Isomerization of cyanopropyne in solid argon

Thomas Custer,[*a] Urszula Szczepaniak,[a,b,e] Marcin Gronowski,[a] Nathalie Piétri,[c] Isabelle Couturier-Tamburelli,[c] Jean-Claude Guillemin,[d] Michał Turowski,[a] and Robert Kołos [a]

a. *Institute of Physical Chemistry, Polish Academy of Sciences, Kasprzaka 44/52, 01-224 Warsaw, Poland.*
b. *Institut des Sciences Moléculaires d'Orsay (ISMO), CNRS, Univ. Paris-Sud, Université Paris-Saclay, F-91405 Orsay, France.*
c. *UMR CNRS 7345, Physique des Interactions Ioniques et Moléculaires, Equipe ASTRO, Aix-Marseille Université, Case 252, Centre de St-Jérôme, 13397 Marseille cedex 20, France.*
d. *Univ. Rennes, Ecole Nationale Supérieure de Chimie de Rennes, CNRS, ISCR-UMR6226,F-35000 Rennes, France.*
e. *Current address: IRsweep AG, Laubisruetistrasse 44, 8712 Staefa, Switzerland*

Electronic Supplementary Information

Table of Contents

APPENDIX 1-SYNTHESIS **4**

APPENDIX 2-COMPUTATIONS ON THE GROUND STATE POTENTIAL ENERGY SURFACE **4**

ISOMERIZATION. 4
Fig. S1 ..... *5*
Fig. S2 ..... *5*
Fig. S3 ..... *6*
ELECTRON DETACHMENT. 6
Fig. S4 ..... *7*
HETEROLYTIC BOND CLEAVAGE (DEPROTONATION). 7
Fig. S5 ..... *7*
Fig. S6 ..... *8*
HOMOLYTIC BOND CLEAVAGE. 8
Fig. S7 ..... *8*
Table S1 ..... *8*
HYDROGENATION. 9
Fig. S8 ..... *10*
$C_4H_3N^+$ FAMILY 11
Table S2 ..... *11*
Table S3 ..... *12*
$C_4H_2N^-$ FAMILY 14
Table S4 ..... *14*
Table S5 ..... *14*
C_4H_2N FAMILY 15
Table S6 ..... *15*
Table S7 ..... *16*
$C_4H_4N^+$ FAMILY 17
Table S8 ..... *17*
Table S9 ..... *18*
C_4H_4N FAMILY 19
Table S10 ..... *19*
Table S11 ..... *20*
SINGLET C_4H_3N FAMILY ($^{14}N/^{15}N$ COMPARISON) 21
Table S12 ..... *21*
Table S13 ..... *24*
Table S14 ..... *27*
Table S15 ..... *30*

Table S16 ..... *33*
Table S17 ..... *36*
TRIPLET C_4H_3N FAMILY ($^{14}N/^{15}N$ COMPARISON) 39
Table S18 ..... *39*
Table S19 ..... *41*
Table S20 ..... *43*
Table S21 ..... *45*
Table S22 ..... *47*
Table S23 ..... *49*

APPENDIX 3-PHOTOPRODUCT DETAILS 51

ALLENYL CYANIDE (2) 51
Fig. S9 ..... *52*
Fig. S10 ..... *52*
Fig. S11 ..... *53*
Fig. S12 ..... *53*
Fig. S13 ..... *54*
Fig. S14 ..... *54*
PROPARGYL CYANIDE (3) 55
Fig. S15 ..... *55*
Fig. S16 ..... *56*
Fig. S17 ..... *56*
Fig. S18 ..... *57*
Fig. S19 ..... *57*
Fig. S20 ..... *58*
Fig. S21 ..... *58*
Fig. S22 ..... *59*
ALLENYL ISOCYANIDE (6) 59
Fig. S23 ..... *60*
Fig. S24 ..... *60*
Fig. S25 ..... *61*
Fig. S26 ..... *61*
Fig. S27 ..... *62*
Fig. S28 ..... *62*
Fig. S29 ..... *63*
Fig. S30 ..... *63*
Fig. S31 ..... *64*
PROPARGYL ISOCYANIDE (10) 64
Table S24 ..... *65*
Table S25 ..... *66*
Fig. S32 ..... *66*
Fig. S33 ..... *67*
Fig. S34 ..... *67*
Fig. S35 ..... *68*
Fig. S36 ..... *68*
Fig. S37 ..... *69*
Fig. S38 ..... *69*
Fig. S39 ..... *70*
Fig. S40 ..... *70*
Fig. S41 ..... *71*
Fig. S42 ..... *71*
Fig. S43 ..... *72*
Fig. S44 ..... *72*

1,2,3-BUTATRIEN-1-IMINE (4) 73
Fig. S45 ..... *73*
Fig. S46 ..... *74*
Fig. S47 ..... *74*
Fig. S48 ..... *75*
Fig. S49 ..... *75*
Fig. S50 ..... *76*
Fig. S51 ..... *76*
1-ISOCYANO-1-PROPYNE (9) 77
Fig. S52 ..... *77*
Fig. S54 ..... *78*
Fig. S55 ..... *79*
Fig. S56 ..... *79*
Fig. S57 ..... *80*
3-CYANOCYCLOPROPENE (8) 80
Table S26 ..... *81*
Fig. S58 ..... *81*
Fig. S59 ..... *82*
Fig. S60 ..... *82*
Fig. S61 ..... *83*
Fig. S62 ..... *83*
Fig. S63 ..... *84*
1-CYANO-2-PROPENEYLIDENE (TRIPLET) (19) 84
Fig. S64 ..... *84*
Fig. S65 ..... *85*
Fig. S66 ..... *85*
Fig. S67 ..... *86*
Fig. S68 ..... *86*
Fig. S69 ..... *87*
ACETYLENE 87
Fig. S70 ..... *87*
FULL SPECTRA 88
Fig. S71 ..... *88*
Fig. S72 ..... *88*
Fig. S73 ..... *89*
Fig. S74 ..... *89*
Fig. S75 ..... *90*
Fig. S76 ..... *90*

APPENDIX 4-RATE COEFFICIENTS AND EXCITED STATE POTENTIAL ENERGY SURFACE 91

Table S27 ..... *91*
Fig. S77 ..... *91*
Fig. S78 ..... *92*
Fig. S79 ..... *92*
Fig. S80 ..... *92*
Fig. S81 ..... *93*
Fig. S82 ..... *93*
Fig. S83 ..... *93*
Fig. S84 ..... *94*

REFERENCES 94

Appendix 1-Synthesis

Chemical Handling and Synthesis Methods for synthesizing the parent cyanopropyne (**1**) have been described recently[1, 2] and involve a two-step sequence starting from the reaction of methyl 2-butynoate with aqueous ammonia (28%) to produce an amide, followed by the dehydration of this amide on phosphorus pentaoxide under vacuum conditions. The ^{15}N isotopologue of cyanopropyne (**1**) employs the same steps but replaces aqueous ammonia, having normal isotopic abundances, with ammonia-^{15}N. Methods for synthesizing isonitriles **6**[3, 4] and **10**[3] have also been described recently and require heating a mixture of N-2-propyn-1-yl formamide combined with p-toluenesulfonyl chloride and trioctylamine in excess to 80 °C under vacuum to form propargyl isocyanide (**10**). To form allenyl isocyanide (**6**) the propargyl isocyanide product **10** is trapped on KOH and allenyl isocyanide (**6**) is further distilled under vacuum[4, 5]. Allenyl cyanide (**2**) and propargyl cyanide (**3**) can be formed in good yield by flash vacuum pyrolysis of allenyl isocyanide (**6**) and propargyl isocyanide (**10**) respectively at 700 °C [6]. Although all of these chemicals should be treated with care, particular caution should be used in working with isomers **3** and **6**. At room temperature, both are potentially explosive in their pure form.

A brief comment regarding purity, storage, and handling of these chemicals specific to these FT-IR and matrix isolation measurements is helpful. Our FT-IR measurements indicate that in samples of ^{14}N-**1** and ^{15}N-**1**, which are white solids which melt near room temperature to form a clear liquid, the only observable bands not associated with these species themselves come from trace impurities inherent to our experimental apparatus (e.g., leaks in the vacuum system giving rise to CO_2 or H_2O signals or trace impurities in Ar gas used for forming matrices). Samples of **2** were found to contain traces of **3** on the order of a percent. Both **1** and **2** seem to be safely storable in small amounts in evacuated glass containers for long periods without significant decomposition (storage at -20 °C for **1** and storage at -78 °C in dry ice for **2**). Samples of **6** were contaminated with **10** and vice versa although both also appear to be stable stored in small quantities in an evacuated vessel at -78 °C for extended periods. Propargyl cyanide (**3**) is much less stable. Although fresh samples can be quite pure, significant contamination with **2** and even minimal contamination by **1** have been observed. The origin of these impurities may be partly synthetic as a chain of reactions starting from allenyl isocyanide (**6**) and proceeding through propargyl isocyanide (**10**) is used in its synthesis. The presence of **1** may also be due to contamination of equipment from previous experiments working with **1**. We have also observed that prolonged (a period of several weeks) storage of small amounts of **3** in an intially evacuated glass vessel at -78 °C resulted in its conversion into isomer **2**, eventually followed by polymerization. Contamination of **3** by **2** could often be reduced by almost completely transfering a sample in-vacuo to a second vessel and using residual material from the first vessel for experiments. The successful use of this procedure suggests that **2** has a lower vapor pressure than **3**. Sequential IR spectra show that concentrations of the gas phase species placed in a glass gas-cell at low pressures decrease in concentration over time and at different rates.

Propargyl cyanide (3-Butynenitrile) 3. ^{1}H NMR (C_6D_6, 400 MHz) δ 1.70 ($_1H$, $^4J_{HH}$ = 2.9 Hz, CH); 2.27 (2H, $^4J_{HH}$ = 2.9 Hz, CH_2). ^{13}C NMR (C_6D_6, 100 MHz) δ 8.53 ($^1J_{CH}$ =139.4 Hz, (t), CH_2), 72.2 ($^2J_{CH}$ = 51.3 Hz, (d), CCH); 72.7 ($^1J_{CH}$ = 254.6 Hz, (d), CH); 114.8 (s, CN).

Allenyl cyanide (2,3-Butadienenitrile) 2. ^{1}H NMR (C_6D_6, 400 MHz) δ 4.33 (m, 2H, CH2); 4.37 (m, 1H, CH). ^{13}C NMR (C_6D_6, 100 MHz) δ 67.2 ($^1J_{CH}$ = 183.4 Hz, (d), CH); 79.7 ($^1J_{CH}$ = 171.6 Hz, (t), CH_2); 112.9 (s, CN); 218.0 (s, C=C=C).

Cyanopropyne-^{15}N (2-Butynenitrile-^{15}N) 1^{15}N. ^{1}H NMR ($CDCl_3$, 400 MHz) δ 2.04 (s, 3H, CH_3). ^{13}C NMR ($CDCl_3$, 100 MHz) δ 4.25 (^1JC_H = 133.5 Hz (q), CH_3), 54.7 (qd, $^3J_{CH}$ = 8.7 Hz, $^2J_{CN}$ = 4.4 Hz, C-Me), 83.4 (qd, $^2J_{CH}$ = 11.0 Hz, $^3J_{CN}$ = 8.0 Hz, C-CN), 105.4 (qd, $^4J_{CH}$ = 3.7 Hz, $^1J_{CN}$ = 20.3 Hz, CN).

2-Butynamide-^{15}N. ^{1}H NMR (DMSO-d6, 400 MHz) δ 1.92 (s, 3H, CH_3), 7.36 (d, 1H, $^1J_{NH}$ = 87.6 Hz,NH), 7.82 (d, 1H, $^1J_{NH}$ = 89.6 Hz, NH). ^{13}C NMR (DMSO-d6, 100 MHz) δ 2.88 (q, $^1J_{CH}$ = 132.0 Hz, CH_3), 75.7 (dq, $^2J_{CN}$ = 11.6 Hz, $^3J_{CH}$ = 5.1 Hz, CCN), 82.4 (dq, $^3J_{CN}$ = 1.4 Hz, $^2J_{CH}$ = 11.0 Hz, C-Me), 154.2 (d, $^1J_{CN}$ = 18.9 Hz, C=O).

Appendix 2-Computations on the ground state potential energy surface

Isomerization. Production of new isomers is one of the most likely processes following photolysis of a species isolated in a noble gas matrix due to the "cage effect"[7-9]. While absorption of light of a certain energy by a species in the gas-phase or solution may result in cleavage of bonds and production of separated fragments, lack of any path for efficient exit of such a fragment from a matrix cage, depending on a number of factors, often makes it much less likely to occur. One very common isomerization reaction is conversion of cyano species to isocyano species. The transition states for this process on the ground state PES and connecting various pairs of C_4H_3N isomers are presented in Fig. S1. Taking into account the precision of B3LYP computations, the calculated activation energies for isomerization of **2** to **6** and from **3** to **10** are the same. The activation energy for isomerization of **1** to **9** is slightly higher. This is related to larger electron delocalization of pi electrons in **1** as compared to **2** and **3**.

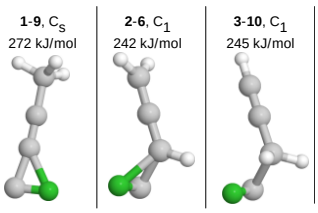

Fig. S1.Transition states connecting cyanides with respective isocyanides and their activation energies. Numbers separated by a hyphen correspond to C4H3N isomers (PES minima depicted in Fig. 1) connected by the transition state.

Another frequently encountered isomerization process in rare gas photolysis experiments is a hydrogen shift. For CH_3C_3N, this means H atom movement along the CCCCN chain. Transition states for hydrogen shifts between a variety of isomers are presented in Fig. S2. No transition state directly linking **1** with **2** on the ground singlet PES was found. This reaction involves species **19**, as discussed later. Activation energies for hydrogen shift processes considered here range from 310 to 374 kJ/mol. We did not find any transition states directly linking cyclic isomers **7** and **8** with any of the isomers **1**-**6** or **9**-**11**.

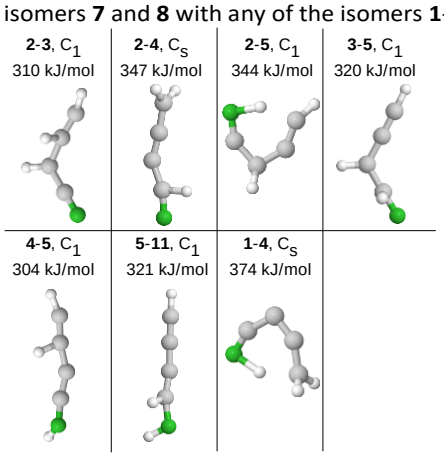

Fig. S2. Transition states for hydrogen shifts along the CCCCN chain and their activation energies. Numbers separated by a hyphen correspond to C_4H_3N isomers (PES minima depicted in Fig. 1) connected by the transition state.

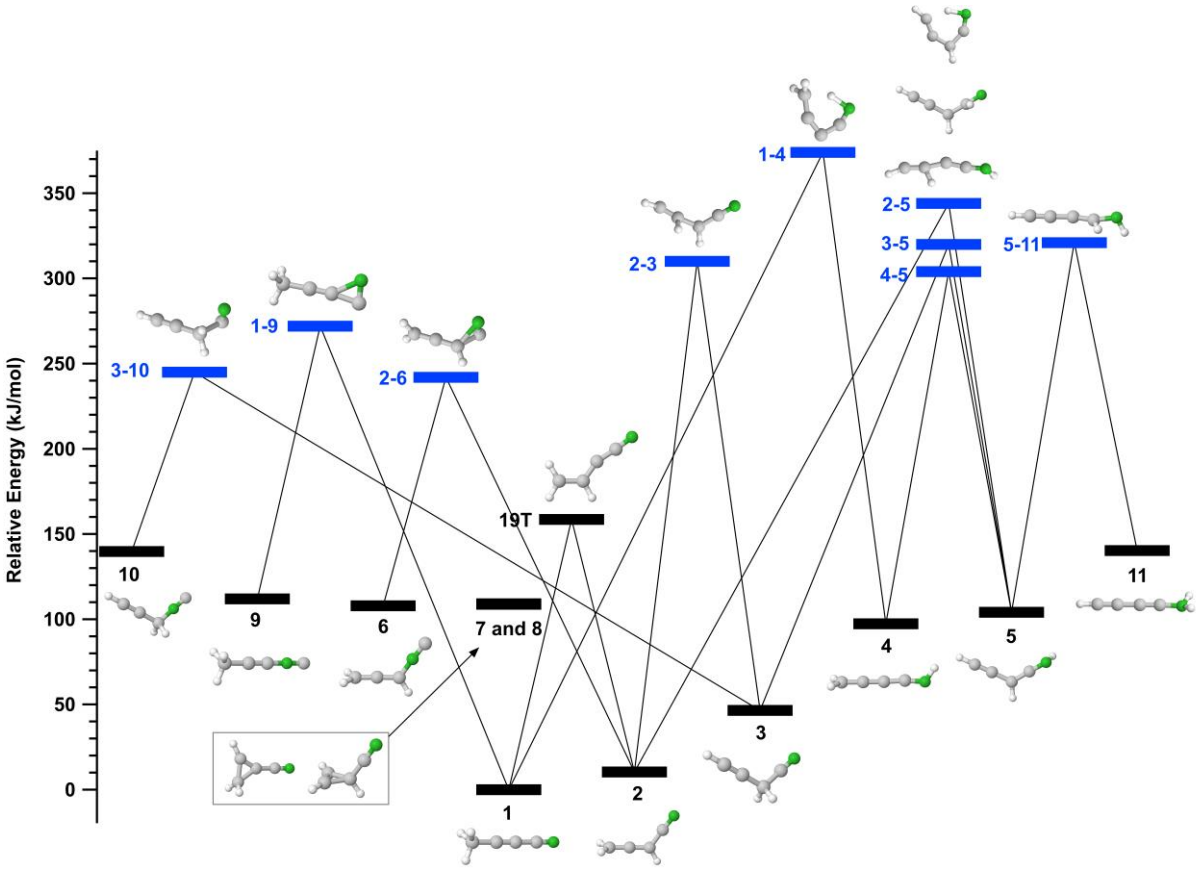

Fig. S3. Potential energy diagram depicting ground state species and transition states connecting them. No transition state was found connecting 7 or 8 to any other species. 19T is a triplet ground state and not a transition state. For further details about 19T see Fig. 7 of the main text or Appendix 4.

Electron detachment. Loss of one electron from a C_4H_3N isomer leads to a molecular cation $C_4H_3N^+$. The electron can readily leave the matrix cage where it was originally released. The ultimate fate of both cation and electron in a matrix environment depends in a complicated way on experimental conditions, as well as the nature of the host, guest, ionic photoproducts, and even impurities/dopants[10,11]. For now, it is important to answer the question as to whether an electron can be detached from various C_4H_3N family members at all. The production of H_3C-CC-CN^+ from **1** in a noble gas matrix was demonstrated experimentally by Fulara et al.[12]. They photolyzed **1** using a neon discharge lamp with an energy of ~1600 kJ/mol. This is far higher than the measured gas-phase ionization energy of 1 which has been reported as 1039 kJ/mol[13]. Our theoretical predictions give a value of 995 kJ/mol which is smaller than the measured one, but within the typical precision of DFT calculations (see adiabatic ionization energies in Fig. 1, main text). Isolation in a matrix environment often decreases the ionization potential of a species[11]. Neglecting the reduction in ionization potential for our system in Ar for now, one-photon 248 nm (482 kJ/mol) or 193 nm (620 kJ/mol) laser photolysis cannot ionize any of the 12 lowest energy isomers depicted in Fig. 1. The microwave discharge hydrogen flow lamp (peak intensity at 121.6 nm or 984 kJ/mol) may have sufficient energy to ionize all isomers but **1**, **3**, **8**, or **10** depending on the accuracy of the theoretical results. Of the pure chemicals we have available, only **2** and **6** have a chance of being ionized by this radiation. From an energetic point of view, only two-photon 193 nm absorption can lead to ionization of species **1**. The structures of ionized species are presented in Fig. S4. Although molecular geometries corresponding to minima on the $C_4H_3N^+$ and C_4H_3N potential energy surfaces are similar, their energetic order is significantly different. For the molecular cation, species **4**$^+$ has the lowest energy, closely followed by **5**$^+$ and more distantly by **11**$^+$, **12**$^+$ and then **2**$^+$.

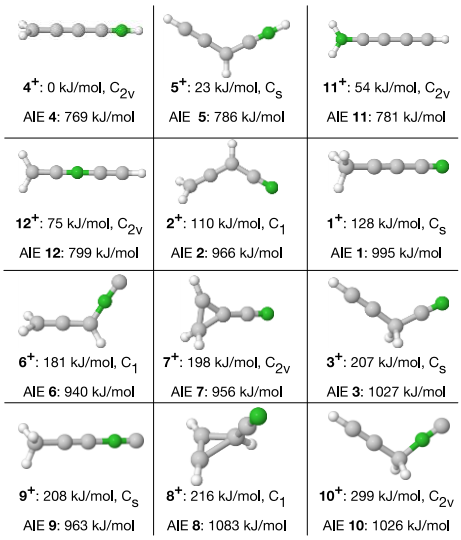

Fig. S4. Structures of twelve $C_4H_3N^+$ isomers together with energies relative to **4**$^+$. Results of B3LYP/aug-cc-pVTZ computations. Numbering reflects structural similarity to the respective neutral species of Fig. 1. Adiabatic ionization energies (AIE) of the respective neutral C_4H_3N precursors calculated at the same level of theory are also given.

Heterolytic bond cleavage (deprotonation). Anions C_3N^-[14, 15] and C_5N^-[16], isoelectronic with their precursors, were shown to be formed in the course of HC_3N and HC_5N photolyses, respectively. Several isomeric anions may be considered as potential products of the photolysis of **1**. Our PES screening calculations resulted in 8 ground state singlet structures with energies lower than the global minimum on the triplet PES (165 kJ/mol for **A1**, H_2CCCCN^-). The three highest energy isomers are separated from those below (Fig. S5) by a modest energy gap. Although H_2CCCCN^- (species **A1**, Fig. S5) seems to be the most stable anion, HCC-CH-CN$^-$ (**A2**) has an energy only 13 kJ/mol higher, a difference smaller than the precision of our calculations. Regardless, such anions are not expected as products of photolysis of any of the C_4H_3N isomers, as deprotonation is a strongly endothermic process (1467 kJ/mol is predicted for dissociation of CH_3CCCN to H^+ and H_2CCCCN^-).

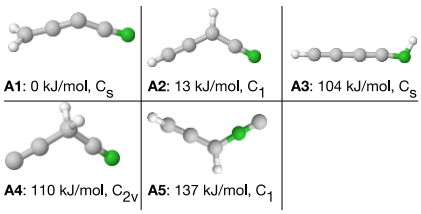

Fig. S5. Structures for $C_4H_2N^-$ anions optimized at the B3LYP/aug-cc-pVTZ level of theory along with their energy relative to the lowest energy isomer. Numbering does not imply structural similarity to species from previous Figs.

Dissociation of neutral isomers into H^- and a corresponding cation is even less likely. Without any free protons available in the matrix, production of protonated ions with $C_4H_4N^+$ composition by the addition of mobile H^+ to available neutral species can be neglected. Nevertheless, calculations for such species may be of broader interest outside of this work and can be found below in Fig. S6.

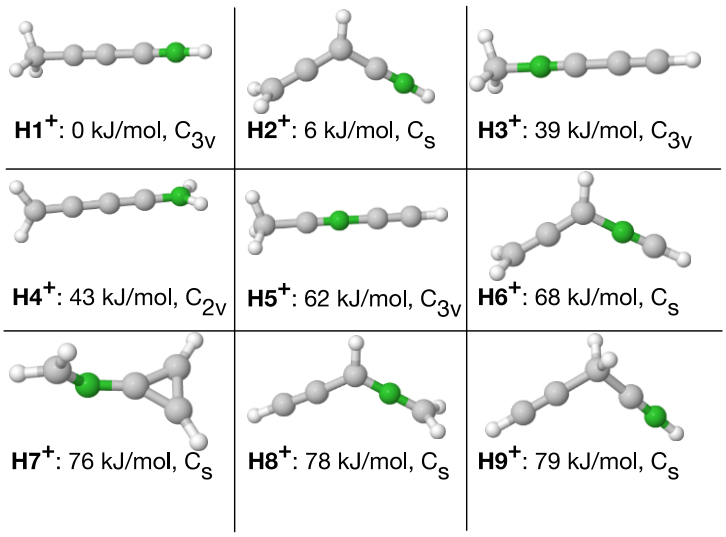

Fig. S6. Structures for $C_4H_4N^+$ isomers optimized at the B3LYP/aug-cc-pVTZ level of theory along with their energy relative to the lowest energy isomer. Numbering does not imply structural similarity to species from other Figs. in the main text.

Homolytic bond cleavage. Here, the lowest energy homolytic bond cleavage processes invariably involve C-H bonds. These processes are thermodynamically accessible at all photolysis wavelengths used in this study for all molecules depicted in Fig. 1 (main text). Unlike C-C bond cleavage, where the resulting fragments may have difficulty exiting a matrix cage, H atom is small and may readily migrate in the matrix leaving a bulky radical behind. While the PES for C_4H_2N is less complicated than for $C_4H_2N^-$ a number of minima could still be found. The lowest energy radicals are presented in Fig. S7. The radical H_2CCCCN, **R1**, is expected to be the lowest energy isomer although the energetic separation between **R1** and **R2** (HCC-CH-CN) is smaller than the precision of our calculations. We found six structures with energies smaller than 200 kJ/mol relative to **R1**. The abstraction of hydrogen from the C_4H_3N isomers which we have in pure form (i.e. **1**, **2**, **3**, **6**, and **10**) requires reaction enthalpies on the order of 350 kJ/mol.

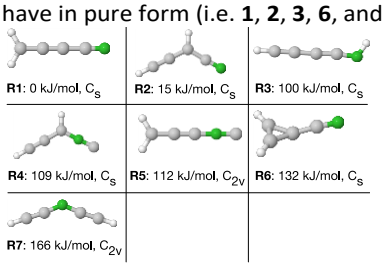

Fig. S7. Structures for molecules of C_4H_2N composition optimized at the B3LYP/aug-cc-pVTZ level of theory along with their energy relative to the lowest energy isomer. Numbering does not imply structural similarity to species from previous Figs.

Table S1. The reaction enthalpy at 0 K for dissociation of selected C_4H_3N isomers organized in order of decreasing energy. Numbers in first column correspond to those in Fig. 1. For reference, the photon energies of the light sources used in these experiments are also given.

Parent Isomer	Products		ΔH 0 K (kJ/mol)
H_2 discharge lamp (984 kJ/mol)			
1	H_3CCC	CN	650
193 nm Excimer Laser (620 kJ/mol)			
11	H_2NCC	HCC	607
1	H_3C	C_3N	558[a]
9	CH_3CC	CN	537
11	NH_2	HCCCC	519
5	HCCNH	HCC	510
9	CH_3	CCNC	510
248 nm Excimer Laser (482 kJ/mol)			
8	cycl-C_3H_3	CN	459
2	H_2CCCH	CN	453
10	H_2CNC	HCC	451
3	H_2CCCH	CN	417

12	HCCNCCH (**R7**)	H	374
2	HCC-CH-CN (**R2**)	H	355
6	H_2CCCH	CN	355
6	H_2CCNC (**R5**)	H	355
4	HCCCCNH (**R3**)	H	354
5	HCCCCNH (**R3**)	H	354
7	H_2CCCH	CN	354
6	HCC-CH-NC (**R4**)	H	352
12	H_2CCN	HCC	352
1	H_2CCCCN (**R1**)	H	351
9	H_2CCCNC (**R5**)	H	351
2	H_2CCCCN (**R1**)	H	340
10	H_2CCCH	CN	323
10	HCC-CH-NC (**R4**)	H	320
3	HCC-CH-CN (**R2**)	H	319
11	HNCCCCH (**R3**)	H	311
5	HCC-CH-CN (**R2**)	H	261
4	H_2CCCCN (**R1**)	H	254
3	HCCCCN	H_2	243[b]
8	cycl-CH-CH-C	HCN	195[c]

a) The value could only be estimated, as DFT calculations were hampered by the proximity[14, 17] of the ground and the lowest excited electronic state of C_3N.

b) The ground electronic state of HCCCCN is of triplet multiplicity. The activation energy on singlet PES is 360 kJ/mol.

c) The activation energy for this reaction is 269 kJ/mol.

Observing products of C-C bond breakage in a cryogenic matrix, following the separation of two bulky fragments, is generally not likely. Should a C-C bond break, the resulting fragments would more likely recombine, a situation dealt with here under isomerization. Nevertheless, the production of CN radical has been observed upon photolysis of gas-phase HC_3N, albeit with a low quantum yield[18]. It has also been observed upon photolysis of NCCN in an Ar matrix[19]. While it is unlikely that the CN radical would be able to leave the matrix cage in which it is formed, such an event cannot be ruled out completely. The occurrence of chain elongation reactions, which have also been reported for matrix-isolated nitriles, may depend on mobility of larger molecular fragments driven out of their matrix cage and on excess energy provided by light.[20] With this in mind, possibilities for C-C bond dissociation should at least be considered. The reaction enthalpies at 0 K for gas-phase homolytic bond breakage of precursors **1**-**12** are collected in Table S1. In addition to the requirement that precursors possess excited states amenable to absorption of a photon of a particular energy, a necessary condition for these endothermic reactions to occur is that the photon energy surpass the dissociation energy in addition to any activation energy and some excess energy required to exit a particular matrix cage. We have checked that excited state PESs do not cross the ground state PES for the processes listed in Table S1. Therefore, these reactions are not expected to occur for photon energies below that of the respective ground state dissociation enthalpy. The only two dissociation reactions requiring activation are marked in Table S1 with their respective activation energies given in the footnote. The majority of the processes collected in Table S1 are simply loss of a hydrogen atom. A few exceptions include loss of CN for species such as **6**, **7**, and **10**, the loss of CCH from amine **12**, loss of H_2 from **3**, and loss of HCN from cyclic species **8**. Reactions involving species **1** are the most likely to be observed here. Irradiation by the excimer laser using either 193 nm (620 kJ/mol) or 248 nm (482 kJ/mol) should not dissociate **1** into H_3CCC and CN or CH_3 and C_3N. Ignoring details of the excited state PES and the matrix cage effect, these processes cannot be excluded for the H_2 discharge lamp.

Hydrogenation. H atoms may appear following photolysis of **1** or other isomers (see discussion of homolytic bond cleavage) or of unavoidable impurities and may then migrate through the matrix and attach to other species. The most stable molecules of C_4H_4N composition are presented in Fig. S8. Rotamers **H1** and **H2** are separated by only 3 kJ/mol which is not significant, given the precision of our calculations. Both can be considered as the products of hydrogen atom addition to allenyl cyanide, **2**. The calculated energies of these endothermic reactions are 262 and 259 kJ/mol respectively.

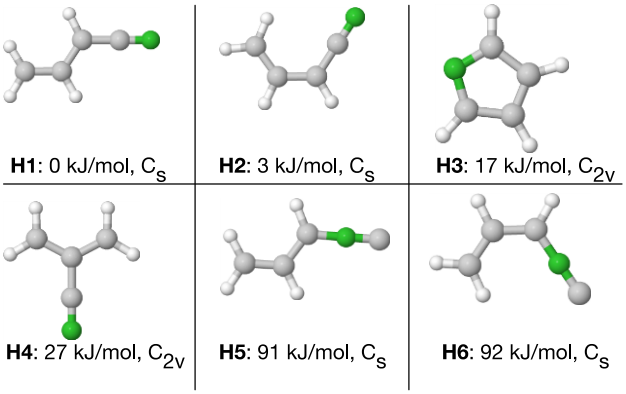

Fig. S8. Structures for molecules of the C_4H_4N composition, optimized at the B3LYP/aug-cc-pVTZ level of theory, along with their energies relative to the lowest energy isomer. Numbering does not imply structural similarity to species from previous Figs.

$C_4H_3N^+$ family

Table S2-Frequencies (unscaled) and intensities for $C_4H_3N^+$ isomers. Corresponding structures in Fig. S4.

1⁺		**2⁺**		**3⁺**		**4⁺**		**5⁺**		**6⁺**	
freq	IR int.	freq	IR int.	freq	IR int.	freq	IR int.	freq	IR int.	freq	IR int.
cm^{-1}	km/mol	cm^{-1}	km/mol	cm^{-1}	km/mol	cm^{-1}	km/mol	cm^{-1}	km/mol	cm^{-1}	km/mol
135	1	128	6	138	3	126	10	136	4	126	2
136	3	273	8	265	15	133	11	235	126	203	6
248	78	334	11	333	9	282	133	353	31	265	5
350	9	343	6	338	9	379	0	365	8	297	9
446	37	503	108	581	3	400	135	431	9	424	51
509	1	565	6	642	8	415	0	595	121	562	14
518	19	801	27	696	40	493	2	620	10	812	5
683	1	865	51	752	27	551	0	677	16	881	25
921	29	924	30	888	50	745	5	697	22	934	36
1229	26	965	21	1010	39	860	37	716	38	987	17
1235	22	1109	5	1118	0	990	1	974	8	1169	6
1311	125	1313	51	1231	167	1331	22	1146	2	1330	44
1420	8	1386	14	1286	144	1449	8	1382	14	1414	22
2027	527	1745	60	2056	1037	2058	129	2079	123	1826	20
2280	24	2192	377	2293	486	2303	772	2298	308	2065	793
2903	284	3051	190	2832	111	3121	78	3143	51	3050	176
3020	64	3098	57	2872	174	3216	34	3405	119	3118	33
3021	65	3125	92	3358	146	3704	1305	3692	1043	3122	85

Table S2 (cont.)-Frequencies (unscaled) and intensities for $C_4H_3N^+$ isomers. Corresponding structures in Fig. S4.

7⁺		**8⁺**		**9⁺**		**10⁺**		**11⁺**		**12⁺**	
freq	IR int.	freq	IR int.	freq	IR int.	freq	IR int.	freq	IR int.	freq	IR int.
cm^{-1}	km/mol	cm^{-1}	km/mol	cm^{-1}	km/mol	cm^{-1}	km/mol	cm^{-1}	km/mol	cm^{-1}	km/mol
176	1	145	2	127	1	129	0	145	15	143	9
195	1	198	17	142	5	269	0	154	18	151	8
352	0	232	8	236	45	289	19	304	1	350	1
479	11	401	15	262	2	330	1	393	0	378	1
534	1	544	8	393	49	503	22	500	3	445	0
662	25	670	50	445	29	687	43	520	2	468	0
731	12	699	9	475	3	774	15	661	190	685	28
953	36	793	42	705	5	866	11	693	38	708	34
953	6	826	12	915	21	944	61	705	23	784	14
1035	12	929	38	1241	23	1097	25	754	0	814	45
1086	45	1007	16	1270	17	1265	6	1138	3	985	1
1193	54	1113	6	1312	109	1322	334	1439	9	1323	40
1293	102	1308	1	1431	6	1454	13	1636	61	1425	0
1637	8	1752	1	1957	822	2075	1703	2061	364	2048	289
2214	284	2133	220	2297	64	2219	144	2251	4	2153	177
2912	208	3146	32	2901	226	3043	24	3397	160	3122	108
2939	62	3183	170	3026	49	3131	0	3452	379	3224	51
3227	86	3319	148	3031	54	3382	113	3549	167	3402	134

Table S3-Coordinates of optimized structures of $C_4H_3N^+$ isomers. Corresponding structures in Fig. S4.

4+	**5+**	**11+**
H,1.663398479,3.0735378321,0.	C,-2.3583158817,-0.4356349581,-0.0212446596	C,2.6805217867,-0.0000003384,-0.0123432677
N,1.1854474803,2.1895460741,0.	C,-1.2788497181,0.1291613175,-0.0059429351	C,1.4595336099,-0.0000002111,0.014192982
C,0.6359710993,1.1734096013,0.	C,-0.0869184506,0.7977580106,0.006638342	C,0.1365805533,-0.0000000731,0.0429422605
C,0.0065433841,0.0094068395,0.	C,1.11068486,0.1160104441,0.1489335586	C,-1.1005390087,0.000000056,0.0698379708
C,-0.5823779581,-1.0797630491,0.	N,2.114890921,-0.4286703026,0.2649520484	N,-2.3791770149,0.0000001894,0.0976405691
C,-1.2193728195,-2.2577568988,0.	H,2.9931298772,-0.9083288226,0.3703509316	H,-2.9083683488,-0.8679384319,0.1091487814
H,-1.4813319795,-2.7422063149,0.934156848	H,-0.0280542903,1.8776536258,-0.0929977757	H,-2.9083681677,0.867938921,0.1091487814
H,-1.4813319795,-2.7422063149,-0.934156848	H,-3.3047243176,-0.9293813147,-0.0348015103	H,3.7486446171,-0.0000004499,-0.0355562847

Table S3 (cont.)-Coordinates of optimized structures of $C_4H_3N^+$ isomers. Corresponding structures in Fig. S4.

12+	2+	1+
C,-0.0071700509,-2.4440547569,0.2027205419	C,-2.1435927957,-0.7199805013,0.0168556717	N,-2.5315763626,-0.5036699294,0.
C,-0.0071697945,-1.1109256552,0.0797245432	C,-1.0791436459,-0.0004016082,-0.0328229976	C,-1.3773107231,-0.2766303278,0.
N,-0.0071695689,0.0620961406,-0.0285036487	C,0.0252346166,0.7749128385,-0.0823392983	C,-0.0700641797,-0.0190364304,0.
C,-0.0071693246,1.3321578182,-0.1456876995	C,1.3009455813,0.2279373466,0.0461702155	C,1.1467217855,0.217637471,0.
C,-0.0071690925,2.5384493056,-0.2570051841	N,2.3713077658,-0.2125776159,0.1706593323	C,2.5271911143,0.5067783146,0.
H,-0.007168888,3.6020353937,-0.3551577615	H,-0.0751216632,1.8552041511,-0.1954697047	H,3.0155931264,0.1414399232,-0.9091509067
H,0.932075041,-2.9833471708,0.2524804798	H,-2.3766731062,-1.3267133461,0.8945582417	H,2.6323482398,1.6102503102,0.
H,-0.9464153502,-2.9833468921,0.2524795844	H,-2.8475787527,-0.7495292648,-0.8176114607	H,3.0155931264,0.1414399232,0.9091509067

Table S3 (cont.)-Coordinates of optimized structures of $C_4H_3N^+$ isomers. Corresponding structures in Fig. S4.

6+	7+	3+
C,-2.0677637889,-0.8580118472,0.0151951662	N,-0.8913271445,-2.1717824021,0.	C,-2.2076946363,-0.6617966374,0.
C,-1.0356921569,-0.0980995431,-0.0205933521	C,-0.4715730811,-1.0859375386,0.	C,-1.1619312826,-0.0156185683,0.
C,0.0345416306,0.7445335425,-0.0547874566	C,0.0377500823,0.1845659703,0.	C,0.0198728132,0.7797442995,0.
N,1.2811927269,0.2963210116,0.0516449841	C,-0.1852450106,1.5233459443,0.	C,1.2921965996,0.0949688377,0.
C,2.4259878425,-0.035350025,0.1166761873	C,1.1992360499,1.0893599918,0.	N,2.3264476204,-0.4211715071,0.
H,-0.1147232439,1.8173236254,-0.1697582942	H,1.8194359382,1.1974163744,0.905136776	H,-0.0348542503,1.4898760446,0.8545049579
H,-2.3250288598,-1.4245469024,0.9127591094	H,-0.9048157726,2.3307102877,0.	H,-0.0348542503,1.4898760446,-0.8545049579
H,-2.7231721505,-0.9700648617,-0.8511363441	H,1.8194359382,1.1974163744,-0.905136776	H,-3.1165937236,-1.2321161031,0.

Table S3 (cont.)-Coordinates of optimized structures of $C_4H_3N^+$ isomers. Corresponding structures in Fig. S4.

9+	8+	10+
C,-2.52104325,0.650070777,0.	C,0.626269897,0.2220900713,0.3493413964	C,2.0719965034,-0.8154180525,0.
N,-1.353740467,0.34630138,0.	C,-0.212666724,1.430208633,0.6836872414	C,1.1342873194,-0.0327933104,0.
C,-0.129322071,0.027643819,0.	N,-0.3635773249,-2.0739306827,-0.1603502378	C,0.0124233189,0.8847238873,0.
C,1.071596521,-0.288209149,0.	C,-0.4400765933,1.4216565803,-0.55678871	N,-1.2068736265,0.1067854173,0.
C,2.446056979,-0.625632211,0.	C,0.0875973612,-1.0222571518,0.0770155578	C,-2.226033098,-0.4415611684,0.
H,3.016483813,0.324753783,0.	H,-0.6763944167,1.4152696873,-1.6061915804	H,0.014699513,1.5138978408,0.8930021211
H,2.733101761,-1.162432104,0.908815029	H,-0.2483141756,2.0261500231,1.5878784735	H,0.014699513,1.5138978408,-0.8930021211
H,2.733101761,-1.162432104,-0.908815029	H,1.7051239763,0.3330478394,0.405407859	H,2.9047607095,-1.4884188678,0.

$C_4H_2N^-$ family

Table S4-Frequencies (unscaled) and intensities for $C_4H_2N^-$ isomers. Corresponding structures in Fig. S5.

A1		A2		A3		A4		A5	
freq	IR int.	Freq	IR int.	freq	IR int.	freq	IR int.	freq	IR int.
cm^{-1}	km/mol	cm^{-1}	km/mol	cm^{-1}	km/mol	cm^{-1}	km/mol	cm^{-1}	km/mol
106	2	158	2	39	66	136	16	159	3
275	6	348	117	53	43	252	1	340	31
399	4	392	406	139	2	319	7	344	16
508	20	412	51	453	68	373	3	435	115
542	36	513	39	461	15	552	5	499	119
552	112	574	34	480	0	873	10	594	235
625	3	629	8	521	5	928	1	611	172
798	11	719	37	526	1	961	15	764	36
1015	0	962	1	746	39	1230	0	958	4
1304	42	1155	14	1072	277	1305	51	1175	5
1461	16	1372	8	1420	290	1446	1	1374	1
2033	708	2017	958	2065	42	2079	103	1964	800
2197	929	2209	431	2208	2892	2319	54	2126	29
3104	26	3126	17	3454	9	2940	113	3153	20
3164	29	3325	6	3481	120	2945	17	3216	17

Table S5-Coordinates of optimized structures of $C_4H_2N^-$ isomers. Corresponding structures in Fig. S5.

A1	A2	A3
N,-0.0068977314,-0.2616681822,2.6101339945	C,2.3773658786,-0.0127359615,0.2749613161	C,-2.5996138331,0.0145613308,-0.0000009642
C,-0.0002167255,0.0185106875,1.4723252921	C,1.2101076393,0.3502260169,0.0765201861	C,-1.3727801854,0.0003868613,-0.0000002288
C,0.0096369021,0.4632305935,0.1809523232	C,-0.0903903446,0.8008205568,-0.0098287112	C,-0.03090357,-0.0148225342,-0.0000003694
C,0.0037077113,0.0339079759,-1.0086724159	C,-1.2069114442,-0.0375039863,-0.0062061314	C,1.2145931147,-0.0004348601,-0.0000014092
C,-0.0007293486,-0.3200436117,-2.2992741236	N,-2.1643060242,-0.7074506914,-0.0085123667	N,2.488126241,-0.1144086761,0.0000075579
H,0.9222135342,-0.4938943759,-2.8395675283	H,-0.282634505,1.8642652494,-0.0912250912	H,2.9732640766,0.7778902958,-0.000064941
H,-0.9277143422,-0.460781087,-2.8422815419	H,3.2612788002,-0.3361831839,-0.233868323	H,-3.6578228438,0.0245455824,-0.0000006453

Table S5 (cont.)-Coordinates of optimized structures of $C_4H_2N^-$ isomers. Corresponding structures in Fig. S5.

A4	A5
C,-2.3787125721,-0.4554361609,0.	C,2.2769093004,-0.408375522,-0.1580718613
C,-1.2526965719,0.0580794018,0.	C,1.1438945658,0.1031086617,0.0013205787
C,0.0120682392,0.7710174752,0.	C,-0.0784389205,0.7024367724,0.0202810204
N,1.2077507204,-0.069885727,0.	N,-1.2608100056,-0.0054913493,0.0081789028
C,2.1699137653,-0.7229775608,0.	C,-2.2900759863,-0.5673538467,0.0024665276
H,0.1232026823,1.4174638261,0.8783507376	H,-0.1922192836,1.7773435547,0.0423672311
H,0.1232026823,1.4174638261,-0.8783507376	H,3.0058233298,-0.7659272709,0.5517286008

C_4H_2N family

Table S6-Frequencies (unscaled) and intensities for C_4H_2N isomers. Corresponding structures in Fig. S7.

R1		R2		R3		R4		R5		R6		R7	
freq	IR int.	Freq	IR int.	freq	IR int.	freq	IR int.	freq	IR int.	freq	IR int.	freq	IR int.
cm^{-1}	km/mol	cm^{-1}	km/mol	cm^{-1}	km/mol	cm^{-1}	km/mol	cm^{-1}	km/mol	cm^{-1}	km/mol	cm^{-1}	km/mol
138	0	146	3	131	5	142	2	139	0	133	10	143	3
150	0	362	11	140	1	302	3	158	0	205	1	408	0
362	5	370	8	417	2	326	1	320	4	425	11	421	0
416	9	409	5	432	16	369	13	359	4	530	13	425	5
496	2	579	38	462	5	548	43	407	2	635	54	486	108
539	4	610	2	518	0	597	10	449	0	705	0	504	12
724	0	673	14	526	54	642	9	743	46	798	9	584	0
763	44	675	41	619	33	694	37	754	0	877	0	587	70
1020	0	957	7	757	1	981	12	1025	0	974	3	605	5
1308	0	1131	12	1013	296	1161	14	1328	0	1039	13	909	10
1467	2	1377	11	1496	65	1394	29	1472	1	1437	10	1335	8
2054	3	2053	34	2040	114	2040	83	2062	67	1694	14	1903	86
2226	26	2225	0	2049	112	2119	65	2125	20	2161	41	2126	16
3139	0	3163	2	3459	115	3182	0	3138	0	3247	17	3463	124
3227	1	3455	68	3473	33	3456	76	3225	0	3294	4	3469	22

Table S7-Coordinates of optimized structures of C_4H_2N isomers. Corresponding structures in Fig. S7.

R1	R2	R3
C,-1.6916343302,0.,-0.783492	C,2.2703808631,-0.4198303875,-0.0000533258	C,-0.45521748,3.1342179616,-0.3297375077
C,-0.3438437433,0.,-0.783492	C,1.1790722178,0.1101426806,0.0000050108	N,-0.0818700983,1.9494699084,-0.190362967
C,0.8876075082,0.,-0.783492	C,-0.0483597405,0.7366152666,0.0000726307	C,1.1332949399,-1.5900105097,-0.4122309697
C,2.2381358727,0.,-0.783492	C,-1.2569237752,0.0321816331,0.000170982	C,0.7362453157,-0.4369637098,-0.3323840182
N,3.4006174697,0.,-0.783492	N,-2.2734407359,-0.5253365654,0.000271709	C,0.3062335641,0.8067865334,-0.2352347028
H,-2.2454403886,0.9288746059,-0.783492	H,-0.0993854403,1.8182995467,0.0000473512	H,1.4784725275,-2.590880665,-0.4849210812
H,-2.2454403886,-0.9288746059,-0.783492	H,3.2221386109,-0.8909601741,-0.0001033579	H,-0.775607769,3.6792614811,0.5575292464

Table S7 (cont.)-Coordinates of optimized structures of C_4H_2N isomers. Corresponding structures in Fig. S7.

R4	R5	R6
C,-2.2335657935,-0.3974246764,0.0009973545	C,-2.4272454509,0.000375239,-0.0000196046	C,-1.1257883068,-0.0008291348,-0.0030446491
C,-1.129818047,0.1051038383,0.0004788161	C,-1.07422322,0.0002048034,0.000024626	C,0.2170704444,0.000134543,0.2422242511
C,0.1067697937,0.7139583407,-0.0001410462	C,0.1525910453,0.0000498273,-0.0000104768	N,-2.2896395223,-0.0016517995,-0.1033377208
N,1.2572203464,0.002996258,0.0003957914	N,1.4454399233,-0.0001138018,0.0000033442	C,1.4810985133,-0.6545076631,0.0152120404
C,2.2773970596,-0.5838956044,0.0007255487	C,2.6287614653,-0.0002637781,-0.0000092925	C,1.4802426414,0.6563348071,0.014994714
H,0.201042522,1.7908872308,-0.0010768842	H,-2.9822786485,-0.9276330729,0.0000044735	H,2.0186127814,1.5813138391,-0.0847818418
H,-3.1965708812,-0.844863387,0.0014534196	H,-2.9820471146,0.9285217274,-0.0000663123	H,2.0207064486,-1.5788006246,-0.0842327938

Table S7 (cont.)-Coordinates of optimized structures of C_4H_2N isomers. Corresponding structures in Fig. S7.

R7
C,-2.2961183668,-0.3127614603,0.0002699518
C,-1.1539437781,0.1107402241,0.0001480403
N,-0.0000328769,0.6919345803,-0.0006107242
C,1.1539983971,0.1109664794,0.0000511767
C,2.296249468,-0.312321354,0.0002130003
H,3.2785859883,-0.7118790503,0.0012672278
H,-3.2783519618,-0.7125704192,0.0019473274

$C_4H_4N^+$ family

Table S8-Frequencies (unscaled) and intensities for $C_4H_4N^+$ isomers. Corresponding structures in Fig. S6.

H1$^+$		**H2$^+$**		**H3$^+$**		**H4$^+$**		**H5$^+$**		**H6$^+$**		**H7$^+$**		**H8$^+$**		**H9$^+$**	
freq	IR int.	Freq	IR int.	freq	IR int.	freq	IR int.	freq	IR int.	freq	IR int.	freq	IR int.	freq	IR int.	freq	IR int.
cm^{-1}	km/mol	cm^{-1}	km/mol	cm^{-1}	km/mol	cm^{-1}	km/mol	cm^{-1}	km/mol	cm^{-1}	km/mol	cm^{-1}	km/mol	cm^{-1}	km/mol	cm^{-1}	km/mol
128	11	135	4	140	9	133	14	148	7	146	10	144	37	139	6	125	6
128	11	306	49	140	9	153	17	148	7	320	26	199	12	219	26	297	20
387	0	332	107	282	0	288	2	341	2	338	10	453	3	266	6	341	19
387	0	376	9	282	0	385	0	341	2	371	1	457	8	312	7	368	3
413	136	394	1	543	14	509	2	487	0	603	27	670	1	605	21	570	59
413	136	601	121	543	14	561	0	487	0	635	27	778	1	650	6	575	131
553	0	623	14	675	6	665	0	706	0	642	10	813	58	741	35	592	85
553	0	644	2	782	27	689	196	741	30	804	21	961	0	799	22	742	38
686	18	835	29	782	27	750	4	741	30	828	32	993	4	978	7	769	31
1021	8	930	46	1130	2	921	45	1028	10	938	3	1026	10	1002	35	876	1
1021	8	945	3	1133	1	938	3	1028	10	954	41	1110	24	1093	28	914	0
1226	0	976	2	1133	1	1145	3	1178	22	963	1	1171	31	1132	5	974	6
1395	12	1129	33	1439	5	1331	3	1390	9	1144	22	1193	18	1196	20	1231	0
1427	16	1335	34	1462	20	1461	36	1427	18	1346	3	1393	29	1419	27	1317	4
1427	16	1426	8	1462	20	1640	73	1427	18	1436	11	1534	16	1521	32	1409	24
2246	118	2003	277	2197	134	1975	0	2228	198	2009	125	1691	2	2049	193	2246	32
2398	1380	2340	331	2458	405	2227	649	2419	12	2291	2	2002	254	2217	264	2372	95
3017	52	3113	87	3050	29	3108	118	3021	75	3116	64	3084	0	3067	28	2999	39
3086	11	3138	40	3138	8	3189	43	3097	22	3181	30	3194	3	3104	25	3030	25
3086	11	3191	34	3138	8	3452	316	3097	22	3195	25	3239	64	3169	18	3438	95
3704	1210	3702	1008	3404	118	3546	154	3419	131	3372	403	3277	60	3420	90	3668	812

Table S9-Coordinates of optimized structures of $C_4H_4N^+$ isomers. Corresponding structures in Fig. S6.

H1+	H2+	H3+
N,0,0.0000024225,-0.0000054457,-2.4961415453	C,-2.2935494411,-0.5324938909,0.	C,0.,0.,-2.4944240195
C,0,-0.0000049514,0.0000097245,-1.346520224	C,-1.1808283749,0.1082468141,0.	N,0.,0.,-1.0673536639
C,0,-0.000009792,0.0000208817,-0.0139084814	C,-0.052161253,0.8024095246,0.	C,0.,0.,2.6311079773
C,0,-0.0000104925,0.0000246226,1.2002722283	C,1.1718581976,0.1315755632,0.	C,0.,0.,1.4276768426
C,0,0.0000060447,-0.0000010292,2.6301686434	N,2.1877155275,-0.3966955219,0.	C,0.,0.,0.0795460913
H,0,0.513531866,-0.8894844136,3.0045238889	H,3.0773329502,-0.8653954796,0.	H,1.0331361243,0.,-2.8384533615
H,0,0.5135314714,0.889467262,3.0045605473	H,-0.0177831763,1.8879717608,0.	H,0.,0.,3.7001624243
H,0,-1.0270581266,-0.000008234,3.0045624078	H,-2.7789975992,-0.8098883704,0.9308069895	H,-0.5165680621,-0.8947221292,-2.8384533615
H,0,0.0000115578,-0.0000233682,-3.5012963622	H,-2.7789975992,-0.8098883704,-0.9308069895	H,-0.5165680622,0.8947221292,-2.8384533615

Table S9 (cont.)-Coordinates of optimized structures of $C_4H_4N^+$ isomers. Corresponding structures in Fig. S6.

H4+	H5+	H6+
C,0.,0.,-0.0565832569	C,0.,0.,-2.5186415868	C,-2.1659016212,-0.6240485773,0.
C,0.,0.,1.1887379696	C,0.,0.,-1.0836204566	N,-1.2022944856,-0.0162613169,0.
N,0.,0.,2.4591664096	N,0.,0.,0.0670392317	C,2.3147060237,-0.293618076,0.
C,0.,0.,-2.633834035	C,0.,0.,1.3684437472	C,1.1264346785,0.2026942656,0.
C,0.,0.,-1.3423706198	C,0.,0.,2.5673416864	C,-0.0609120196,0.7671196574,0.
H,0.,0.9324780927,-3.1911069799	H,0.,0.,3.634508317	H,-0.2520373131,1.8323960072,0.
H,-0.8666507585,0.,2.9900967997	H,-0.5155541151,0.8929659215,-2.8808544246	H,2.8306177349,-0.5101883257,-0.9301022736
H,0.,-0.9324780927,-3.1911069799	H,-0.5155541151,-0.8929659215,-2.8808544246	H,-3.070809589,-1.2021231329,0.
H,0.8666507585,0.,2.9900967997	H,1.0311082304,0.,-2.8808544246	H,2.8306177349,-0.5101883257,0.9301022736

Table S9 (cont.)-Coordinates of optimized structures of $C_4H_4N^+$ isomers. Corresponding structures in Fig. S6.

H7+	H8+	H9+
N,-0.9317107567,-0.0000001353,-0.2423766597	C,2.1744334773,-0.529974691,0.	N,2.1062366462,-0.3499397982,0.
C,1.545993125,0.6654078008,0.0403186714	N,1.0951983368,0.0827734539,0.	C,1.1241121898,0.2236261556,0.
C,1.5459931959,-0.6654078076,0.0403186714	C,-2.3675732763,-0.3461120566,0.	C,-2.1579882099,-0.7983097815,0.
C,0.3191677175,-0.0000000687,-0.0245588935	C,-1.2546001539,0.1065387634,0.	C,-1.2505091942,-0.0208371334,0.
C,-2.1195405584,-0.0000001986,0.1621651018	C,0.0035828382,0.7198483072,0.	C,-0.1492073997,0.9316288523,0.
H,-2.361050909,-0.0000002114,1.2231188677	H,2.6488896398,-0.7994534,0.9427057314	H,-0.1545303505,1.5836123156,0.8830063216
H,-2.9249692343,-0.0000002415,-0.5654237357	H,0.0714074038,1.8082009976,0.	H,-2.976740645,-1.4798292609,0.
H,2.0870067458,-1.5978784555,0.0638364859	H,-3.3525704609,-0.7569363553,0.	H,2.9724715782,-0.8670270551,0.
H,2.0870065756,1.5978785063,0.0638364859	H,2.6488896398,-0.7994534,-0.9427057314	H,-0.1545303505,1.5836123156,-0.8830063216

C_4H_4N family

Table S10-Frequencies (unscaled) and intensities for C_4H_4N isomers. Corresponding structures Fig. S8.

H1		H2		H3		H4		H5		H6	
freq	IR int.	freq	IR int.	freq	IR int.	freq	IR int.	freq	IR int.	freq	IR int.
cm^{-1}	km/mol	cm^{-1}	km/mol	cm^{-1}	km/mol	cm^{-1}	km/mol	cm^{-1}	km/mol	cm^{-1}	km/mol
161	1	159	4	496	0	203	4	163	1	153	3
181	6	238	2	543	20	291	1	169	4	238	1
405	0	407	1	663	5	397	0	365	1	342	0
469	4	478	0	715	68	533	10	388	0	416	1
573	9	550	19	831	0	541	0	537	2	548	20
574	0	661	0	850	0	600	1	564	11	657	4
765	4	733	17	882	11	650	9	745	3	717	11
883	46	890	34	926	0	787	3	861	47	869	36
927	0	940	1	936	0	803	0	933	2	964	2
1009	24	1001	8	1044	2	832	66	997	26	987	9
1087	4	1040	1	1080	6	987	1	1127	8	1042	5
1206	1	1156	2	1090	40	1043	0	1201	1	1187	2
1289	3	1257	2	1203	3	1314	2	1291	3	1250	1
1332	1	1421	1	1298	0	1365	1	1349	1	1430	6
1476	11	1443	12	1360	45	1485	18	1477	15	1444	14
1537	2	1543	3	1433	24	1525	5	1535	2	1542	2
2227	5	2244	5	1559	2	2341	8	2102	99	2115	101
3147	3	3150	1	3197	15	3158	0	3148	2	3155	2
3158	1	3160	5	3201	1	3163	3	3162	0	3165	3
3170	1	3191	0	3228	5	3263	0	3180	4	3201	2
3243	4	3246	2	3247	1	3264	1	3244	4	3250	2

Table S11-Coordinates of optimized structures of C_4H_4N isomers. Corresponding structures Fig. S8.

H1	H2	H3
C,-2.2969136881,-0.3151322625,0.	C,-1.5529202545,-0.9771198619,0.	N,0.,0.,-1.2121610445
C,-0.9472999313,-0.5226781209,0.	C,-1.2808555168,0.3624494489,0.	C,1.0626587339,0.,-0.3934548236
N,2.5240141373,0.1035874444,0.	N,2.1636464449,-0.432502502,0.	C,-1.0626587339,0.,-0.3934548236
C,1.3782429409,0.2807828772,0.	C,1.1829878633,0.1835528079,0.	C,0.6786467456,0.,1.0109682453
C,-0.0031003595,0.5104837194,0.	C,-0.0027083762,0.9356595818,0.	C,-0.6786467456,0.,1.0109682453
H,-0.3273205966,1.5436086599,0.	H,0.1078747838,2.0109288374,0.	H,-1.348559797,0.,1.8547937097
H,-2.7122927407,0.6838761508,0.	H,-0.7613972139,-1.7142105048,0.	H,1.348559797,0.,1.8547937097
H,-0.5739032845,-1.5398869729,0.	H,-2.1113564132,1.0580643471,0.	H,2.0696078206,0.,-0.7864709322
H,-2.9900854774,-1.1427554954,0.	H,-2.5713713173,-1.3353161543,0.	H,-2.0696078206,0.,-0.7864709322

Table S11 (cont.)-Coordinates of optimized structures of C_4H_4N isomers. Corresponding structures Fig. S8.

H4	H5	H6
C,0.0000027833,0.4438592832,0.	C,-2.3662014194,-0.0023698663,0.	C,-1.6532285612,-0.8775682177,0.
C,0.0000071383,1.0908530445,1.2265986758	C,-1.0566254042,-0.3901848458,0.	C,-1.2806379773,0.437457377,0.
C,0.0000071383,1.0908530445,-1.2265986758	C,2.4312726208,-0.2471734512,0.	C,2.0468402608,-0.6142936138,0.
C,-0.0000096774,-0.9985115213,0.	N,1.3034027281,0.0863357017,0.	N,1.1106048973,0.0957992736,0.
N,-0.0000189581,-2.1496198726,0.	C,0.0149910967,0.503712092,0.	C,0.0306521654,0.9172921444,0.
H,0.0000018195,0.5396051101,-2.1534232055	H,-0.1346681728,1.5751057558,0.	H,0.247542592,1.9752296429,0.
H,0.0000144666,2.1701799008,-1.2686406299	H,-0.8150409347,-1.4464960851,0.	H,-2.0489496727,1.2007673464,0.
H,0.0000018195,0.5396051101,2.1534232055	H,-3.1632933895,-0.729943135,0.	H,-2.6960803465,-1.1558364848,0.
H,0.0000144666,2.1701799008,1.2686406299	H,-2.645409023,1.042817367,0.	H,-0.9209663438,-1.6726222779,0.

Singlet C_4H_3N family ($^{14}N/^{15}N$ comparison)

Table S12-Frequencies in cm^{-1} (scaled by 0.96) for singlet $C_4H_3{}^{14}N$ isomers. Numbering according Custer et al 2016[21]. Reprinted (adapted) with permission from [21]. Copyright (2016) American Chemical Society.

1	2	3	4	5	6	7	8	9	10	11	12	13	14	15	16	17	18
2966.8	3069.4	3329.1	3342.0	3332.2	3061.8	3141.6	3176.3	2963.3	3328.6	3478.0	3337.6	3166.1	3324.2	3328.0	3150.7	3329.5	3329.9
2966.8	3015.4	2934.3	3080.3	3329.0	3034.5	3008.5	3129.3	2963.3	2944.0	3394.6	3102.9	3121.6	3050.7	3098.7	2993.7	3066.8	3038.7
2908.9	2998.5	2907.6	3007.9	3022.0	2992.4	2938.6	2972.5	2907.3	2916.9	3331.7	3024.3	2995.7	2965.7	3001.6	2926.9	3011.7	2978.6
2294.7	2241.0	2271.2	2161.6	2115.8	2109.8	2232.6	2240.6	2284.8	2150.4	2242.7	2130.3	2115.3	2122.5	2060.5	2096.2	2123.4	2103.1
2170.5	1959.1	2150.3	1933.4	2030.3	1966.1	1742.4	1671.5	2059.7	2138.7	2078.9	2038.5	1655.3	1707.1	1953.2	1757.1	1682.8	1916.2
1410.2	1405.0	1392.9	1448.3	1343.8	1414.2	1461.5	1314.4	1414.9	1415.2	1572.3	1396.3	1324.6	1449.8	1449.9	1463.1	1311.5	1379.8
1410.2	1295.8	1287.8	1312.5	1109.2	1314.2	1114.7	1091.8	1414.9	1321.1	1258.9	1236.0	1112.1	1210.5	1299.1	1139.7	1197.1	1178.1
1357.3	1091.6	1196.8	949.4	951.3	1116.4	1056.0	1007.3	1359.9	1228.7	1129.6	942.1	1013.9	1067.2	1091.5	1060.4	1009.7	956.6
1131.3	959.4	952.2	940.8	924.9	969.2	1036.5	970.0	1165.1	954.6	691.2	836.6	993.2	1001.1	806.8	1040.2	962.6	865.2
1007.5	912.4	901.3	757.2	818.2	929.4	972.4	924.4	1009.8	945.2	647.5	703.1	907.0	953.6	724.5	974.7	904.2	812.3
1007.5	862.3	863.5	732.4	674.8	880.4	971.4	869.3	1009.8	876.1	550.7	639.9	877.9	838.1	706.5	968.6	765.3	683.0
645.9	839.8	679.4	694.9	610.9	838.1	910.2	827.4	667.3	691.1	511.6	591.6	846.8	688.2	628.3	906.0	676.0	625.8
524.5	622.9	663.8	560.7	607.4	614.0	750.2	790.2	450.6	657.3	475.3	563.1	827.9	642.2	513.4	731.4	670.8	590.2
524.5	588.9	553.5	471.0	568.1	582.2	620.3	620.4	450.6	531.4	459.0	540.7	632.8	630.3	477.5	632.9	620.0	561.1
348.5	365.7	349.3	409.5	423.8	317.4	521.0	551.2	304.9	305.6	403.9	421.7	480.3	504.0	415.8	458.3	529.4	422.8
348.5	361.6	339.9	366.4	369.6	291.6	484.0	536.5	304.9	274.2	323.0	369.0	479.5	499.3	297.2	398.7	500.9	333.0
141.4	300.9	303.8	136.6	334.9	260.6	202.0	220.3	148.1	242.7	149.1	282.9	196.5	206.8	233.6	194.5	221.4	325.7
141.4	138.5	135.3	122.8	135.7	135.8	194.5	210.3	148.1	129.7	138.2	130.4	181.0	189.8	129.3	182.0	197.4	141.7

Table S12 (cont.)-Frequencies in cm^{-1} (scaled by 0.96) for singlet $C_4H_3{}^{14}N$ isomers. Numbering according to Fig. 1 and Custer et al 2016[21]. Reprinted (adapted) with permission from [21]. Copyright (2016) American Chemical Society.

19	20	21	22	23	24	25	26	27	28	29	30	31	32	33	34	35	36
3108.0	3098.8	3056.8	3434.5	2978.0	3073.9	3001.3	2971.2	3243.0	3107.7	2943.4	3163.6	3060.7	3099.6	3050.8	3107.7	3318.5	3200.1
3012.6	3016.8	3043.4	3340.3	2978.0	3001.3	2995.5	2956.7	3167.2	3027.0	2916.9	3096.6	2961.9	3048.2	2935.3	3016.7	3108.5	3161.7
2963.8	3006.7	2978.7	3337.8	2912.5	2955.4	2922.1	2926.2	3121.7	3018.8	2887.7	3073.2	2899.2	2939.8	2900.6	2971.5	2916.8	3096.8
2054.8	2055.1	2036.2	2164.5	2289.8	2134.2	2243.0	2266.1	2062.7	1671.8	2273.7	1449.3	2210.7	1706.2	2210.5	1918.2	1690.3	1561.1
1535.6	1503.3	1616.5	2147.7	1962.9	1860.9	1649.0	1684.8	1628.9	1596.5	1723.5	1336.7	1477.2	1609.4	1473.4	1561.1	1604.9	1374.4
1387.5	1388.5	1465.5	1420.1	1426.4	1457.7	1418.0	1404.6	1370.9	1384.1	1403.1	1264.7	1287.0	1448.5	1379.9	1378.1	1352.6	1298.9
1274.1	1281.8	1341.3	1160.7	1426.4	1337.6	1415.6	1279.5	1109.9	1304.8	1294.7	1178.7	1220.4	1230.6	1151.5	1270.1	1245.3	1184.1
1223.8	1264.1	1070.9	937.0	1398.2	971.9	1341.4	1200.6	991.4	1261.1	1197.4	1151.0	1101.9	1151.6	1053.8	1175.5	1169.4	1122.3
1042.8	1023.4	997.3	693.1	1146.3	860.3	1045.1	1021.0	939.0	1080.5	991.8	1031.4	1004.4	1073.2	970.0	1061.3	1088.9	1106.9
1028.6	969.4	869.7	691.7	1095.8	793.0	997.8	942.7	816.8	998.9	910.5	1001.5	925.7	984.4	891.7	1028.0	1057.2	1005.1
962.7	937.7	806.2	594.3	1095.8	765.7	993.3	879.0	800.2	979.9	897.1	930.1	834.7	934.0	853.3	968.7	919.2	920.7
837.4	829.9	774.4	492.3	686.1	753.7	717.6	803.8	755.8	977.5	805.4	841.8	774.7	838.6	759.2	875.8	890.2	783.2
645.2	664.5	624.1	482.1	509.7	474.8	528.2	631.9	690.0	707.8	532.0	804.3	653.0	747.9	631.1	634.0	772.0	697.0
564.6	528.1	608.9	413.3	509.7	432.8	509.6	495.3	585.8	707.6	528.4	709.3	561.4	706.6	504.5	542.2	746.8	667.3
417.6	421.6	508.2	397.5	164.4	398.1	277.3	357.4	553.4	500.0	348.7	602.4	489.6	521.9	481.3	405.0	551.7	639.1
322.2	320.6	352.7	335.7	164.4	314.5	204.1	209.8	306.1	359.0	247.4	554.7	308.0	365.1	307.1	266.3	296.1	632.3
171.0	218.0	210.3	218.2	41.6	155.0	189.5	155.9	231.0	200.8	130.0	515.8	184.8	190.9	176.5	186.9	213.5	629.0
55.7	137.7	189.2	139.2	41.6	121.0	142.9	98.3	189.3	97.9	118.5	418.4	103.9	179.7	121.1	83.3	66.7	99.8

Table S12 (cont.)-Frequencies in cm^{-1} (scaled by 0.96) for singlet $C_4H_3{}^{14}N$ isomers. Numbering according to Fig. 1 and Custer et al 2016[21]. Reprinted (adapted) with permission from [21]. Copyright (2016) American Chemical Society.

37	38	39	40	41	42	43	44	45	46	47	48	49	50	51	52	53	54
3099.7	3322.4	2965.7	3322.3	3377.3	3386.2	3039.4	3317.9	3040.0	3369.8	3466.1	2983.0	3436.4	2991.4	3366.7	3474.5	3008.9	3556.8
3037.0	3129.7	2965.7	3055.6	3109.6	3111.7	2998.4	3000.1	2967.2	3329.8	2997.6	2974.3	3139.6	2982.0	3046.7	3126.6	2995.7	3441.0
3013.4	2971.7	2903.8	2844.5	3024.4	3022.5	2969.3	2951.8	2929.8	3024.8	2931.7	2935.2	3134.7	2911.9	2981.2	3075.6	2944.5	3058.0
1908.7	1735.9	2270.2	2031.3	2035.4	2030.3	2245.7	1950.3	1969.4	2119.3	2066.5	2132.1	1737.7	2105.4	2017.0	1651.5	1742.7	1636.6
1531.1	1375.6	1970.6	1702.5	1613.1	1619.9	1330.4	1588.9	1722.2	1536.0	1523.4	1675.9	1426.9	1647.7	1508.0	1397.3	1370.3	1554.8
1379.7	1253.0	1402.8	1332.9	1282.7	1282.0	1289.6	1367.7	1467.6	1307.8	1392.1	1426.8	1341.1	1409.6	1406.9	1347.6	1309.5	1274.9
1273.2	1163.2	1402.8	1125.7	1111.8	1117.3	1162.5	1306.6	1362.5	1156.3	1023.7	1313.9	1325.7	1408.2	1280.2	1256.8	1183.5	1214.8
1209.6	1143.8	1352.7	1021.0	1016.4	1009.0	1037.0	1201.9	1147.9	986.7	979.4	1233.2	1190.8	1338.6	1012.0	1157.9	1152.5	1059.9
1021.7	1020.9	1126.2	960.3	926.2	917.6	991.2	1100.3	1130.5	951.6	965.2	1045.0	1180.5	1066.2	995.9	1116.1	1073.2	1019.7
978.2	950.0	996.3	832.8	872.8	859.3	902.7	1076.2	1045.0	894.7	902.3	945.6	1039.9	993.3	864.5	1021.7	1066.4	938.9
955.7	908.4	996.3	800.9	808.4	804.2	863.7	985.3	982.3	680.0	825.5	903.2	964.4	977.1	801.4	993.0	889.0	773.8
871.9	837.1	684.2	649.4	684.7	677.3	718.6	925.3	902.8	674.2	693.5	819.3	883.5	742.6	658.5	859.3	866.0	674.6
673.6	776.2	476.1	576.4	584.5	582.8	691.7	696.7	711.0	604.8	618.0	648.1	709.0	479.8	624.8	811.1	789.4	656.0
493.2	693.0	476.1	516.2	579.5	562.1	603.9	529.3	487.7	549.0	568.0	427.0	665.8	435.6	501.4	732.3	691.0	549.4
369.4	651.5	229.7	426.0	456.7	464.5	449.1	404.3	331.7	522.2	500.8	262.3	603.7	262.8	404.2	601.7	569.7	508.5
310.6	494.3	229.7	236.8	288.8	266.6	436.4	251.4	228.1	428.6	348.6	192.8	529.9	210.9	289.4	542.5	566.3	376.3
203.9	409.0	116.9	143.1	202.2	194.0	192.0	150.2	180.0	220.5	168.9	154.5	454.0	196.4	205.6	437.5	544.8	284.7
146.1	273.6	116.9	133.3	129.5	134.4	177.6	112.6	89.3	194.8	158.4	102.1	445.1	153.6	190.8	256.5	346.8	279.7

Table S13-Frequencies in cm^{-1} (scaled by 0.96) for singlet $C_4H_3{}^{15}N$ isomers. Numbering according to Fig. 1 and Custer et al 2016[21].

1	2	3	4	5	6	7	8	9	10	11	12	13	14	15	16	17	18
2966.8	3069.4	3329.1	3334.4	3332.0	3061.8	3141.6	3176.3	2963.3	3328.6	3467.6	3337.6	3166.1	3324.2	3328.0	3150.7	3329.5	3329.9
2966.8	3015.4	2934.3	3080.3	3321.6	3034.5	3008.5	3129.3	2963.3	2944.0	3390.4	3102.9	3121.6	3050.7	3098.7	2993.7	3066.7	3038.7
2908.9	2998.5	2907.6	3007.9	3022.0	2992.4	2938.6	2972.5	2907.3	2916.8	3331.7	3024.3	2995.7	2965.7	3001.6	2926.9	3011.7	2978.4
2286.8	2212.9	2242.1	2158.9	2115.6	2071.4	2206.1	2211.7	2279.7	2149.4	2241.8	2128.4	2077.9	2122.4	2060.4	2057.7	2123.4	2102.6
2151.5	1959.1	2150.3	1925.3	2017.2	1966.1	1740.3	1671.4	2024.9	2101.3	2078.5	2023.7	1655.2	1689.0	1915.3	1756.9	1658.0	1876.4
1410.2	1404.7	1392.9	1442.2	1337.8	1414.1	1461.4	1314.4	1414.9	1415.2	1567.2	1389.7	1324.0	1449.4	1449.3	1463.1	1310.9	1379.3
1410.2	1295.4	1287.6	1308.5	1103.5	1313.7	1114.2	1091.1	1414.9	1320.7	1248.6	1220.1	1112.0	1205.3	1295.5	1139.3	1196.8	1177.0
1357.2	1090.2	1196.8	949.4	945.7	1115.6	1056.0	1007.3	1359.9	1227.3	1124.5	941.9	1013.9	1066.7	1088.2	1060.4	1007.1	955.5
1126.0	959.4	949.7	935.1	923.0	969.2	1036.5	970.0	1163.6	953.3	682.5	827.2	993.1	1000.6	805.2	1040.1	961.8	865.1
1007.5	907.5	901.2	757.2	816.0	926.4	971.4	921.9	1009.8	944.0	647.5	703.1	906.4	951.5	724.5	974.0	903.4	810.1
1007.5	862.3	859.7	724.4	674.8	880.4	971.1	866.6	1009.8	873.8	550.7	639.7	875.0	830.3	706.3	968.5	765.0	683.0
639.5	839.8	679.4	692.8	610.5	838.1	907.3	827.4	663.1	691.1	511.5	586.4	846.7	688.2	627.6	904.4	675.3	624.7
523.2	622.2	663.8	559.4	604.9	611.2	750.1	790.1	446.4	657.3	473.5	560.5	827.6	641.7	506.1	730.8	665.1	583.6
523.2	585.8	551.0	471.0	568.1	577.2	615.7	619.0	446.4	526.0	456.4	540.2	631.4	622.1	476.4	629.2	620.0	561.0
347.7	364.3	347.0	408.2	422.6	316.0	519.2	550.1	301.5	305.4	403.6	421.5	474.0	503.9	412.8	451.5	529.3	415.1
347.7	360.3	338.5	366.1	368.7	287.0	482.5	534.4	301.5	270.2	322.8	368.7	472.6	497.4	293.9	393.8	494.3	332.7
140.1	299.9	303.6	135.6	334.5	257.1	200.5	218.4	147.9	238.1	148.2	282.7	194.8	206.4	231.6	192.7	219.8	321.8
140.1	136.9	133.6	122.1	134.4	135.5	192.6	207.7	147.9	129.4	137.5	129.1	179.2	189.0	129.1	180.6	196.5	141.5

Table S13 (cont.)-Frequencies in cm^{-1} (scaled by 0.96) for singlet $C_4H_3{}^{15}N$ isomers. Numbering according to Fig. 1 and Custer et al 2016[21].

19	20	21	22	23	24	25	26	27	28	29	30	31	32	33	34	35	36
3108.0	3098.8	3056.7	3427.0	2978.0	3073.9	3001.3	2971.2	3235.8	3107.7	2943.4	3163.6	3060.7	3099.6	3050.8	3107.7	3311.1	3200.1
3012.6	3016.8	3043.4	3340.2	2978.0	3001.2	2995.5	2956.7	3167.2	3027.0	2916.9	3096.6	2961.9	3048.2	2935.3	3016.7	3108.5	3161.7
2963.8	3006.7	2978.7	3337.8	2912.4	2955.3	2922.1	2926.2	3121.7	3018.8	2887.7	3073.2	2899.2	2939.8	2900.6	2971.5	2916.8	3096.8
2028.7	2029.1	2035.7	2163.8	2265.8	2124.2	2215.3	2237.0	2055.3	1660.7	2244.6	1440.4	2183.0	1688.1	2182.8	1884.1	1690.1	1559.5
1535.6	1503.3	1598.9	2145.0	1953.6	1831.8	1648.3	1684.8	1626.6	1595.3	1723.5	1335.0	1476.8	1600.2	1473.1	1560.9	1588.0	1373.0
1387.3	1388.1	1460.8	1409.1	1426.2	1456.1	1418.0	1404.6	1360.8	1383.9	1403.1	1262.5	1286.7	1442.8	1379.4	1378.0	1342.8	1295.3
1273.8	1280.1	1339.7	1141.8	1426.2	1337.5	1415.5	1279.4	1103.8	1296.4	1294.5	1177.6	1220.4	1230.2	1150.9	1270.1	1245.0	1176.1
1221.6	1263.9	1068.8	920.8	1398.2	971.9	1341.3	1200.6	991.4	1258.3	1197.3	1143.0	1101.6	1148.6	1053.5	1174.9	1168.1	1115.5
1041.4	1022.3	997.3	693.1	1134.0	858.5	1041.1	1020.9	937.8	1074.3	989.3	1027.7	1002.3	1070.9	969.4	1059.6	1087.6	1100.4
1028.6	969.3	869.7	691.7	1094.0	793.0	997.8	939.4	816.6	998.9	910.4	1000.4	922.3	983.8	886.4	1028.0	1055.0	1003.7
962.7	937.4	806.0	593.4	1094.0	765.7	993.3	877.0	800.2	977.5	896.7	923.0	833.8	933.2	853.2	968.7	919.1	915.1
834.0	825.0	772.8	491.0	685.6	749.9	712.5	802.2	753.3	974.7	800.8	838.7	774.7	838.2	758.7	874.0	890.1	783.2
644.6	663.4	618.3	482.1	508.3	467.3	527.0	630.9	683.2	707.3	530.2	801.6	652.7	740.3	629.1	633.6	771.9	696.7
562.2	526.5	607.5	411.2	508.3	432.8	508.4	493.7	585.8	703.9	528.3	708.2	558.7	701.8	503.3	533.3	746.8	666.5
416.1	420.5	502.4	397.5	163.5	389.9	276.0	355.0	552.5	495.1	346.3	599.9	488.5	519.7	480.9	402.0	546.9	638.2
320.3	320.4	352.6	335.7	163.5	313.0	203.6	207.9	305.1	358.8	245.7	553.1	305.9	363.1	305.0	260.6	295.8	623.6
169.2	216.4	210.1	217.0	40.9	154.7	187.8	155.5	230.1	200.3	129.9	512.2	182.6	189.4	174.3	186.3	211.4	622.0
55.4	136.0	188.2	138.5	40.9	121.0	142.2	97.8	187.9	96.8	117.4	415.6	103.5	178.4	120.8	83.3	66.2	99.5

Table S13 (cont.)-Frequencies in cm^{-1} (scaled by 0.96) for singlet $C_4H_3{}^{15}N$ isomers. Numbering according to Fig. 1 and Custer et al 2016[21].

37	38	39	40	41	42	43	44	45	46	47	48	49	50	51	52	53	54
3099.7	3315.1	2965.7	3314.7	3369.3	3378.2	3039.4	3310.5	3040.0	3361.5	3457.4	2983.0	3428.2	2991.4	3358.4	3466.3	3008.9	3545.6
3037.0	3129.7	2965.7	3055.6	3109.6	3111.7	2998.4	3000.1	2967.2	3329.8	2997.6	2974.3	3139.6	2982.0	3046.7	3126.6	2995.7	3436.7
3013.4	2971.6	2903.8	2844.5	3024.4	3022.5	2969.3	2951.8	2929.8	3024.8	2931.7	2935.2	3134.7	2911.9	2981.2	3075.6	2944.5	3058.0
1874.5	1720.1	2234.5	2018.4	2020.7	2015.5	2217.6	1950.3	1969.2	2119.3	2052.8	2093.8	1737.6	2066.7	2016.4	1651.4	1721.9	1625.4
1531.1	1375.5	1970.6	1702.4	1612.9	1619.7	1330.2	1573.4	1692.3	1515.5	1516.2	1675.9	1415.0	1647.6	1500.6	1395.2	1370.2	1553.7
1379.7	1251.6	1402.8	1326.6	1277.7	1277.2	1288.8	1358.0	1464.3	1306.8	1391.7	1426.8	1334.1	1409.6	1399.2	1336.5	1308.4	1271.6
1273.2	1159.1	1402.8	1120.3	1105.4	1110.8	1162.3	1304.4	1360.9	1142.8	1022.8	1313.5	1323.0	1408.2	1270.9	1254.5	1183.5	1214.8
1208.5	1140.5	1352.7	1019.1	1016.1	1008.8	1035.2	1201.3	1146.6	986.5	978.4	1231.8	1186.4	1338.6	1004.4	1146.3	1151.7	1056.7
1021.0	1020.8	1114.2	955.5	923.4	915.1	991.1	1100.1	1127.4	951.0	965.0	1044.2	1180.5	1064.9	995.9	1113.8	1067.3	1016.2
978.2	949.1	996.3	830.7	868.3	854.9	900.1	1073.1	1044.5	892.5	899.0	944.0	1032.8	993.2	864.5	1019.7	1065.6	934.1
955.2	906.2	996.3	799.2	807.2	802.8	862.6	985.1	978.8	679.9	825.2	901.5	956.6	976.7	796.6	987.6	888.2	768.9
869.6	833.5	684.1	649.1	684.4	676.7	718.3	925.3	901.7	671.4	689.2	818.4	874.2	739.4	655.0	850.2	864.1	674.4
671.0	773.1	466.6	574.5	584.1	581.0	689.9	696.3	704.2	604.7	614.2	647.0	708.9	476.2	624.7	811.0	787.0	654.9
487.7	691.0	466.6	515.7	577.2	561.2	603.1	524.4	485.9	544.3	566.5	420.0	665.8	427.6	499.8	732.0	690.9	548.9
366.7	651.0	229.6	424.8	455.4	463.6	447.5	401.5	327.7	521.1	500.2	257.6	603.7	260.9	402.3	601.3	565.6	508.4
305.1	493.1	229.6	235.3	288.2	266.2	434.9	251.2	226.8	426.5	347.3	191.5	521.9	209.2	288.2	537.7	558.6	374.8
202.5	406.1	116.2	142.7	200.8	192.6	190.5	149.7	179.2	219.1	167.7	154.1	454.0	195.7	205.6	436.2	541.6	283.5
145.8	271.8	116.2	132.6	128.8	133.6	175.8	111.5	89.0	194.5	157.7	102.1	444.8	152.9	190.1	255.1	345.3	277.4

Table S14-^{14}N-^{15}N Frequency difference in cm^{-1} for singlet C_4H_3N isomers. Numbering according to Fig. 1 and Custer et al 2016[21].

1	2	3	4	5	6	7	8	9	10	11	12	13	14	15	16	17	18
0.0	0.0	0.0	7.6	0.2	0.0	0.0	0.0	0.0	0.0	10.4	0.0	0.0	0.0	0.0	0.0	0.0	0.0
0.0	0.0	0.0	0.0	7.4	0.0	0.0	0.0	0.0	0.0	4.2	0.0	0.0	0.0	0.0	0.0	0.1	0.0
0.0	0.0	0.0	0.0	0.0	0.0	0.0	0.0	0.0	0.1	0.0	0.0	0.0	0.0	0.0	0.0	0.0	0.2
7.9	28.1	29.1	2.7	0.2	38.4	26.5	28.9	5.1	1.0	0.9	1.9	37.4	0.1	0.1	38.5	0.0	0.5
19.0	0.0	0.0	8.1	13.1	0.0	2.1	0.1	34.8	37.4	0.4	14.8	0.1	18.1	37.9	0.2	24.8	39.8
0.0	0.3	0.0	6.1	6.0	0.1	0.1	0.0	0.0	0.0	5.1	6.6	0.6	0.4	0.6	0.0	0.6	0.5
0.0	0.4	0.2	4.0	5.7	0.5	0.5	0.7	0.0	0.4	10.3	15.9	0.1	5.2	3.6	0.4	0.3	1.1
0.1	1.4	0.0	0.0	5.5	0.8	0.0	0.0	0.0	1.4	5.1	0.2	0.0	0.5	3.3	0.0	2.6	1.0
5.3	0.0	2.5	5.7	1.9	0.0	0.0	0.0	1.5	1.4	8.7	9.5	0.0	0.5	1.7	0.1	0.8	0.2
0.0	4.9	0.1	0.0	2.1	2.9	0.9	2.5	0.0	1.2	0.0	0.0	0.6	2.1	0.0	0.7	0.8	2.2
0.0	0.0	3.8	8.0	0.0	0.0	0.3	2.7	0.0	2.3	0.0	0.2	3.0	7.8	0.2	0.0	0.3	0.0
6.3	0.0	0.0	2.0	0.5	0.0	2.9	0.0	4.2	0.0	0.0	5.2	0.0	0.0	0.6	1.6	0.7	1.1
1.4	0.6	0.0	1.3	2.4	2.8	0.1	0.1	4.2	0.0	1.7	2.5	0.3	0.5	7.3	0.6	5.7	6.7
1.4	3.1	2.6	0.0	0.0	5.0	4.7	1.4	4.2	5.4	2.6	0.5	1.4	8.2	1.1	3.7	0.0	0.0
0.8	1.4	2.3	1.3	1.2	1.4	1.8	1.1	3.4	0.2	0.3	0.2	6.4	0.2	3.0	6.8	0.1	7.7
0.8	1.3	1.4	0.2	0.9	4.5	1.5	2.1	3.4	4.0	0.3	0.3	6.9	1.9	3.3	5.0	6.6	0.4
1.2	1.0	0.2	1.0	0.4	3.5	1.5	1.9	0.3	4.6	0.8	0.1	1.8	0.5	1.9	1.8	1.6	3.9
1.2	1.6	1.6	0.7	1.4	0.4	1.9	2.6	0.3	0.3	0.7	1.3	1.9	0.8	0.2	1.4	0.9	0.3

Table S14 (cont.)-^{14}N-^{15}N Frequency difference in cm^{-1} for singlet C_4H_3N isomers. Numbering according to Fig. 1 and Custer et al 2016[21].

19	20	21	22	23	24	25	26	27	28	29	30	31	32	33	34	35	36
0.0	0.0	0.1	7.5	0.0	0.0	0.0	0.0	7.2	0.0	0.0	0.0	0.0	0.0	0.0	0.0	7.4	0.0
0.0	0.0	0.0	0.1	0.0	0.1	0.0	0.0	0.0	0.0	0.0	0.0	0.0	0.0	0.0	0.0	0.0	0.0
0.0	0.0	0.0	0.0	0.1	0.1	0.0	0.0	0.0	0.0	0.0	0.0	0.0	0.0	0.0	0.0	0.0	0.0
26.1	26.0	0.5	0.7	24.0	10.0	27.7	29.1	7.4	11.1	29.1	8.9	27.7	18.1	27.7	34.1	0.2	1.6
0.0	0.0	17.6	2.7	9.3	29.1	0.7	0.0	2.3	1.2	0.0	1.7	0.4	9.2	0.3	0.2	16.9	1.4
0.2	0.4	4.7	11.0	0.2	1.6	0.0	0.0	10.1	0.2	0.0	2.2	0.3	5.7	0.5	0.1	9.8	3.6
0.3	1.7	1.6	18.9	0.2	0.1	0.1	0.1	6.1	8.4	0.2	1.1	0.0	0.4	0.6	0.0	0.3	8.0
2.2	0.2	2.1	16.2	0.0	0.0	0.1	0.0	0.0	2.8	0.1	8.0	0.3	3.0	0.3	0.6	1.3	6.8
1.4	1.1	0.0	0.0	12.3	1.8	4.0	0.1	1.2	6.2	2.5	3.7	2.1	2.3	0.6	1.7	1.3	6.5
0.0	0.0	0.0	0.0	1.8	0.0	0.0	3.3	0.1	0.0	0.1	1.1	3.4	0.6	5.3	0.0	2.2	1.4
0.0	0.4	0.2	0.9	1.8	0.1	0.0	2.0	0.0	2.4	0.4	7.1	0.9	0.8	0.1	0.0	0.0	5.7
3.4	5.0	1.6	1.3	0.5	3.8	5.1	1.6	2.6	2.8	4.6	3.1	0.0	0.3	0.4	1.8	0.1	0.0
0.6	1.1	5.8	0.0	1.4	7.5	1.1	1.0	6.8	0.5	1.8	2.7	0.3	7.6	2.0	0.3	0.1	0.3
2.5	1.7	1.4	2.1	1.4	0.0	1.3	1.5	0.0	3.7	0.1	1.1	2.7	4.8	1.2	8.9	0.0	0.8
1.5	1.2	5.7	0.0	0.8	8.2	1.3	2.3	1.0	4.9	2.4	2.5	1.1	2.2	0.4	3.0	4.8	0.9
2.0	0.2	0.2	0.0	0.8	1.5	0.5	1.9	1.0	0.2	1.7	1.7	2.1	2.0	2.1	5.7	0.2	8.6
1.8	1.5	0.2	1.1	0.6	0.3	1.7	0.4	0.9	0.5	0.2	3.6	2.2	1.5	2.3	0.6	2.0	7.0
0.3	1.7	1.0	0.7	0.6	0.0	0.8	0.5	1.4	1.1	1.1	2.8	0.5	1.3	0.3	0.0	0.5	0.3

Table S14 (cont.)-^{14}N-^{15}N Frequency difference in cm^{-1} for singlet C_4H_3N isomers. Numbering according to Fig. 1 and Custer et al 2016[21].

37	38	39	40	41	42	43	44	45	46	47	48	49	50	51	52	53	54
0.0	7.3	0.0	7.6	8.0	8.0	0.0	7.4	0.0	8.3	8.7	0.0	8.2	0.0	8.3	8.2	0.0	11.2
0.0	0.0	0.0	0.0	0.0	0.0	0.0	0.0	0.0	0.0	0.0	0.0	0.0	0.0	0.0	0.0	0.0	4.3
0.0	0.1	0.0	0.0	0.0	0.0	0.0	0.0	0.0	0.0	0.0	0.0	0.0	0.0	0.0	0.0	0.0	0.0
34.2	15.8	35.7	12.9	14.7	14.8	28.1	0.0	0.2	0.0	13.7	38.3	0.1	38.7	0.6	0.1	20.8	11.2
0.0	0.1	0.0	0.1	0.2	0.2	0.2	15.5	29.9	20.5	7.2	0.0	11.9	0.1	7.4	2.1	0.1	1.1
0.0	1.4	0.0	6.3	5.0	4.8	0.8	9.7	3.3	1.0	0.4	0.0	7.0	0.0	7.7	11.1	1.1	3.3
0.0	4.1	0.0	5.4	6.4	6.5	0.2	2.2	1.6	13.5	0.9	0.4	2.7	0.0	9.3	2.3	0.0	0.0
1.1	3.3	0.0	1.9	0.3	0.2	1.8	0.6	1.3	0.2	1.0	1.4	4.4	0.0	7.6	11.6	0.8	3.2
0.7	0.1	12.0	4.8	2.8	2.5	0.1	0.2	3.1	0.6	0.2	0.8	0.0	1.3	0.0	2.3	5.9	3.5
0.0	0.8	0.0	2.0	4.5	4.5	2.6	3.1	0.5	2.2	3.4	1.6	7.1	0.1	0.0	2.0	0.8	4.8
0.4	2.2	0.0	1.7	1.1	1.5	1.1	0.2	3.5	0.1	0.3	1.7	7.8	0.4	4.8	5.3	0.8	4.9
2.3	3.6	0.1	0.3	0.4	0.6	0.3	0.0	1.0	2.8	4.3	0.9	9.3	3.2	3.6	9.2	1.9	0.2
2.6	3.1	9.5	1.9	0.4	1.8	1.8	0.4	6.8	0.0	3.8	1.1	0.1	3.6	0.1	0.1	2.4	1.1
5.5	2.0	9.5	0.5	2.3	0.9	0.8	4.9	1.8	4.7	1.5	7.0	0.0	8.0	1.6	0.2	0.0	0.5
2.8	0.5	0.1	1.3	1.3	0.9	1.7	2.8	4.0	1.1	0.5	4.7	0.0	1.9	1.9	0.3	4.1	0.1
5.5	1.3	0.1	1.5	0.6	0.4	1.5	0.2	1.4	2.1	1.4	1.3	8.0	1.7	1.2	4.9	7.7	1.6
1.4	2.9	0.7	0.4	1.3	1.5	1.5	0.6	0.8	1.5	1.2	0.5	0.0	0.7	0.0	1.3	3.2	1.2
0.3	1.8	0.7	0.7	0.7	0.7	1.8	1.1	0.3	0.3	0.7	0.1	0.3	0.6	0.7	1.4	1.6	2.3

Table S15-IR Intensities in km/mol for singlet $C_4H_3{}^{14}N$ isomers. Numbering according to Fig. 1 and Custer et al 2016[21]. Reprinted (adapted) with permission from [21]. Copyright (2016) American Chemical Society.

1	**2**	**3**	**4**	**5**	**6**	**7**	**8**	**9**	**10**	**11**	**12**	**13**	**14**	**15**	**16**	**17**	**18**
1	1	70	45	73	0	4	2	3	67	48	112	2	84	118	6	74	104
1	2	0	0	49	4	20	7	3	0	38	2	4	16	1	27	2	5
6	1	1	5	10	0	49	15	12	5	119	11	16	30	1	58	8	3
135	24	5	1444	19	193	37	18	1	18	321	102	161	3	36	173	5	13
0	92	1	20	588	17	21	26	134	170	0	607	30	13	271	12	31	427
10	4	9	100	8	15	4	4	9	8	25	4	25	5	23	6	3	10
10	1	12	16	6	18	1	4	9	46	70	3	9	8	16	3	17	9
0	0	0	0	268	4	1	0	2	1	0	1	0	1	4	1	13	13
0	0	5	435	67	0	21	46	3	29	6	9	37	30	22	26	20	31
2	8	0	66	62	26	4	7	1	2	40	82	11	1	27	18	20	640
2	46	7	0	38	40	0	11	1	19	54	40	44	6	72	0	19	34
0	23	38	59	18	21	18	0	0	35	2	0	0	34	7	5	51	9
4	3	44	1	7	0	23	2	0	45	76	10	9	49	24	36	3	15
4	4	2	0	58	10	4	67	0	7	159	58	63	1	62	5	46	56
7	7	4	17	18	7	7	4	5	11	38	2	0	5	13	5	9	23
7	6	9	0	6	2	22	18	5	4	1	1	16	11	0	10	6	24
0	2	9	1	32	1	0	2	0	0	10	0	1	1	1	0	11	6
0	3	4	4	1	2	3	4	0	3	12	4	2	5	12	2	2	1

Table S15 (cont.)-IR intensities in km/mol for singlet $C_4H_3{}^{14}N$ isomers. Numbering according to Fig. 1 and Custer et al 2016[21]. Reprinted (adapted) with permission from [21]. Copyright (2016) American Chemical Society.

19	**20**	**21**	**22**	**23**	**24**	**25**	**26**	**27**	**28**	**29**	**30**	**31**	**32**	**33**	**34**	**35**	**36**
1	1	5	66	3	0	2	4	2	1	0	3	3	0	3	1	6	13
7	8	5	35	3	0	1	24	3	9	2	1	8	9	5	8	1	1
25	0	12	211	21	7	4	2	7	2	27	1	20	21	19	20	26	3
19	11	0	15	1763	510	24	4	194	71	3	93	4	5	4	237	21	12
60	22	38	351	236	83	46	87	98	2	69	9	22	8	17	74	53	1
92	34	2	23	11	93	9	10	37	15	6	44	1	3	4	96	25	6
4	9	0	51	11	21	11	11	178	11	8	9	13	12	3	2	36	7
65	1	50	0	58	0	1	5	21	4	1	13	4	19	1	131	23	1
1	11	1	51	5	722	2	1	1	60	5	13	24	11	8	4	5	0
23	18	46	16	0	58	12	6	3	19	2	12	29	26	13	20	8	7
27	23	8	15	0	20	1	8	7	11	1	70	67	3	133	24	23	16
5	5	22	112	17	35	2	7	54	31	0	5	272	22	235	5	38	3
11	6	28	0	12	1	3	19	0	1	3	8	176	7	3	0	28	5
6	5	2	29	12	2	3	7	58	19	23	46	1	3	95	1	28	46
5	69	19	0	7	11	6	0	4	1	0	25	16	5	66	2	2	55
22	8	0	6	7	1	1	2	3	3	19	58	7	8	3	13	13	129
3	8	9	89	1	2	2	30	13	2	2	46	13	7	3	2	17	2
2	2	6	1	1	3	11	17	1	0	8	102	12	13	15	0	52	14

Table S15 (cont.)-IR intensities for singlet $C_4H_3{}^{14}N$ isomers. Numbering according to Fig. 1 and Custer et al 2016[21]. Reprinted (adapted) with permission from [21]. Copyright (2016) American Chemical Society.

37	**38**	**39**	**40**	**41**	**42**	**43**	**44**	**45**	**46**	**47**	**48**	**49**	**50**	**51**	**52**	**53**	**54**
2	7	0	26	79	86	6	14	6	40	228	12	17	2	68	39	0	64
4	2	0	10	7	7	7	1	5	81	6	14	5	2	4	6	10	78
1	12	3	28	8	8	14	11	22	8	11	5	1	2	9	5	3	1
174	196	449	571	651	658	40	580	708	13	1479	203	0	142	13	52	339	404
25	5	588	22	15	19	37	4	151	53	147	107	6	17	50	12	1	3
39	38	11	5	3	4	9	10	24	5	4	6	8	10	22	6	26	5
5	34	11	2	3	1	17	13	54	7	16	41	33	17	23	2	6	27
41	64	11	13	8	12	13	22	12	21	47	12	8	1	23	15	36	11
10	5	25	323	32	26	18	4	112	17	4	2	6	4	1	8	58	3
15	35	3	62	341	306	23	4	20	7	25	40	37	2	47	22	1	39
40	10	3	1	63	56	8	27	52	35	22	19	38	15	72	21	6	30
4	72	2	9	79	46	52	2	33	35	546	7	0	0	8	0	14	11
3	51	2	4	8	18	20	83	10	48	47	21	65	0	14	6	3	23
2	37	2	42	65	64	12	3	14	23	5	10	0	8	5	87	10	13
11	21	1	27	11	51	1	32	48	35	98	1	55	2	30	119	23	3
38	41	1	10	19	27	10	2	24	41	108	4	46	2	16	49	15	7
5	27	1	10	16	10	9	12	6	14	5	22	0	2	12	145	9	23
2	3	1	18	35	22	7	24	24	2	4	15	170	10	7	45	2	185

Table S16-IR intensities for singlet $C_4H_3{}^{15}N$ isomers. Numbering according to Fig. 1 and Custer et al 2016[21].

1	**2**	**3**	**4**	**5**	**6**	**7**	**8**	**9**	**10**	**11**	**12**	**13**	**14**	**15**	**16**	**17**	**18**
1	1	70	42	89	0	4	2	3	67	48	112	2	84	118	6	74	104
1	2	0	0	31	4	20	7	3	0	36	2	4	16	1	27	2	5
6	1	1	5	10	0	49	15	12	5	119	12	16	30	1	58	8	3
133	23	5	1419	22	184	37	17	0	1	318	82	152	3	34	164	5	16
1	92	1	22	568	16	21	26	129	178	0	615	30	12	257	12	30	404
10	4	9	96	8	15	4	4	9	8	22	4	25	5	24	6	3	10
10	1	12	18	5	18	1	4	9	46	69	4	9	8	18	3	17	8
0	0	0	0	268	4	1	0	2	1	0	1	0	1	4	1	13	13
1	0	5	436	68	0	21	46	3	29	6	8	37	30	23	26	20	32
2	9	0	66	61	27	0	6	1	2	40	82	10	1	27	18	20	641
2	46	7	0	38	40	5	12	1	19	54	40	46	5	72	0	19	34
0	23	38	59	21	21	18	0	0	35	2	0	0	34	7	5	46	9
4	3	44	2	4	0	23	2	0	45	50	11	9	47	23	37	7	15
4	4	2	0	58	9	4	68	0	7	185	57	64	2	64	5	46	56
7	7	4	17	17	7	7	4	5	11	36	2	0	5	11	5	9	21
7	6	9	0	6	2	22	16	5	4	1	1	15	11	0	10	6	25
0	2	9	1	33	1	0	1	0	0	10	0	1	1	1	0	11	5
0	3	3	4	1	2	3	4	0	3	11	4	2	5	12	2	2	1

Table S16 (cont.)-IR intensities for singlet $C_4H_3{}^{15}N$ isomers. Numbering according to Fig. 1 and Custer et al 2016[21].

19	20	21	22	23	24	25	26	27	28	29	30	31	32	33	34	35	36
1	1	5	65	3	0	2	4	2	1	0	3	3	0	3	1	6	13
7	8	5	36	3	0	1	24	3	9	2	1	8	9	5	8	1	1
24	0	12	211	21	7	4	2	7	2	27	1	20	21	19	20	26	3
20	11	0	15	1789	471	24	3	183	72	3	85	4	6	3	221	20	13
60	22	37	345	185	97	46	87	95	2	69	9	22	7	17	75	50	1
92	34	1	19	11	97	9	10	36	15	6	45	1	4	4	96	25	5
4	9	0	53	11	21	11	11	180	10	8	9	13	12	3	2	36	7
64	1	49	0	58	0	1	5	21	6	1	14	4	17	1	132	24	1
0	11	1	51	5	723	2	1	2	56	5	11	25	11	9	5	5	1
23	18	46	16	0	57	12	6	3	19	2	11	29	26	13	20	8	7
27	22	8	15	0	20	1	9	7	31	1	70	66	3	134	24	23	14
5	5	22	116	17	35	2	7	53	12	0	6	272	22	234	5	38	3
11	6	25	0	12	1	3	19	0	19	3	8	176	7	3	0	28	6
6	5	1	25	12	2	2	7	58	1	23	47	1	2	99	1	28	50
4	69	20	0	7	10	6	0	4	1	0	25	16	5	61	2	2	47
22	8	0	6	7	1	1	2	3	3	18	57	7	8	3	12	13	5
3	8	9	89	1	2	2	29	13	2	2	45	12	7	3	2	16	126
2	2	6	1	1	3	11	17	1	0	8	101	12	12	15	0	51	14

Table S16 (cont.)-IR intensities for singlet $C_4H_3{}^{15}N$ isomers. Numbering according to Fig. 1 and Custer et al 2016[21].

37	**38**	**39**	**40**	**41**	**42**	**43**	**44**	**45**	**46**	**47**	**48**	**49**	**50**	**51**	**52**	**53**	**54**
2	7	0	25	76	83	6	13	6	39	219	11	16	2	65	40	0	64
4	2	0	10	7	7	7	1	5	81	6	14	5	2	4	6	10	74
1	12	3	28	8	8	14	11	22	8	11	5	1	2	9	5	3	1
164	188	424	554	637	644	39	580	714	13	1471	193	0	136	13	52	337	397
25	5	591	22	15	19	37	3	139	51	138	107	6	17	44	12	1	1
39	35	11	5	3	4	9	9	27	5	4	6	11	10	23	7	26	6
5	24	11	2	3	1	17	14	50	7	17	41	32	17	23	1	6	28
42	80	11	11	8	12	13	23	5	21	45	12	8	1	21	13	37	11
11	5	27	327	27	22	18	4	111	17	4	2	6	5	1	9	55	3
15	35	3	61	347	308	23	4	20	7	29	40	34	2	47	23	1	43
40	10	3	1	63	57	9	27	52	35	20	20	38	15	73	21	6	29
4	71	2	9	79	46	51	2	34	34	537	7	0	0	7	0	13	12
3	54	2	4	12	17	19	82	9	48	48	21	65	0	14	6	4	21
2	34	2	42	61	65	12	3	14	24	6	10	0	8	5	87	10	13
11	21	1	27	11	50	1	32	47	34	98	1	54	2	29	117	12	3
38	41	1	10	19	28	10	2	24	42	108	5	46	2	17	51	24	7
4	27	1	10	16	10	9	12	7	13	5	22	0	2	12	143	9	43
2	3	1	18	34	22	6	24	23	2	4	15	170	10	7	44	2	164

Table S17- ^{14}N-^{15}N IR intensity difference in km/mol for singlet C_4H_3N isomers. Numbering according to Fig. 1 and Custer et al 2016[21].

1	2	3	4	5	6	7	8	9	10	11	12	13	14	15	16	17	18
0	0	0	3	-17	0	0	0	0	0	0	0	0	0	0	0	0	0
0	0	0	0	18	0	0	0	0	0	2	0	0	0	0	0	0	0
0	0	0	0	0	0	0	0	0	0	0	0	0	0	0	0	0	0
2	1	0	25	-3	9	0	1	1	17	3	21	9	0	2	8	0	-4
-1	0	0	-3	20	1	1	0	5	-8	0	-8	0	1	14	0	1	23
0	0	0	4	0	0	0	0	0	0	2	1	0	0	-1	0	0	0
0	0	0	-2	1	0	0	0	0	0	2	-1	0	0	-2	0	0	0
0	0	0	0	-1	0	0	0	0	0	0	0	0	0	0	0	0	0
0	0	0	-1	-1	0	0	0	0	0	0	1	0	0	-1	0	0	0
0	0	0	0	1	-1	4	0	0	0	0	0	1	0	0	0	0	-1
0	0	0	0	0	0	-5	-1	0	-1	0	0	-2	0	0	0	0	0
0	0	0	1	-3	0	0	0	0	0	0	0	0	0	0	0	4	0
0	0	0	0	3	0	0	0	0	0	26	-1	0	2	1	0	-5	0
0	0	0	0	0	0	0	-1	0	0	-26	1	0	-1	-3	0	0	0
0	0	0	0	0	0	0	0	0	0	2	0	0	0	2	0	0	2
0	0	0	0	0	0	0	1	0	0	0	0	1	0	0	0	0	-1
0	0	0	0	0	0	0	0	0	0	0	0	0	0	0	0	0	1
0	0	0	0	0	0	0	0	0	0	0	0	0	0	0	0	0	0

Table S17 (cont.)- ^{14}N-^{15}N IR intensity difference in km/mol for singlet C_4H_3N isomers. Numbering according to Fig. 1 and Custer et al 2016[21].

19	20	21	22	23	24	25	26	27	28	29	30	31	32	33	34	35	36
0	0	0	1	0	0	0	0	0	0	0	0	0	0	0	0	0	0
0	0	0	-1	0	0	0	0	0	0	0	0	0	0	0	0	0	0
0	0	0	0	-1	0	0	0	0	0	0	0	0	0	0	0	0	0
-1	0	0	0	-26	39	0	0	11	0	0	8	0	-1	0	16	1	0
0	0	2	6	50	-14	0	0	3	0	0	0	0	1	0	-1	3	0
1	0	0	4	0	-3	0	0	1	0	0	-1	0	0	0	0	-1	1
-1	0	0	-2	0	0	0	0	-2	1	0	0	0	0	0	0	0	0
1	0	1	0	0	0	0	0	0	-1	0	-1	0	1	0	-1	-1	-1
0	0	0	0	-1	0	0	0	0	4	0	2	-1	0	0	-1	0	0
0	0	0	0	0	0	0	0	0	0	0	1	0	0	0	0	0	0
0	0	0	0	0	0	0	-1	0	-20	0	-1	1	0	-1	0	0	3
0	0	0	-4	0	0	0	0	1	18	0	-1	0	0	1	0	0	0
0	0	3	0	0	0	0	0	0	-18	0	0	-1	0	0	0	0	-1
0	0	0	3	0	0	0	0	0	18	0	-1	0	0	-4	0	0	-5
0	0	-1	0	0	1	0	0	0	0	0	0	0	0	4	0	0	8
0	0	0	0	0	0	0	0	0	0	0	1	0	0	0	0	0	125
0	0	0	0	0	0	0	0	0	0	0	1	0	0	0	0	0	-124
0	0	0	0	0	0	0	0	0	0	0	1	0	0	0	0	0	0

Table S17 (cont.)- ^{14}N-^{15}N IR intensity difference in km/mol for singlet C_4H_3N isomers. Numbering according to Fig. 1 and Custer et al 2016[21].

37	38	39	40	41	42	43	44	45	46	47	48	49	50	51	52	53	54
0	0	0	1	3	3	0	0	0	1	9	0	1	0	3	0	0	0
0	0	0	0	0	0	0	0	0	0	0	0	0	0	0	0	0	3
0	0	0	0	0	0	0	0	0	0	0	0	0	0	0	0	0	0
10	7	25	17	15	14	1	1	-6	0	8	10	0	6	0	0	3	7
0	0	-3	0	0	0	0	1	13	2	9	0	0	0	6	0	0	1
0	3	0	0	0	0	0	1	-3	0	0	0	-3	0	-1	-1	0	0
0	10	0	1	0	0	0	-1	3	0	-1	0	0	0	0	1	0	0
-1	-15	0	3	0	0	0	0	7	0	1	0	0	0	1	1	-1	0
0	0	-1	-3	6	4	0	0	0	0	0	0	0	0	0	-1	4	0
0	0	0	1	-6	-2	0	0	0	0	-4	0	3	0	0	-1	0	-4
0	0	0	0	0	-1	-1	0	-1	-1	1	-1	0	0	-2	0	0	1
0	1	0	0	1	0	1	0	-1	1	9	0	0	0	1	0	1	0
0	-3	0	0	-4	2	1	0	1	0	-1	0	0	0	0	0	0	1
0	3	0	0	4	-1	0	0	0	0	-1	0	0	0	0	0	0	0
0	0	0	0	0	1	0	0	1	2	0	0	1	0	0	1	11	0
1	0	0	0	0	0	0	0	0	-1	1	0	0	0	-1	-2	-10	0
0	0	0	0	0	0	0	0	0	1	0	0	0	0	0	2	0	-20
0	0	0	0	0	0	0	0	0	0	0	0	0	0	0	0	0	20

Triplet C_4H_3N family ($^{14}N/^{15}N$ comparison)

Table S18- Frequencies in cm^{-1} (scaled by 0.96) for triplet $C_4H_3{}^{14}N$ isomers. Numbering according to Fig. 1 and Custer et al 2016[21].

1	2	3	4	5	6	7	8	9	10	11	12	13	14	15	16	17	18
2953.0	3058.4	3328.2	3287.1	3331.0	3056.4	3028.3	3045.3	2964.8	2937.8	3473.9	3328.7	3043.3	3131.1	3316.0	3046.8	3318.2	3321.4
2928.0	2953.3	2897.6	3041.8	3319.4	2977.8	3002.4	3032.5	2906.1	2919.2	3315.8	3092.5	3030.8	3039.1	3081.8	2998.8	3020.6	2988.3
2846.5	2940.7	2789.4	2971.6	2965.5	2943.3	2939.0	2904.7	2820.8	2841.0	3262.0	2967.8	2909.3	2939.5	2951.7	2914.5	2744.2	2951.0
1954.1	2148.2	2129.8	1783.7	1980.3	2028.5	2030.6	2242.0	1882.3	2133.9	1798.7	1970.2	2114.1	1913.9	1830.8	1951.9	2011.3	2004.0
1702.7	1431.7	1577.7	1742.2	1590.8	1435.3	1411.7	1291.4	1524.6	1629.0	1578.7	1416.5	1305.7	1542.2	1500.3	1368.8	1407.0	1512.0
1388.5	1375.5	1326.5	1418.2	1292.9	1376.7	1346.2	1132.4	1393.6	1378.7	1544.1	1363.0	1157.4	1431.0	1420.0	1318.5	1260.9	1326.8
1373.2	1259.8	1212.2	1242.3	1140.4	1280.6	1049.1	1043.6	1364.3	1277.1	1305.3	1235.4	1046.3	1078.6	1267.0	1061.0	1018.1	1139.3
1321.5	1120.3	1103.7	1014.8	1041.4	1131.5	997.0	1014.9	1310.3	1193.5	1122.3	1042.8	1020.3	1034.9	1135.4	1031.9	961.7	1059.1
1043.4	997.0	949.7	977.2	886.7	1023.2	984.7	937.1	1110.5	995.2	788.8	848.0	938.0	964.2	854.8	979.3	914.0	925.8
988.0	859.6	868.8	792.4	732.6	863.5	937.4	911.7	990.5	944.2	633.5	819.5	907.7	840.1	814.6	915.4	765.6	726.5
934.1	802.0	786.4	711.9	695.5	781.3	925.1	809.6	818.1	869.3	603.6	606.8	818.1	660.7	568.2	881.1	717.7	681.0
756.0	727.6	665.1	710.8	631.0	709.8	749.4	797.6	742.2	834.0	551.9	562.7	788.0	601.4	532.3	773.8	653.5	654.9
510.3	605.3	662.2	513.1	555.3	583.0	662.0	707.0	449.7	635.1	464.0	523.6	704.4	505.7	487.0	688.7	593.1	558.5
505.5	538.0	476.4	395.1	531.3	503.0	625.7	699.2	377.1	443.8	434.1	461.2	688.3	377.5	424.1	614.6	542.4	541.5
363.3	427.1	384.0	365.0	402.9	358.9	545.6	492.0	311.8	341.5	391.4	433.5	421.7	340.2	420.1	453.0	457.3	393.6
268.1	321.2	323.2	196.6	390.4	278.0	435.9	424.7	163.2	256.1	246.0	394.4	346.4	254.8	363.2	379.8	286.8	366.6
137.3	183.6	205.4	141.2	171.8	189.2	191.9	198.5	151.1	184.8	142.3	148.5	188.9	174.6	148.4	194.4	203.3	171.5
99.6	148.9	110.1	123.3	163.3	144.9	154.5	197.4	138.4	99.7	119.8	137.7	175.8	144.4	133.8	176.9	143.4	170.7

Table S18 (cont.)- Frequencies in cm^{-1} (scaled by 0.96) for triplet $C_4H_3{}^{14}N$ isomers. Numbering according to Fig. 1 and Custer et al 2016[21].

19	21	22	23	24	25	26	27	28	29	30	35	39	41	42	43	46	47
3121.9	3026.6	3332.1	2973.7	3067.6	3012.8	2974.1	3325.3	3126.4	2930.5	3130.4	3332.8	2967.9	3396.9	3396.8	3007.5	3324.5	3262.8
3029.2	3022.2	3220.9	2972.1	2992.0	2939.7	2928.1	3025.6	3033.1	2923.2	3097.3	3182.0	2958.4	3010.6	3010.6	2971.1	3137.9	2997.7
2957.1	2963.1	3038.8	2899.6	2929.2	2890.8	2911.5	3012.4	2998.7	2903.3	3076.1	2919.7	2881.1	2889.5	2889.5	2938.2	3000.0	2926.4
1815.5	1843.7	2123.7	1910.9	1933.5	2127.2	2257.7	2024.5	1695.5	2266.5	1455.1	1653.4	1786.1	2048.2	2048.2	2228.7	2089.0	1935.2
1489.3	1478.5	1416.5	1758.4	1615.5	1417.6	1541.7	1470.6	1450.1	1553.9	1379.7	1424.3	1694.3	1364.5	1364.5	1406.8	1309.3	1483.5
1455.3	1339.4	1346.1	1430.9	1419.1	1393.9	1397.8	1068.0	1348.9	1398.8	1267.0	1345.5	1403.2	1357.2	1357.1	1297.7	1235.3	1418.6
1318.6	1047.5	1169.9	1421.6	1283.7	1330.0	1264.0	1019.3	1291.4	1285.3	1224.6	1236.1	1382.7	1142.9	1142.9	1188.4	1065.8	1064.4
1208.9	911.7	1031.3	1375.0	1033.8	1144.4	1218.2	955.3	1161.5	1187.0	1061.3	1166.5	1331.0	1059.4	1059.4	1027.0	1041.3	1004.3
1020.0	903.5	846.9	1095.5	993.1	1041.4	1155.5	909.4	998.9	1164.6	1012.1	917.5	1056.0	936.7	936.7	1007.5	966.0	992.1
895.1	887.0	699.1	1071.0	771.6	966.0	958.8	857.5	868.9	953.3	1002.6	853.0	1028.6	855.9	855.9	974.5	935.5	989.5
855.5	845.4	670.8	1032.8	736.4	791.3	905.3	740.1	756.7	857.3	917.8	833.9	971.8	748.6	748.7	957.1	849.7	871.0
757.0	759.8	662.7	753.7	677.8	679.8	839.3	674.1	736.9	821.0	877.1	665.5	815.1	663.9	663.9	845.3	674.5	820.6
575.8	646.9	561.7	440.2	434.9	544.4	613.8	654.1	515.5	641.9	784.1	641.5	436.3	661.9	661.9	785.1	624.7	642.3
449.5	535.0	555.4	299.8	428.6	495.3	501.5	568.2	514.1	605.2	781.6	583.5	347.6	553.0	553.0	620.6	573.3	561.4
448.0	404.7	416.6	283.8	354.7	360.5	426.8	426.0	422.1	381.7	701.2	538.5	303.9	403.2	403.2	533.3	515.7	474.7
397.5	299.6	388.3	142.8	247.5	260.7	355.8	374.0	179.0	352.8	665.2	299.8	156.5	317.5	317.5	480.1	428.4	267.7
132.8	188.2	175.4	128.0	162.3	182.9	192.8	218.1	175.6	153.2	586.1	206.1	138.9	229.5	229.6	222.6	220.2	210.5
89.3	160.6	157.0	111.8	142.1	113.5	82.7	183.1	157.2	108.7	481.8	175.3	126.3	156.8	156.8	195.6	190.7	179.0

Table S19- Frequencies in cm^{-1} (scaled by 0.96) for triplet $C_4H_3{}^{15}N$ isomers. Numbering according to Fig. 1 and Custer et al 2016[21].

1	2	3	4	5	6	7	8	9	10	11	12	13	14	15	16	17	18
2953.0	3058.4	3328.2	3279.7	3323.5	3056.4	3028.3	3045.3	2964.8	2937.8	3464.7	3328.6	3043.3	3131.1	3316.0	3046.8	3318.2	3321.4
2928.0	2953.3	2897.6	3041.8	3319.4	2977.8	3002.4	3032.5	2906.1	2919.2	3315.8	3092.4	3030.8	3039.1	3081.8	2998.8	3020.6	2988.3
2846.5	2940.7	2789.4	2971.6	2965.5	2943.3	2939.0	2904.7	2820.7	2841.0	3256.7	2967.8	2909.3	2939.5	2951.7	2914.5	2744.2	2951.0
1934.7	2121.2	2129.7	1782.4	1980.1	1991.8	2005.8	2213.6	1847.7	2095.7	1798.6	1969.7	2076.0	1911.5	1829.6	1916.6	2011.2	2003.5
1696.3	1431.6	1556.6	1730.4	1571.4	1435.2	1409.0	1290.7	1524.5	1629.0	1570.7	1413.1	1305.4	1533.6	1496.5	1368.6	1388.3	1488.8
1388.5	1375.3	1326.5	1417.3	1291.7	1376.5	1345.3	1132.3	1393.6	1378.6	1542.9	1338.1	1156.8	1430.2	1415.7	1318.2	1258.2	1325.4
1373.2	1258.9	1212.1	1236.4	1136.8	1280.1	1048.9	1041.9	1364.3	1276.7	1294.3	1232.3	1045.4	1076.8	1246.2	1060.4	1016.2	1127.8
1321.5	1119.4	1103.1	1009.0	1039.8	1130.6	996.5	1014.9	1310.3	1192.0	1116.0	1038.8	1020.3	1020.2	1130.8	1031.8	958.8	1057.9
1039.7	993.7	949.3	977.2	885.5	1021.2	983.8	937.1	1108.9	994.8	785.8	842.7	937.8	964.0	854.1	979.1	904.9	923.5
987.5	857.2	868.5	792.4	732.3	862.4	937.0	910.7	990.4	942.5	631.4	819.5	907.1	826.3	807.5	914.6	765.5	725.0
934.1	802.0	784.6	709.1	693.8	781.3	924.4	809.6	817.0	867.6	601.0	602.4	817.9	660.3	565.2	880.6	716.9	680.8
751.6	727.6	665.1	705.9	631.0	709.8	748.5	793.2	740.3	833.3	551.9	562.7	785.7	600.9	532.2	773.4	653.4	654.9
508.9	605.1	662.2	512.6	555.3	582.1	661.7	706.6	443.1	634.2	462.3	520.7	704.2	505.0	485.4	685.8	593.1	555.7
504.3	535.2	475.3	394.7	527.2	496.1	622.0	698.9	370.3	437.2	434.0	460.8	686.1	376.1	423.8	613.6	537.5	541.5
362.0	425.3	379.0	364.6	402.8	352.3	544.3	489.9	308.6	341.2	389.4	432.5	414.9	339.7	419.3	446.5	456.2	392.7
266.9	319.7	323.0	195.9	387.8	275.3	433.6	423.4	163.1	251.1	246.0	393.9	341.6	253.6	360.3	372.6	285.8	362.2
137.0	182.8	204.9	140.6	170.0	188.8	190.1	197.0	150.7	183.1	141.7	147.4	187.9	174.3	148.3	193.1	201.5	170.3
98.5	147.4	108.5	122.5	162.4	144.4	153.4	195.1	138.2	99.6	119.2	136.1	174.1	144.3	133.4	175.9	142.8	169.2

Table S19 (cont.)- Frequencies in cm^{-1} (scaled by 0.96) for triplet $C_4H_3{}^{15}N$ isomers. Numbering according to Fig. 1 and Custer et al 2016[21].

19	21	22	23	24	25	26	27	28	29	30	35	39	41	42	43	46	47
3121.9	3026.6	3332.1	2973.7	3067.6	3012.8	2974.1	3317.5	3126.4	2930.5	3130.4	3325.4	2967.9	3388.4	3388.3	3007.5	3324.5	3255.5
3029.2	3022.2	3214.0	2972.1	2992.0	2939.7	2928.1	3025.6	3033.1	2923.2	3097.3	3182.0	2958.4	3010.6	3010.6	2971.1	3131.1	2997.7
2957.1	2963.1	3038.8	2899.6	2929.2	2890.8	2911.5	3012.4	2998.7	2903.3	3076.1	2919.7	2881.1	2889.5	2889.5	2938.2	3000.0	2926.4
1796.4	1843.7	2122.5	1900.9	1933.3	2099.4	2228.6	2010.2	1678.8	2237.5	1452.7	1653.4	1767.7	2030.6	2030.5	2200.2	2089.0	1923.0
1484.0	1474.8	1405.3	1745.0	1586.8	1417.6	1541.7	1465.1	1449.8	1553.9	1370.2	1422.8	1684.4	1362.6	1362.6	1406.8	1304.0	1479.0
1455.2	1338.4	1343.0	1430.9	1417.2	1393.9	1397.8	1066.1	1346.5	1398.8	1265.9	1341.1	1402.8	1356.7	1356.7	1297.3	1228.3	1417.2
1316.7	1036.0	1155.3	1421.5	1281.9	1330.0	1263.9	1019.2	1288.3	1285.1	1223.9	1219.1	1382.7	1142.6	1142.5	1188.4	1063.6	1063.5
1208.9	905.5	1018.8	1375.0	1031.3	1142.4	1218.2	955.2	1161.3	1187.0	1061.1	1165.1	1331.0	1056.2	1056.2	1024.8	1039.3	1002.8
1019.4	903.4	843.1	1091.8	993.1	1040.8	1155.4	907.8	998.7	1164.5	1002.1	915.6	1045.1	931.7	931.7	1007.5	961.5	991.6
895.1	886.1	698.8	1069.1	771.6	965.9	958.3	851.7	868.9	949.4	999.1	853.0	1027.3	855.7	855.7	974.5	934.0	985.4
855.5	845.4	670.8	1020.2	730.0	788.1	900.0	739.0	756.7	857.2	917.2	833.8	971.8	744.6	744.7	955.7	846.7	864.4
751.7	757.7	656.6	748.1	677.3	677.7	838.1	672.9	735.8	818.8	877.1	664.9	809.9	662.3	662.3	845.1	674.5	820.2
575.8	639.8	561.7	437.3	433.9	543.6	613.2	649.7	514.4	639.2	781.0	641.3	433.8	660.7	660.7	781.5	624.7	641.4
447.5	532.0	554.1	298.7	425.5	494.5	499.9	567.6	514.1	605.1	771.7	583.5	346.8	551.8	551.8	620.3	570.2	559.2
445.8	404.1	415.8	283.8	351.0	359.2	426.2	424.9	412.6	380.5	701.2	534.0	301.7	402.2	402.2	531.7	515.3	473.2
395.6	299.2	387.7	141.8	245.7	258.8	353.4	373.8	178.4	350.4	661.0	299.0	154.5	316.5	316.5	478.5	422.7	267.6
131.8	187.2	174.1	127.4	162.3	180.6	190.6	216.7	175.4	151.0	581.1	205.2	137.4	228.9	228.9	220.6	219.7	209.0
88.7	160.4	156.5	111.5	141.7	113.5	82.3	181.7	155.6	108.5	479.6	173.4	126.3	155.3	155.3	193.3	189.1	177.6

Table S20-^{14}N-^{15}N frequency difference in cm^{-1} for triplet C_4H_3N isomers. Numbering according to Fig. 1 and Custer et al 2016[21].

1	2	3	4	5	6	7	8	9	10	11	12	13	14	15	16	17	18
0.0	0.0	0.0	7.4	7.5	0.0	0.0	0.0	0.0	0.0	9.2	0.1	0.0	0.0	0.0	0.0	0.0	0.0
0.0	0.0	0.0	0.0	0.0	0.0	0.0	0.0	0.0	0.0	0.0	0.1	0.0	0.0	0.0	0.0	0.0	0.0
0.0	0.0	0.0	0.0	0.0	0.0	0.0	0.0	0.1	0.0	5.3	0.0	0.0	0.0	0.0	0.0	0.0	0.0
19.4	27.0	0.1	1.3	0.2	36.7	24.8	28.4	34.6	38.2	0.1	0.5	38.1	2.4	1.2	35.3	0.1	0.5
6.4	0.1	21.1	11.8	19.4	0.1	2.7	0.7	0.1	0.0	8.0	3.4	0.3	8.6	3.8	0.2	18.7	23.2
0.0	0.2	0.0	0.9	1.2	0.2	0.9	0.1	0.0	0.1	1.2	24.9	0.6	0.8	4.3	0.3	2.7	1.4
0.0	0.9	0.1	5.9	3.6	0.5	0.2	1.7	0.0	0.4	11.0	3.1	0.9	1.8	20.8	0.6	1.9	11.5
0.0	0.9	0.6	5.8	1.6	0.9	0.4	0.0	0.0	1.5	6.3	4.0	0.0	14.7	4.6	0.1	2.9	1.2
3.7	3.4	0.5	0.0	1.2	2.0	0.9	0.0	1.6	0.4	3.0	5.3	0.2	0.2	0.7	0.2	9.1	2.3
0.5	2.4	0.4	0.0	0.4	1.1	0.5	1.0	0.2	1.8	2.1	0.0	0.6	13.8	7.1	0.7	0.0	1.5
0.0	0.0	1.8	2.9	1.7	0.0	0.7	0.0	1.0	1.7	2.5	4.4	0.1	0.5	2.9	0.5	0.8	0.2
4.4	0.0	0.0	4.9	0.0	0.0	0.8	4.4	1.9	0.6	0.0	0.0	2.4	0.5	0.0	0.4	0.0	0.0
1.4	0.2	0.0	0.5	0.0	0.9	0.3	0.4	6.7	0.9	1.7	2.9	0.3	0.8	1.6	2.9	0.0	2.8
1.2	2.8	1.0	0.4	4.1	6.8	3.7	0.3	6.8	6.6	0.1	0.4	2.2	1.4	0.2	1.0	4.9	0.0
1.3	1.9	5.0	0.5	0.2	6.6	1.3	2.1	3.2	0.4	2.1	1.0	6.8	0.4	0.8	6.5	1.1	0.9
1.3	1.4	0.1	0.8	2.6	2.7	2.3	1.3	0.0	5.1	0.1	0.5	4.7	1.2	2.9	7.2	1.1	4.4
0.2	0.9	0.4	0.6	1.8	0.4	1.8	1.5	0.4	1.7	0.6	1.1	1.0	0.3	0.1	1.3	1.8	1.3
1.1	1.5	1.6	0.8	0.9	0.4	1.1	2.3	0.2	0.1	0.6	1.6	1.6	0.1	0.4	0.9	0.5	1.6

Table S20 (cont.)-^{14}N-^{15}N frequency difference in cm^{-1} for triplet C_4H_3N isomers. Numbering according to Fig. 1 and Custer et al 2016[21].

19	21	22	23	24	25	26	27	28	29	30	35	39	41	42	43	46	47
0.0	0.0	0.0	0.0	0.0	0.0	0.0	7.8	0.0	0.0	0.0	7.4	0.0	8.5	8.5	0.0	0.0	7.3
0.0	0.0	6.9	0.0	0.0	0.0	0.0	0.0	0.0	0.0	0.0	0.0	0.0	0.0	0.0	0.0	6.8	0.0
0.0	0.0	0.0	0.0	0.0	0.0	0.0	0.0	0.0	0.0	0.0	0.0	0.0	0.0	0.0	0.0	0.0	0.0
19.1	0.0	1.2	10.0	0.2	27.8	29.1	14.3	16.7	29.0	2.4	0.0	18.4	17.6	17.7	28.5	0.0	12.2
5.3	3.7	11.2	13.4	28.7	0.0	0.0	5.5	0.3	0.0	9.5	1.5	9.9	1.9	1.9	0.0	5.3	4.5
0.1	1.0	3.1	0.0	1.9	0.0	0.0	1.9	2.4	0.0	1.1	4.4	0.4	0.5	0.4	0.4	7.0	1.4
1.9	11.5	14.6	0.1	1.8	0.0	0.1	0.1	3.1	0.2	0.7	17.0	0.0	0.3	0.4	0.0	2.2	0.9
0.0	6.2	12.5	0.0	2.5	2.0	0.0	0.0	0.2	0.0	0.2	1.4	0.0	3.2	3.2	2.2	2.0	1.5
0.6	0.1	3.7	3.7	0.0	0.6	0.1	1.6	0.3	0.1	10.0	1.9	10.9	5.0	5.0	0.0	4.5	0.5
0.0	0.9	0.3	1.9	0.0	0.1	0.5	5.8	0.0	3.9	3.5	0.0	1.3	0.3	0.3	0.0	1.5	4.1
0.0	0.0	0.0	12.6	6.4	3.2	5.3	1.1	0.0	0.1	0.6	0.1	0.0	4.0	4.0	1.4	3.0	6.6
5.3	2.1	6.1	5.7	0.6	2.1	1.2	1.1	1.0	2.2	0.0	0.6	5.2	1.6	1.6	0.2	0.0	0.4
0.0	7.0	0.0	2.8	1.0	0.8	0.5	4.4	1.1	2.7	3.1	0.2	2.5	1.2	1.2	3.5	0.0	0.9
2.1	3.0	1.3	1.1	3.1	0.9	1.7	0.7	0.0	0.0	9.9	0.0	0.9	1.2	1.2	0.3	3.0	2.2
2.2	0.6	0.9	0.0	3.7	1.4	0.5	1.1	9.5	1.2	0.1	4.5	2.2	1.0	1.0	1.6	0.4	1.6
1.9	0.4	0.6	1.0	1.8	1.9	2.4	0.2	0.6	2.4	4.1	0.8	2.0	1.0	1.0	1.6	5.7	0.1
1.0	1.0	1.2	0.6	0.0	2.3	2.2	1.4	0.3	2.2	5.0	0.9	1.5	0.7	0.7	2.0	0.5	1.4
0.7	0.2	0.6	0.3	0.4	0.1	0.4	1.3	1.5	0.2	2.2	1.9	0.0	1.5	1.5	2.3	1.6	1.4

Table S21-IR intensities in km/mol for triplet $C_4H_3{}^{14}N$ isomers. Numbering according to Fig. 1 and Custer et al 2016[21].

1	**2**	**3**	**4**	**5**	**6**	**7**	**8**	**9**	**10**	**11**	**12**	**13**	**14**	**15**	**16**	**17**	**18**
0	1	60	28	35	1	9	1	9	14	112	76	1	1	118	6	72	81
2	1	6	2	71	4	1	8	1	1	100	1	7	10	6	2	3	8
2	3	28	16	4	2	0	9	5	11	12	13	11	23	21	1	38	3
4	0	11	56	30	149	3	37	105	201	10	20	125	201	13	82	23	3
38	10	4	126	46	4	2	3	17	6	70	1	10	23	4	13	58	14
8	30	33	1	14	34	8	1	11	23	41	88	2	26	13	4	3	34
13	1	4	7	26	2	4	0	12	21	87	70	9	2	31	7	33	9
13	5	1	285	10	7	13	0	13	4	34	0	1	14	28	6	59	1
30	7	4	1	130	12	8	0	18	11	10	7	2	22	29	14	22	62
5	2	37	38	22	4	6	59	19	20	47	34	30	4	6	8	10	3
6	40	1	2	77	42	7	2	9	5	94	2	7	22	4	14	32	34
1	13	42	55	44	13	14	8	4	4	33	37	16	179	38	1	40	40
1	0	43	0	36	1	10	2	3	14	7	4	1	2	19	3	36	10
3	0	7	0	8	2	7	35	6	8	0	56	26	19	43	41	10	42
1	6	5	3	4	2	5	1	5	1	14	0	8	9	0	5	18	5
6	3	11	0	23	1	6	12	3	1	80	6	25	3	5	2	7	26
0	2	3	8	1	2	2	17	1	6	9	7	11	5	5	3	2	3
4	2	2	7	2	1	0	9	0	2	11	7	5	5	7	3	2	3

Table S21 (cont.)-IR intensities in km/mol for triplet $C_4H_3{}^{14}N$ isomers. Numbering according to Fig. 1 and Custer et al 2016[21].

19	21	22	23	24	25	26	27	28	29	30	35	39	41	42	43	46	47
2	0	87	9	2	4	1	45	2	0	1	4	1	123	123	3	70	9
1	8	5	16	7	4	2	6	1	9	3	48	2	5	5	1	3	12
2	2	7	56	6	4	1	27	0	2	6	28	5	46	46	6	4	30
0	71	3	5	4	119	5	615	27	4	6	22	292	575	575	8	11	375
6	3	30	504	7	4	26	6	5	18	54	28	46	4	4	2	50	15
3	3	20	24	5	6	9	8	8	9	19	93	27	45	45	6	2	14
1	2	28	11	14	7	2	6	20	1	1	37	22	15	15	6	68	19
0	3	5	29	87	70	3	1	6	1	17	29	2	7	7	9	22	28
0	1	117	18	1	476	2	41	5	4	23	0	1	19	19	9	45	84
5	11	45	2	42	1	1	339	15	1	2	40	34	13	13	23	37	198
50	48	36	27	11	614	1	51	47	11	2	62	0	512	512	6	43	4
1	34	6	1	19	478	5	0	9	1	0	85	23	24	24	16	39	6
3	8	56	9	2	26	2	5	78	1	26	65	40	35	35	5	42	35
7	2	18	73	21	410	2	3	6	1	0	27	57	52	52	4	30	45
8	3	2	17	0	45	3	196	62	2	64	9	22	32	32	1	10	9
2	7	22	15	3	17	0	2	1	1	1	48	1	11	11	0	2	1
0	1	1	17	6	16	6	13	1	3	0	2	6	22	22	8	1	4
1	2	4	0	10	0	5	1	0	0	10	13	2	14	14	6	0	2

Table S22-IR intensities in km/mol for triplet $C_4H_3{}^{15}N$ isomers. Numbering according to Fig. 1 and Custer et al 2016[21].

1	**2**	**3**	**4**	**5**	**6**	**7**	**8**	**9**	**10**	**11**	**12**	**13**	**14**	**15**	**16**	**17**	**18**
0	1	60	27	29	1	9	1	9	14	111	76	1	1	118	6	72	81
2	1	6	2	76	4	1	8	1	1	100	1	7	10	6	2	3	8
2	3	28	16	4	2	0	9	5	11	13	13	12	23	21	1	38	3
4	0	11	42	30	141	3	36	100	191	10	20	119	196	14	78	23	3
38	10	4	131	43	4	2	3	17	6	54	1	10	21	4	13	55	13
8	29	33	1	14	34	8	1	11	23	49	96	2	27	12	5	3	34
13	1	4	7	25	2	4	0	12	21	90	60	9	2	29	7	32	8
13	5	1	285	10	8	13	0	13	4	34	0	1	13	28	6	62	2
29	6	4	1	132	12	9	0	18	12	11	7	2	23	29	14	19	61
5	3	37	38	20	4	6	60	19	20	37	34	30	3	6	8	10	3
6	40	1	55	78	42	7	2	9	5	104	2	7	22	4	14	33	33
1	13	42	1	44	13	14	8	4	4	32	37	16	178	38	1	40	40
1	0	43	0	36	1	11	2	3	14	6	5	1	2	19	3	36	10
3	0	7	0	8	2	7	35	6	8	0	55	26	19	43	42	10	42
1	6	5	3	4	2	5	1	5	1	14	0	8	8	0	4	18	5
6	3	11	0	23	1	6	13	3	1	80	6	25	3	5	2	7	25
0	2	3	8	1	2	2	16	1	6	9	7	11	5	5	3	2	3
4	2	2	7	2	1	0	9	0	2	11	7	5	5	7	3	2	3

Table S22 (cont.)-Intensities for triplet $C_4H_3{}^{15}N$ isomers. Numbering according to Fig. 1 and Custer et al 2016[21].

19	21	22	23	24	25	26	27	28	29	30	35	39	41	42	43	46	47
2	0	87	9	2	4	1	43	2	0	1	4	1	119	119	3	70	9
1	8	6	16	7	4	2	6	1	9	3	48	2	5	5	1	3	12
2	2	7	57	6	4	1	27	0	2	6	28	5	46	46	6	4	30
0	71	3	0	4	118	5	597	25	4	4	22	277	561	561	8	11	362
6	3	36	498	6	4	26	7	5	18	53	29	53	2	2	2	48	14
3	3	16	24	5	6	9	8	7	9	18	84	28	47	47	6	3	15
0	2	26	11	14	7	2	6	20	1	1	43	22	15	15	6	67	21
0	3	2	29	88	70	3	1	6	1	18	28	2	8	8	9	21	14
0	1	117	20	1	477	2	48	5	4	5	0	3	17	17	9	39	13
5	11	44	2	42	1	1	327	15	1	18	40	32	13	13	23	41	280
50	48	36	23	10	636	1	55	47	11	2	62	0	509	509	6	45	4
1	34	8	1	19	457	5	1	9	1	0	85	22	44	44	16	38	5
3	8	56	8	2	25	2	4	73	1	0	64	39	18	18	5	42	34
7	2	18	72	20	410	2	4	6	1	27	27	58	52	52	4	30	45
7	3	2	17	0	44	3	195	62	2	64	8	22	31	31	1	10	9
2	7	21	14	3	17	0	2	1	0	1	48	1	12	12	0	2	1
0	1	1	17	6	15	6	13	1	3	0	2	6	21	21	7	1	3
1	2	4	0	10	0	5	1	0	0	10	13	2	14	14	5	0	2

Table S23-^{14}N-^{15}N IR intensity difference in km/mol for triplet C_4H_3N isomers. Numbering according to Fig. 1 and Custer et al 2016[21].

1	2	3	4	5	6	7	8	9	10	11	12	13	14	15	16	17	18
0	0	0	1	7	0	0	0	0	0	1	0	0	0	0	0	0	0
0	0	0	0	-5	0	0	0	0	0	0	0	0	0	0	0	0	0
0	0	0	0	0	0	0	0	0	0	-1	0	0	0	0	0	0	0
-1	0	0	14	1	8	0	1	5	10	0	0	6	5	-1	4	0	0
0	0	0	-4	4	0	0	0	0	0	16	0	0	2	0	0	3	1
0	0	0	0	0	0	0	0	0	0	-8	-8	0	-1	1	0	0	0
0	0	0	0	1	0	0	0	0	0	-3	10	0	0	2	0	1	0
0	0	0	0	0	0	0	0	0	0	1	0	0	1	0	0	-3	0
1	0	0	0	-1	0	-1	0	0	0	-1	0	0	-1	0	0	3	1
0	0	0	0	2	0	0	-1	0	0	10	0	0	1	0	0	0	0
0	0	0	-53	-1	0	0	0	0	0	-10	0	0	0	0	0	0	0
0	0	0	53	0	0	0	1	0	0	0	0	0	0	0	0	0	0
0	0	0	0	0	0	0	0	0	0	1	-1	0	0	0	0	0	0
0	0	0	0	0	0	0	0	0	0	0	1	0	0	0	0	0	0
0	0	0	0	0	0	0	0	0	0	0	0	0	0	0	0	0	0
0	0	0	0	0	0	0	0	0	0	0	0	0	0	0	0	0	0
0	0	0	0	0	0	0	1	0	0	0	0	0	0	0	0	0	1
0	0	0	0	0	0	0	0	0	0	0	0	0	0	0	0	0	0

Table S23 (cont.)-^{14}N-^{15}N IR intensity difference in km/mol for triplet C_4H_3N isomers. Numbering according to Fig. 1 and Custer et al 2016[21].

19	21	22	23	24	25	26	27	28	29	30	35	39	41	42	43	46	47
0	0	0	0	0	0	0	2	0	0	0	0	0	4	4	0	0	1
0	0	0	0	0	0	0	0	0	0	0	0	0	0	0	0	0	0
0	0	0	0	0	0	0	0	0	0	0	0	0	0	0	0	0	0
0	0	0	5	0	1	0	18	2	0	2	0	15	14	14	0	0	12
0	0	-6	5	1	0	0	-1	0	0	1	0	-7	2	2	0	2	1
0	0	4	0	0	0	0	0	1	0	1	9	-1	-1	-1	0	-1	-1
0	1	2	0	0	0	0	0	0	0	0	-5	0	0	0	0	1	-2
0	1	2	0	-2	-1	0	0	0	0	-1	0	0	-1	-1	0	1	14
0	0	0	-2	0	-1	0	-7	0	0	18	0	-1	2	2	0	6	71
0	0	1	0	0	0	0	12	0	0	-16	0	2	0	0	0	-3	-82
0	0	0	4	1	-22	0	-3	0	0	0	0	0	3	3	0	-2	0
0	0	-1	0	0	21	0	0	0	0	0	0	1	-19	-19	0	0	0
0	1	0	1	0	1	0	1	5	0	26	0	0	18	18	0	0	1
0	0	-1	1	1	1	0	0	0	0	-27	0	-1	0	0	0	0	0
0	0	0	0	0	1	0	1	0	0	0	1	0	1	1	0	0	0
0	0	0	0	0	1	0	0	0	0	0	1	0	0	0	0	0	0
0	0	0	0	0	1	0	0	0	0	0	0	0	0	0	0	0	0
0	0	0	0	0	0	0	0	0	0	0	0	0	0	0	0	0	0

Appendix 3-Photoproduct Details

Allenyl cyanide (2)

Beginning with allenyl cyanide (**2**) (Table 2, main text) the next lowest energy C_4H_3N isomer after cyanopropyne (**1**) a qualitative resemblance between bands can be seen for pure **2** and specific product bands appearing upon photolysis of **1** (Fig. 2, main text). However, certain differences are also evident. The most intense portion of a band is often shifted with respect to pure **2**, as can be seen in Column B for the group of bands recognized as due to the ν_4 vibration. Nevertheless, weak features directly matching the positions observed for a matrix spectrum of pure **2** sometimes surround the shifted bands (all columns of Fig. 2, main text). Substructures (splittings) observed in IR spectra of matrix-isolated chemicals are common and are due to occupation of dissimilar matrix sites. Differences between the structures of our reference bands and those of the photo-produced bands of **2** are also likely site splittings. A matrix cage well suited to **1** may not easily accommodate **2**, and some vibrational modes of the photolysis product **2** may be constrained, causing deviations from expected frequencies. Microenvironment related effects may also affect the IR intensities of photoproduct bands[22]. This is also observed here and the relative intensities of product bands do not exactly match what is observed for the pure chemical in Ar although the most intense bands remain strong and the weakest ones remain difficult to detect. This variation in intensity can be seen by comparing relative peak heights from one column to the next in Fig. 2 of the main text where a common absorbance scale is used. On top of these effects, our IR intensity measurements were often uncertain due to difficulties in integrating very small peaks with poorly defined backgrounds caused by interference fringes produced by the particular configuration of the measurement equipment, gradual formation of H_2O and CO_2 ices due to inevitable leaks, and potential interferences from other photolysis products that form simultaneously. A number of potential cases of interference from similar photolysis products will be mentioned later. Higher resolution and signal-to-noise would reduce such problems.

Isotopic substitution of ^{15}N for ^{14}N in the precursor molecule supplied additional arguments for the identification of **2**. In particular, bands tentatively assigned to the ν_3 mode of this product, observed following photolysis of ^{15}N-**1**, are shifted by -25 cm^{-1} with respect to those generated from ^{14}N-**1** (Fig. S11)**.** This is in good agreement with the calculated value of -28 cm^{-1} listed in Table 2 of the main text. Negligible isotopic shifts (less than 1 cm^{-1} or zero) are observed for ν_4, ν_9, and ν_{15}, bands, a result also predicted by calculations. A negligible isotopic shift is observed for features at 1417 and 1415 cm^{-1} in the region of the ν_5 bands (Fig. S14), also in agreement with calculations, although it is likely that this feature has contributions from **3** as well as other species. The peak assigned to ν_8 exhibits a shift of approx. -3 cm^{-1} with a calculated shift on the order of -5 cm^{-1} (Fig. S13).

In addition to peak location, intensity, and isotopic shifts, the evolution of band intensity as a function of photolysis time can also provide support for identification. Its usefulness as a diagnostic depends on a number of interconnected factors including the intensity of the band being integrated, the level of congestion surrounding or underlying that band, the total extent of photolysis for a particular experiment, and the kinetics of different product formation. Integrated intensities plotted as a function of irradiation time for the features detected at 2228, 1986, 918-914, 858, and 836 cm^{-1} share a common rate of growth and agree with the proposed spectral assignments. While we are confident that the bands at 1417 and 1415 cm^{-1} are associated, at least in part, with ν_5 of **2**, they are not unique to this chemical and the time evolution does not aid in its identification.

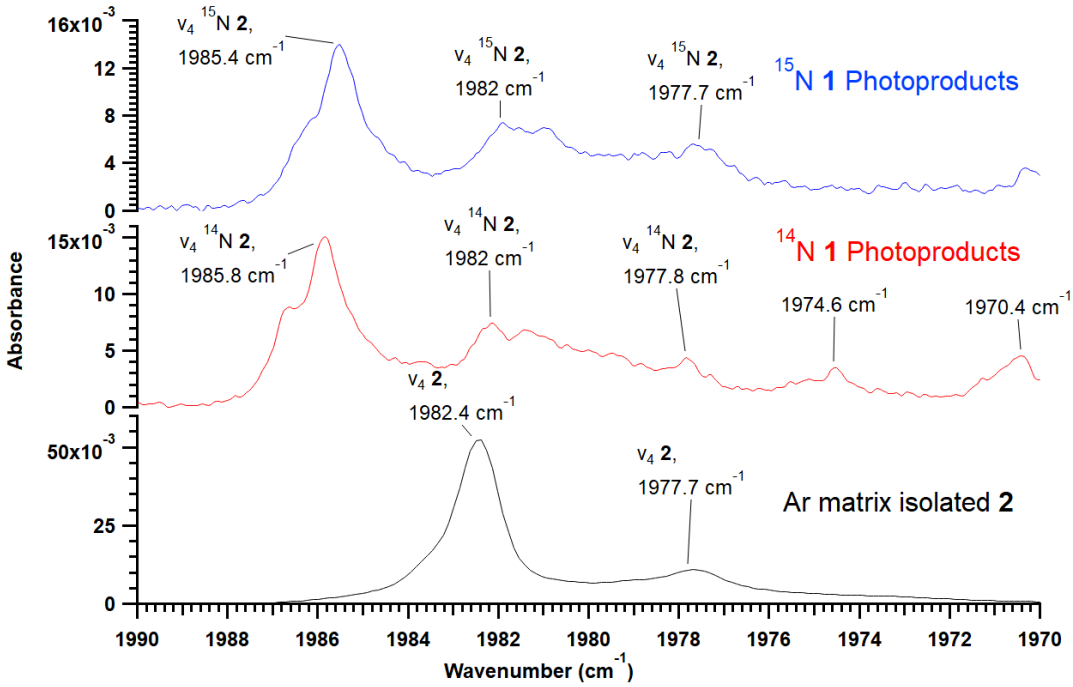

Fig. S9-Allenyl cyanide (**2**) standard (bottom trace) in Ar and as formed following photolysis of ^{14}N-**1** (1365 min, middle trace) and ^{15}N-**1** (741 min, top trace) using Ly-α (121.6 nm) radiation. Predicted ^{14}N-^{15}N frequency shift is 0 cm^{-1}. Calculated intensity is 92 km/mol.

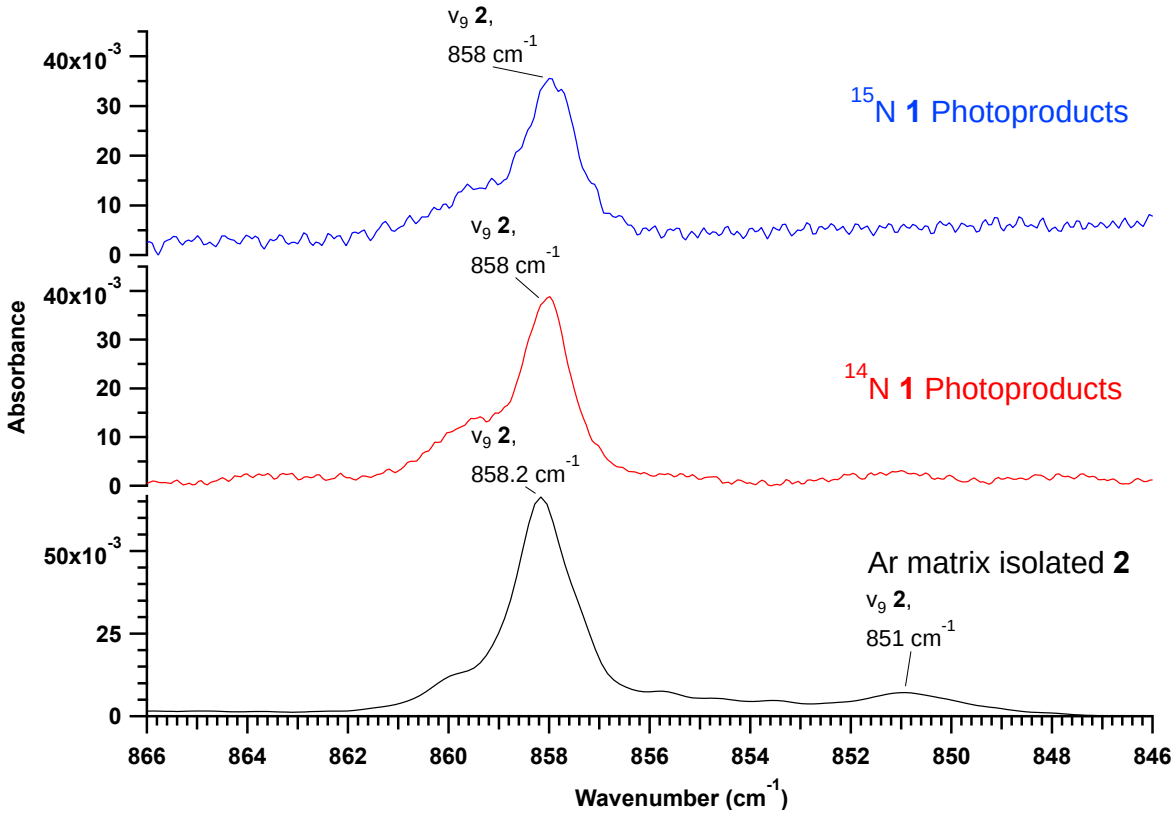

Fig. S10-Allenyl cyanide (**2**) standard (bottom trace) in Ar and as formed following photolysis of ^{14}N-**1** (1365 min, middle trace) and ^{15}N-**1** (741 min, top trace) using Ly-α (121.6 nm) radiation. Predicted ^{14}N-^{15}N frequency shift is 0 cm^{-1}. Calculated intensity is 46 km/mol.

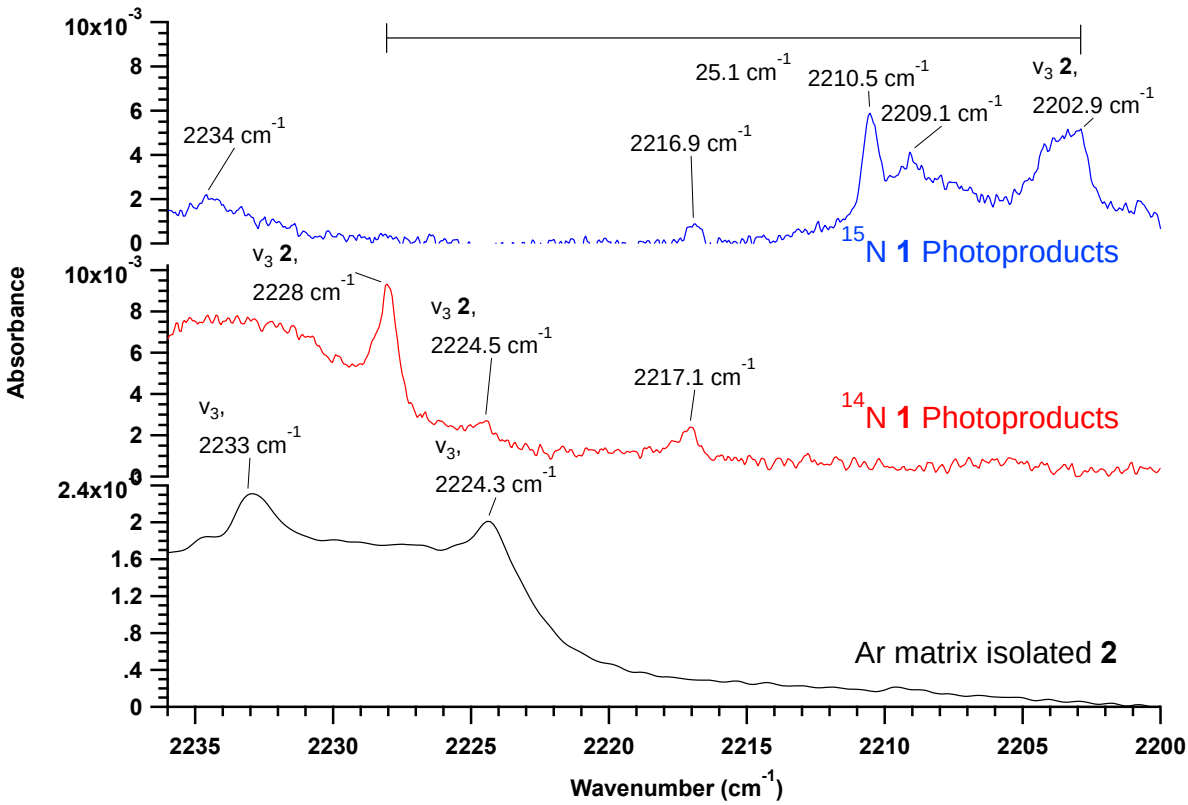

Fig. S11-Allenyl cyanide (**2**) standard (bottom trace) in Ar and as formed following photolysis of ^{14}N-**1** (1365 min, middle trace) and ^{15}N-**1** (741 min, top trace) using Ly-α (121.6 nm) radiation. Predicted ^{14}N-^{15}N frequency shift is -28 cm^{-1}. Calculated intensity is 24 km/mol.

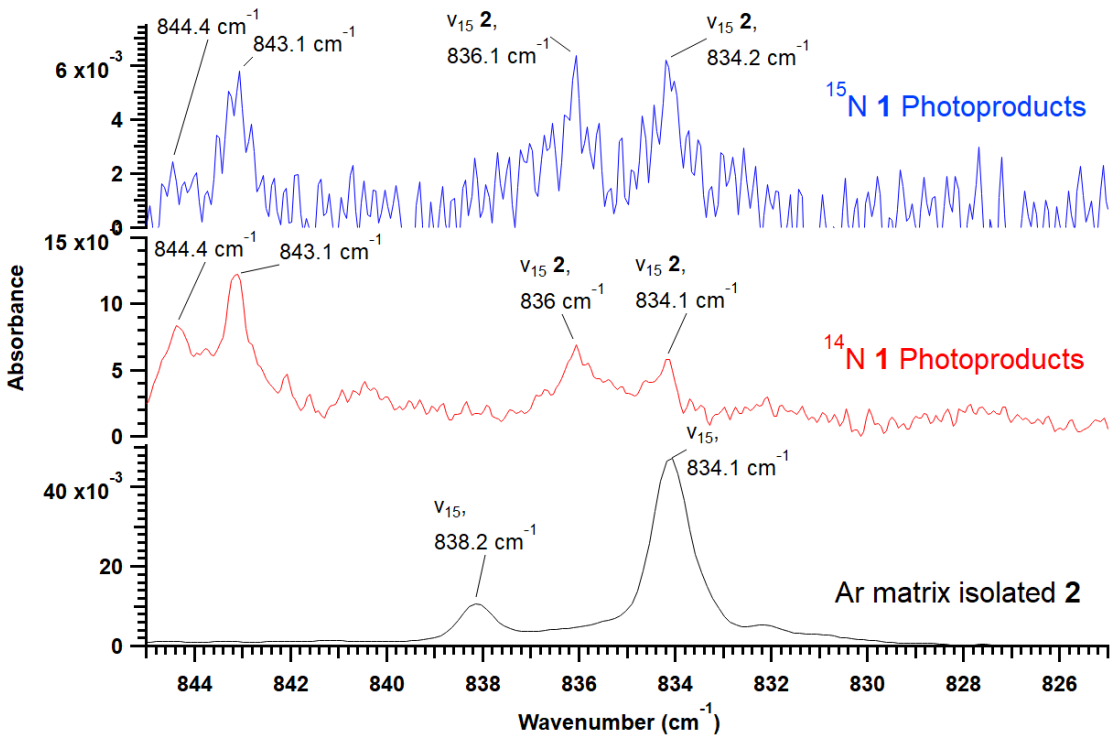

Fig. S12-Allenyl cyanide (**2**) standard (bottom trace) in Ar and as formed following photolysis of ^{14}N-**1** (1365 min, middle trace) and ^{15}N-**1** (741 min, top trace) using Ly-α (121.6 nm) radiation. Predicted ^{14}N-^{15}N frequency shift is 0 cm^{-1}. Calculated intensity is 23 km/mol.

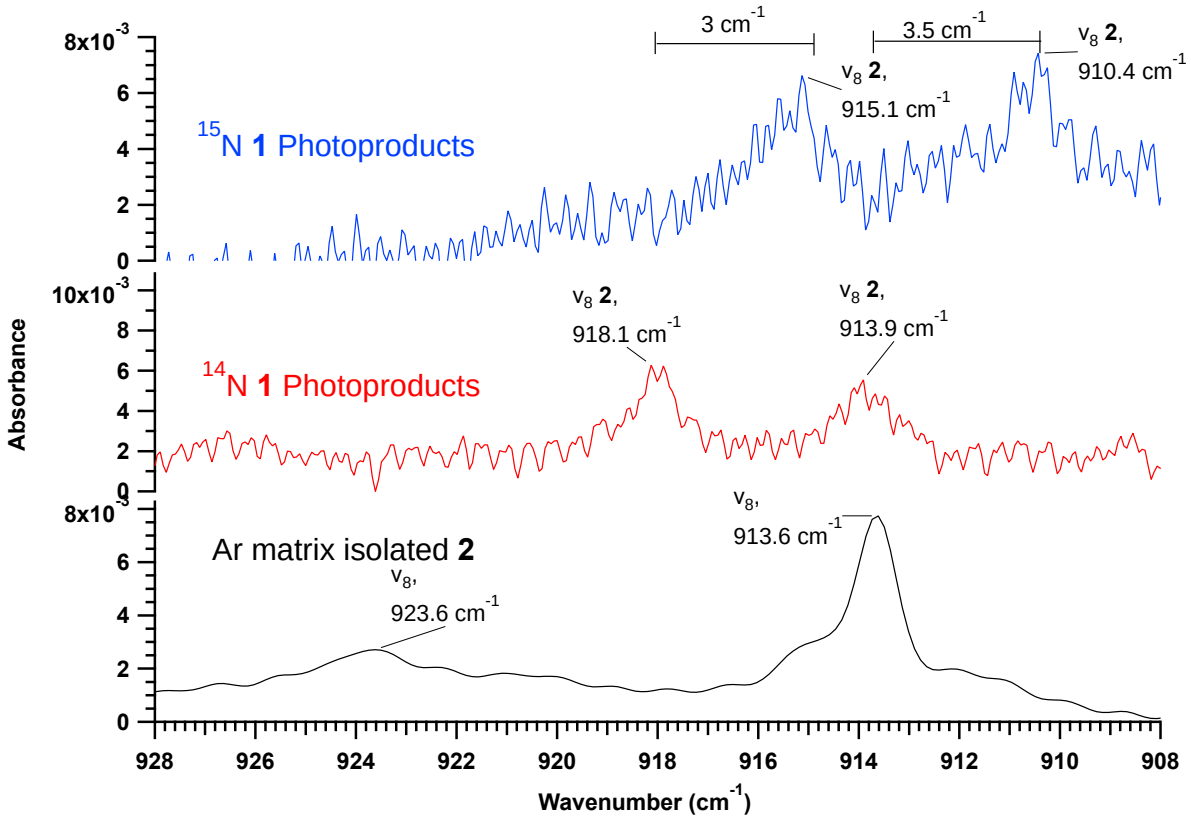

Fig. S13-Allenyl cyanide (**2**) standard (bottom trace) in Ar and as formed following photolysis of ^{14}N-**1** (1365 min, middle trace) and ^{15}N-**1** (741 min, top trace) using Ly-α (121.6 nm) radiation. Predicted ^{14}N-^{15}N frequency shift is -5 cm^{-1}. Calculated intensity is 8 km/mol.

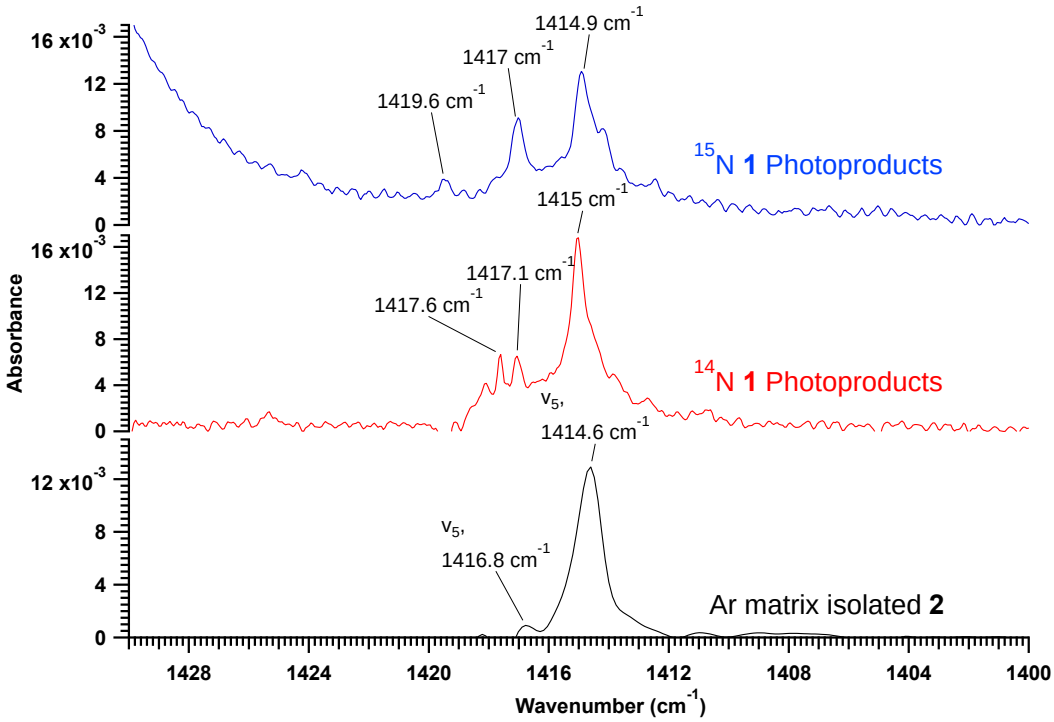

Fig. S14-Allenyl cyanide (**2**) standard (bottom trace) in Ar and as formed following photolysis of ^{14}N-**1** (1365 min, middle trace) and ^{15}N-**1** (741 min, top trace) using Ly-α (121.6 nm) radiation. Predicted ^{14}N-^{15}N frequency shift is 0 cm^{-1}. Calculated intensity is 4 km/mol.

Propargyl cyanide (3)

After allenyl cyanide, the next isomer in order of decreasing thermodynamic stability is propargyl cyanide (**3**) (Table 3, main text). For the pure, Ar-isolated sample, a multiplet structure dominated by two strong bands is observed in the 3320 to 3340 cm^{-1} acetylenic C-H stretching region (Fig. 3, Column A, bottom, main text). While this is not perfectly reproduced in product bands following photolysis of **1**, a strong feature at 3328.4 cm^{-1} falls between the two strongest features for this band observed in the pure sample. The ν_{16} mode has a higher intensity than ν_9 but is out of range of the PIIM measurements pictured in Fig. 3 in the main text. This mode was measured in IPC PAS. While ν_9 has a reproducible position whether it appears as a photolysis product or a pure substance (Fig. 3, Column E, main text) other modes may differ depending on the origin of the chemical (pure substance vs photolysis product). The ν_6 mode of propargyl cyanide standard isolated in Ar has strong features at 1285 and 1292 cm^{-1} (Fig. 3, Column C, bottom, main text). Once again, the matrix sites shift in intensity and position to form a strong feature at 1288.5 cm^{-1} (Fig. 3, Column C, top, main text) when it is formed by photolysis of **1**. This feature exhibits more structure when formed via the 193 nm photolysis of **1** (Fig. 3, Column C, top, main text) where there is a peak at 1288.9 and a weaker band at 1291.4 cm^{-1}. As stated earlier, features at 1417 and 1415 cm^{-1} (Column B) associated with ν_5 have a contribution from both **2** and **3** which cannot be separated. None of the bands of propargyl cyanide mentioned to this point are predicted to exhibit a ^{15}N isotopic shift and none is apparent in the spectra. Only the ν_8, ν_3, and ν_7 bands are predicted to have measurable isotopic shifts (-4, -29, -2 cm^{-1} respectively). Candidates only exist for ν_3 although none is intense making confirmation difficult using their time evolution. The peak visible at 896 (Fig. 3, Column D, main text) appears at 893 cm^{-1} following photolysis of ^{15}N-**1** (Fig. S34 and Fig. S35, Column C) giving an isotopic shift of ~-3 cm^{-1} and is assigned to the ν_8 mode. Overall, bands at 3328, 1289, 896, and 662 share a similar time evolution and seem to be free of interference. As will be discussed later, the time evolution of these peaks differs significantly from those assigned to allenyl cyanide, also suggesting that they belong to a distinct photoproduct. Overall, this evidence makes us confident that propargyl cyanide (**3**) is also formed as a photolysis product of **1**. Like **2**, this photoproduct appears at all photolysis wavelengths tested here.

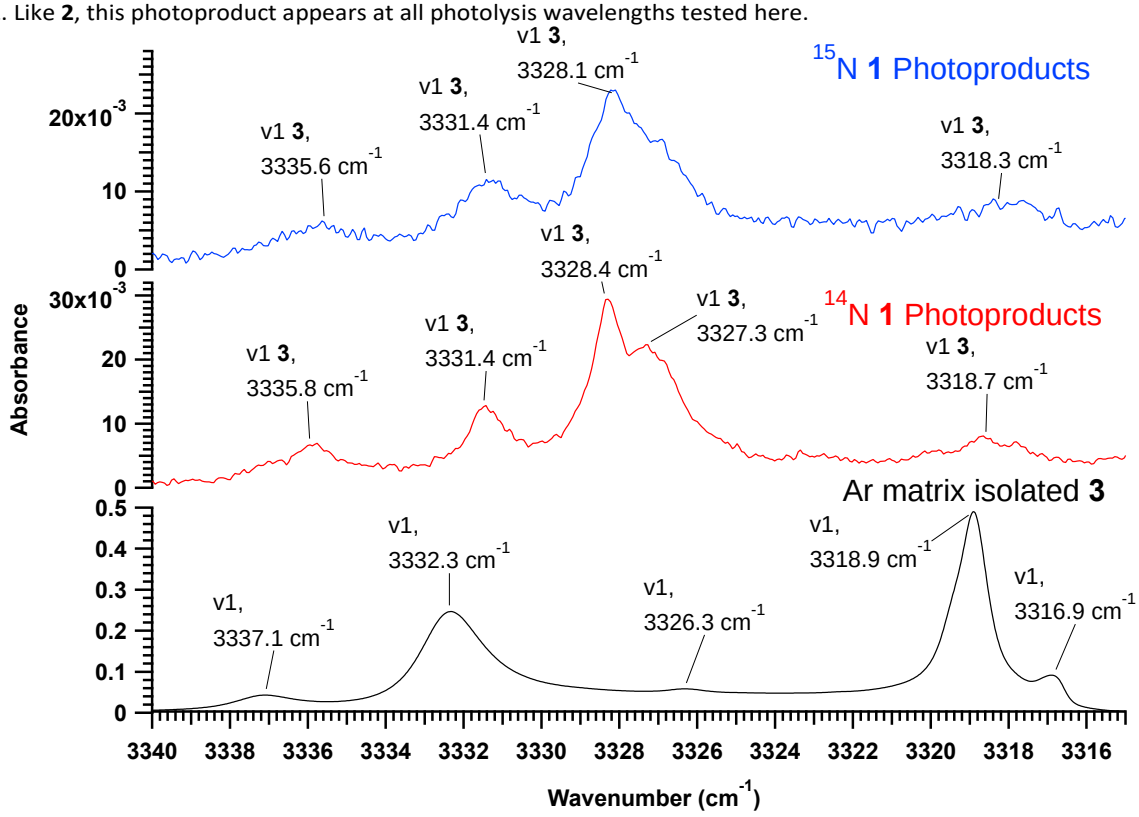

Fig. S15-Propargyl cyanide (**3**) standard (bottom trace) in Ar and as formed following photolysis of ^{14}N-**1** (1365 min, middle trace) and ^{15}N-**1** (741 min, top trace) using Ly-α (121.6 nm) radiation. Predicted ^{14}N-^{15}N frequency shift is 0 cm^{-1}. Calculated intensity is 70 km/mol.

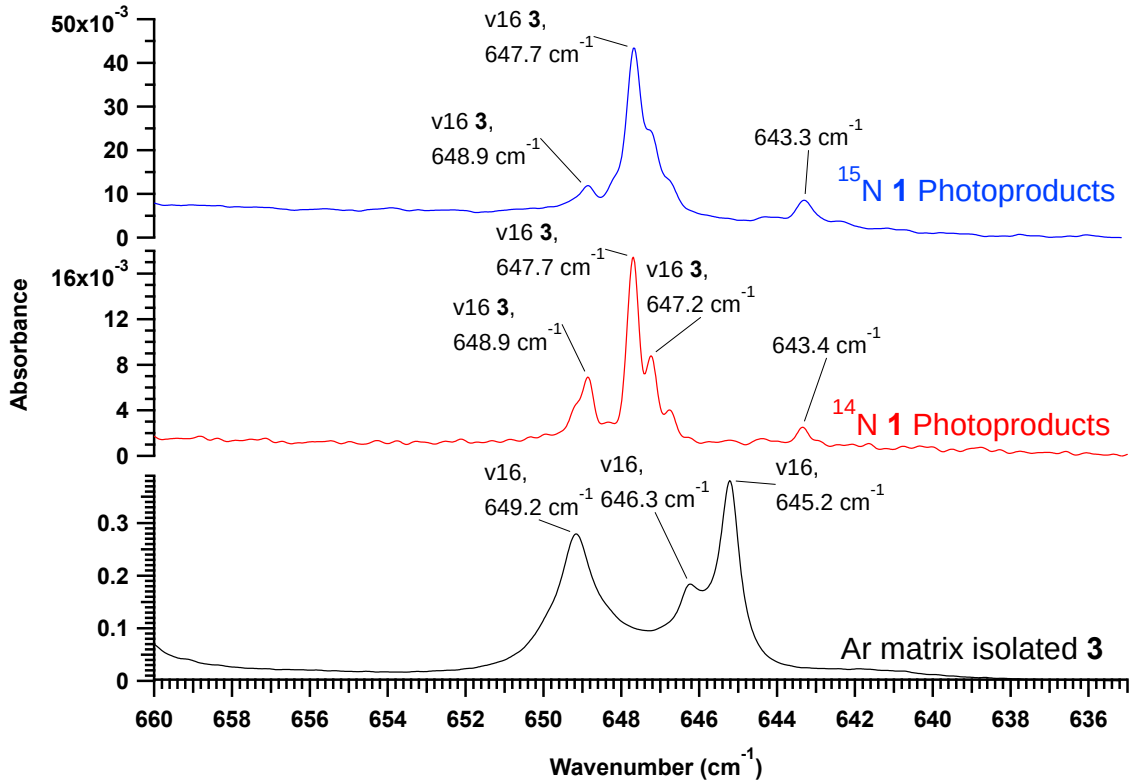

Fig. S16-Propargyl cyanide (**3**) standard (bottom trace) in Ar and as formed following photolysis of ^{14}N-**1** (732 min, middle trace) and ^{15}N-**1** (240 min, top trace) using 193 nm radiation. Predicted ^{14}N-^{15}N frequency shift is 0 cm^{-1}. Calculated intensity is 44 km/mol.

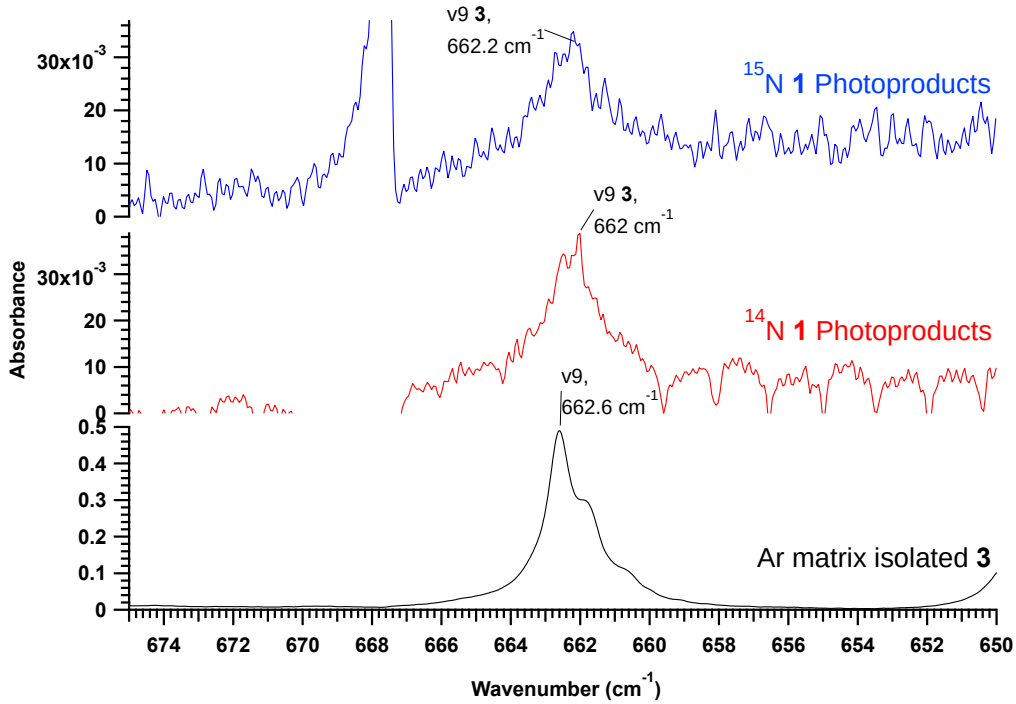

Fig. S17-Propargyl cyanide (**3**) standard (bottom trace) in Ar and as formed following photolysis of ^{14}N-**1** (1365 min, middle trace) and ^{15}N-**1** (741 min, top trace) using Ly-α (121.6 nm) radiation. Predicted ^{14}N-^{15}N frequency shift is 0 cm^{-1}. Calculated intensity is 38 km/mol.

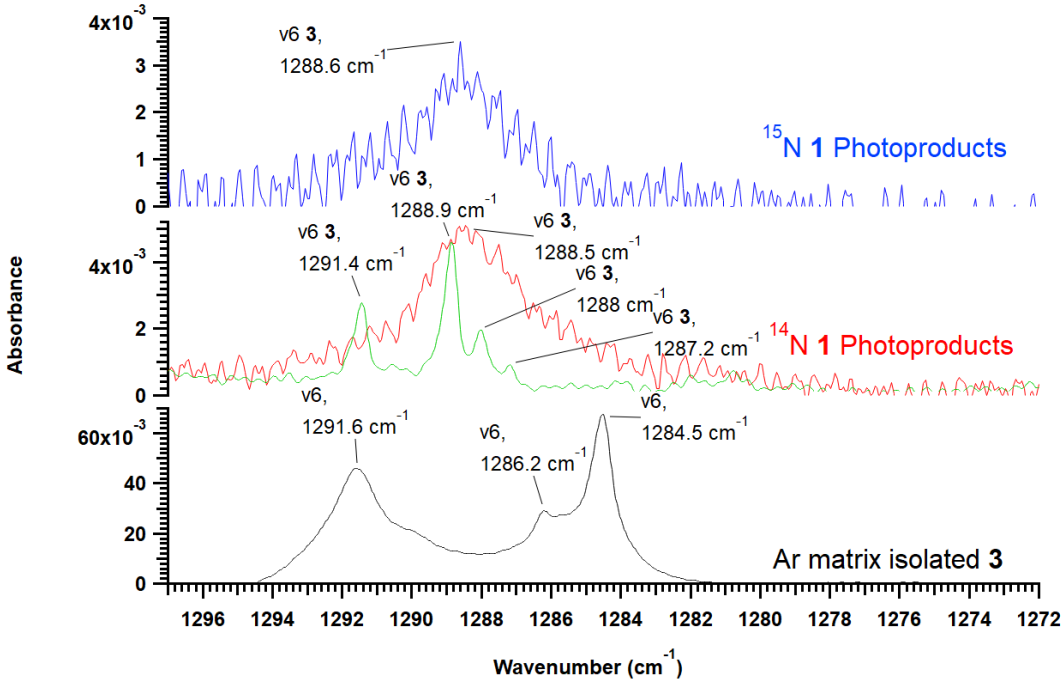

Fig. S18-Propargyl cyanide (**3**) standard (bottom trace) in Ar and as formed following photolysis of ^{14}N-**1** (1365 min, middle trace) and ^{15}N-**1** (741 min, top trace) using Ly-α (121.6 nm) radiation. Green trace from 193 nm photolysis showing site structure of this band more clearly (scale not common with other traces). Predicted ^{14}N-^{15}N frequency shift is 0 cm^{-1}. Calculated intensity is 12 km/mol.

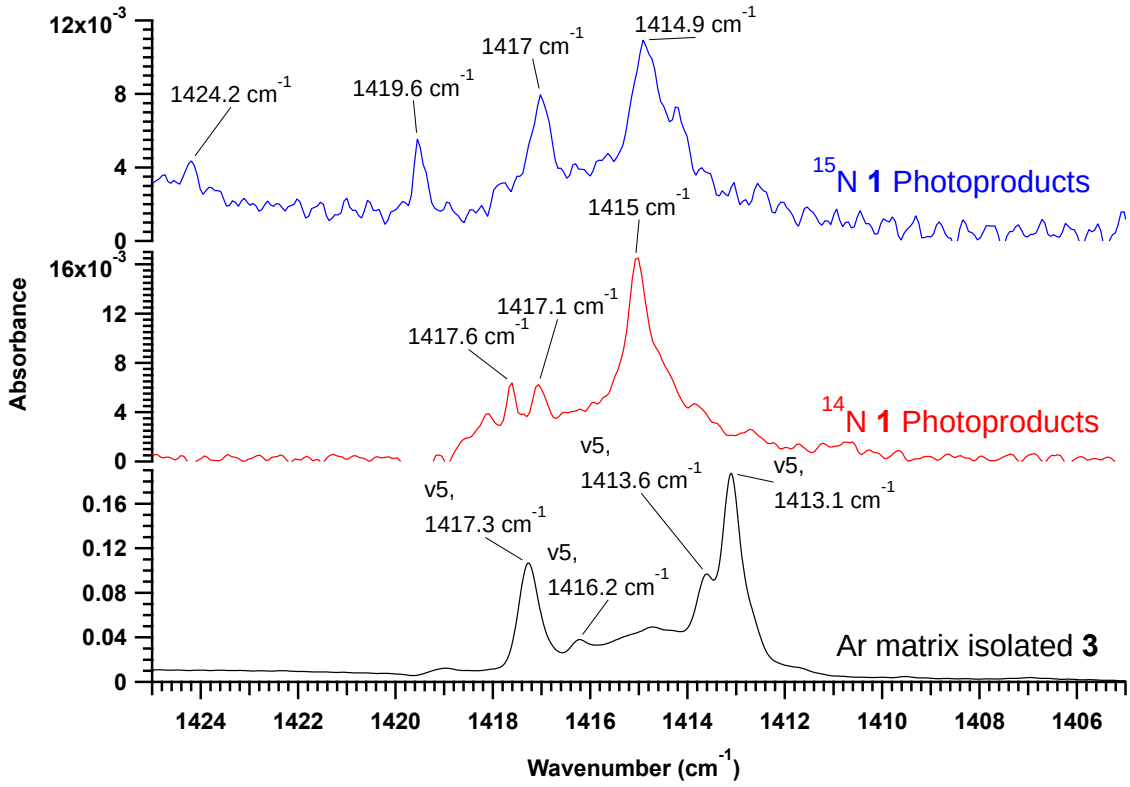

Fig. S19-Propargyl cyanide (**3**) standard (bottom trace) in Ar and as formed following photolysis of ^{14}N-**1** (1365 min, middle trace) and ^{15}N-**1** (741 min, top trace) using Ly-α (121.6 nm) radiation. Predicted ^{14}N-^{15}N frequency shift is 0 cm^{-1}. Calculated intensity is 9 km/mol.

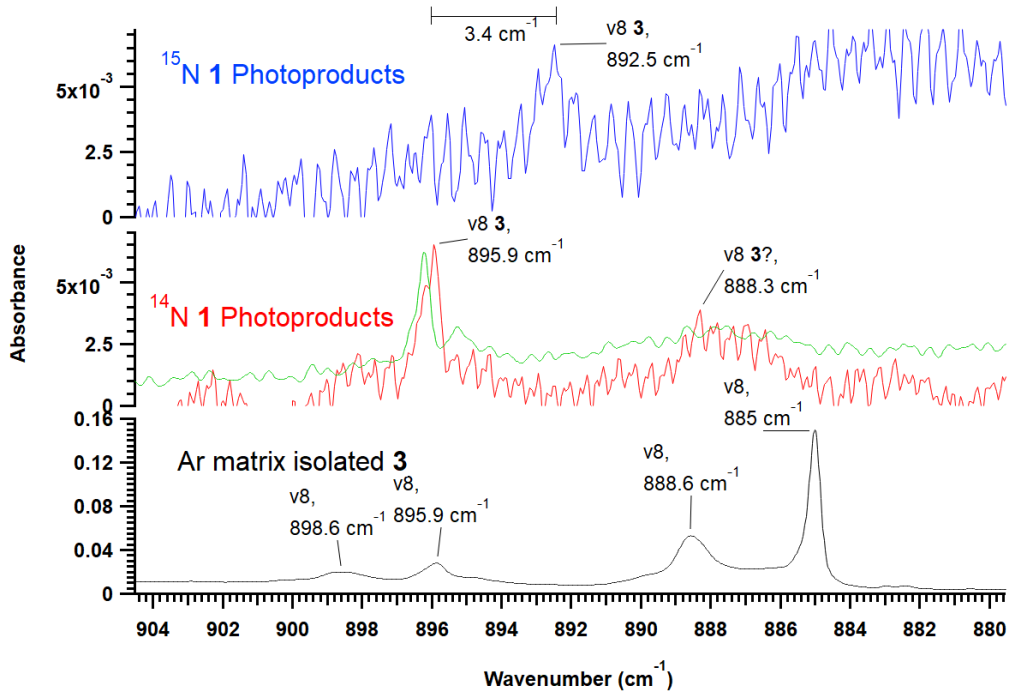

Fig. S20-Propargyl cyanide (**3**) standard (bottom trace) in Ar and as formed following photolysis of ^{14}N-**1** (1365 min, middle trace) and ^{15}N-**1** (741 min, top trace) using Ly-α (121.6 nm) radiation. Green trace from 193 nm photolysis showing site structure of this band more clearly (scale not common with other traces). Predicted ^{14}N-^{15}N frequency shift is -4 cm^{-1}. Calculated intensity is 4 km/mol.

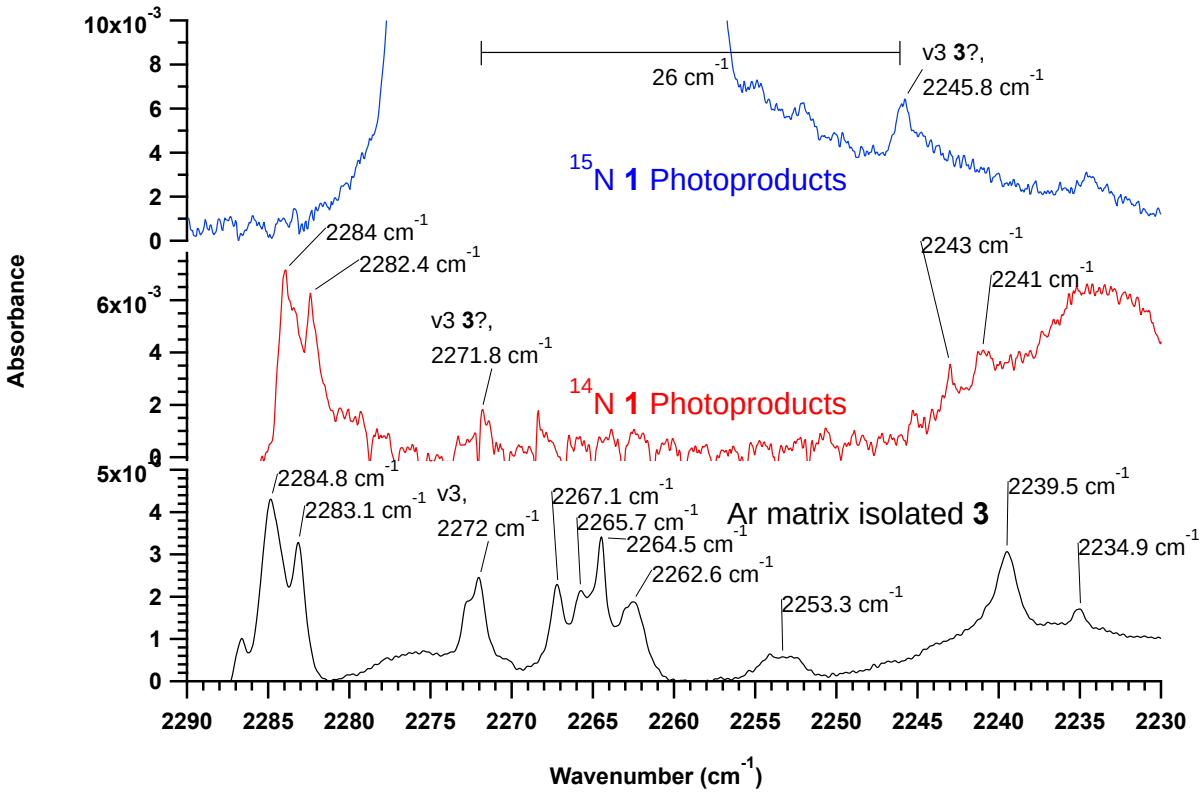

Fig. S21-Propargyl cyanide (**3**) standard (bottom trace) in Ar and as formed following photolysis of ^{14}N-**1** (1365 min, middle trace) and ^{15}N-**1** (741 min, top trace) using Ly-α (121.6 nm) radiation. Predicted ^{14}N-^{15}N frequency shift is -29 cm^{-1}. Calculated intensity is 5 km/mol.

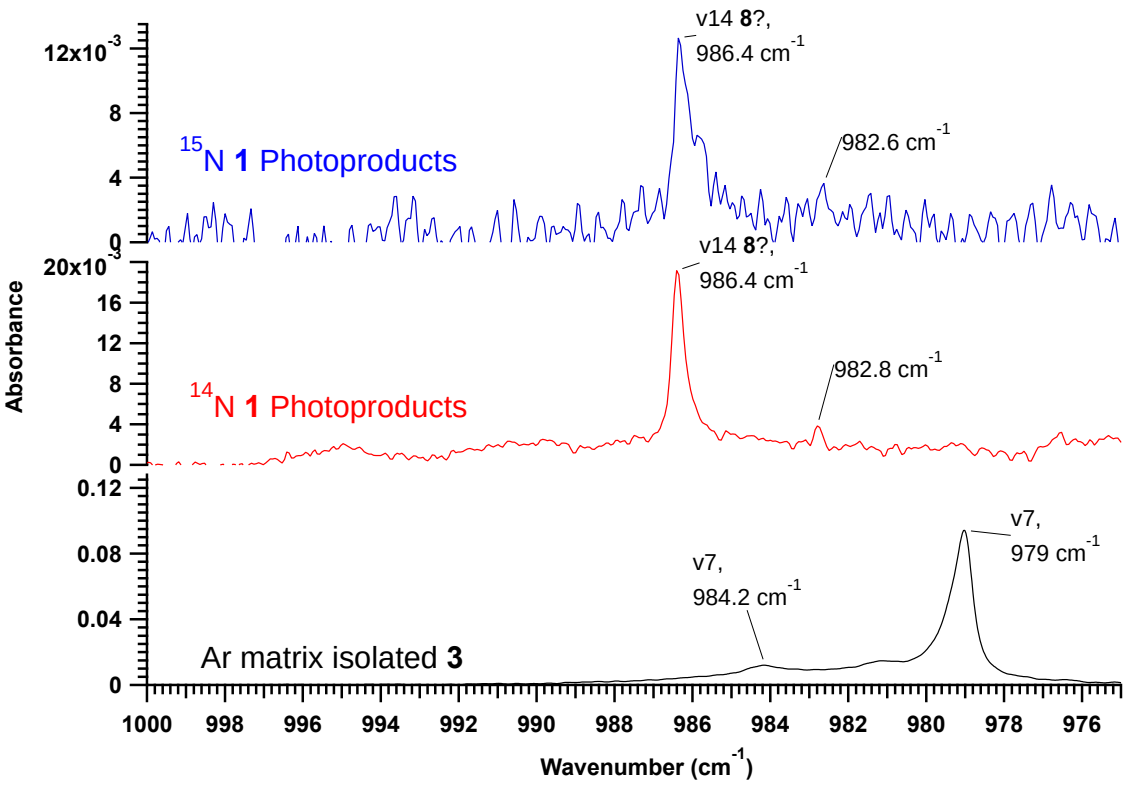

Fig. S22-Propargyl cyanide (**3**) standard (bottom trace) in Ar and as formed following photolysis of ^{14}N-**1** (1365 min, middle trace) and ^{15}N-**1** (741 min, top trace) using Ly-α (121.6 nm) radiation. Predicted ^{14}N-^{15}N frequency shift is -2 cm^{-1}. Calculated intensity is 5 km/mol.

Allenyl Isocyanide (6)

Although cyano/isocyano isomerization is one possible photolysis process in the matrix environment, it is difficult to prove formation of either allenyl isocyanide (**6**) or propargyl isocyanide (**10**) unambiguously from these experiments. Starting with **6**, a potential candidate for ν_3 can be found at 2135 cm^{-1} (see Table 4, main text) following photolysis of ^{14}N-**1** (Fig. 4, Column A, top, main text). A shifted feature can be found at 2097 cm^{-1} starting from ^{15}N-**1** and is pictured in Fig. S34 or S35, column A or Fig. S23. This gives an implied isotope shift of -37 cm^{-1}, close to the value of -38 cm^{-1} predicted by calculations. Evidence of a peak near 876 cm^{-1}, the value for ν_9 observed for authentic **6** isolated in Ar (Fig. 4, Column D, main text), also exists following Ly-α photolysis. This feature is very near the signal-to-noise limit and exhibits no isotope shift (with none expected), which argues for its belonging to **6**. Further evidence can be found for potential ν_8 bands near 948 cm^{-1} and 954 cm^{-1} (Fig. 4, Column C, main text and Fig. S25) which exhibit isotope shifts near -3 cm^{-1}, values close to what are predicted. Moving to the region near ν_{15}, there is no good evidence of a band belonging to **6** with the only visible features already assigned to **2** (Fig. 2, Column E, main text). There is no evidence of production of **6** using 193 nm or 248 nm light for photolysis.

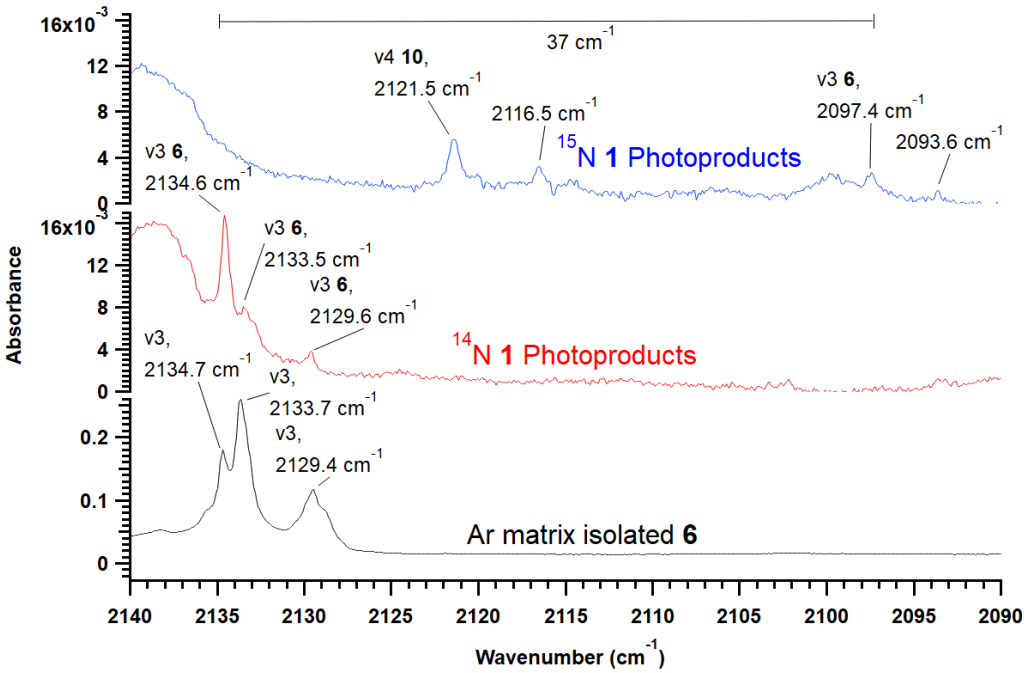

Fig. S23-Allenyl isocyanide (**6**) standard (bottom trace) in Ar and as formed following photolysis of ^{14}N-**1** (1365 min, middle trace) and ^{15}N-**1** (741 min, top trace) using Ly-α (121.6 nm) radiation. Predicted ^{14}N-^{15}N frequency shift is -38 cm^{-1}. Calculated intensity is 193 km/mol.

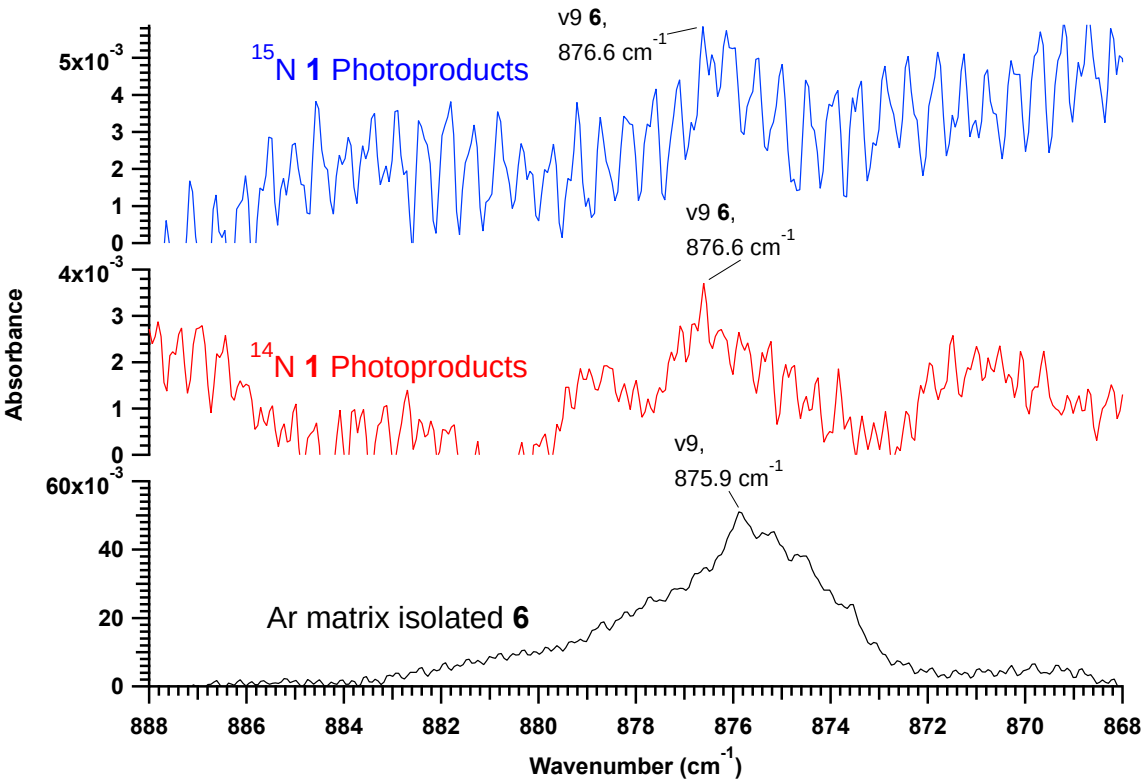

Fig. S24-Allenyl isocyanide (**6**) standard (bottom trace) in Ar and as formed following photolysis of ^{14}N-**1** (1365 min, middle trace) and ^{15}N-**1** (741 min, top trace) using Ly-α (121.6 nm) radiation. Predicted ^{14}N-^{15}N frequency shift is 0 cm^{-1}. Calculated intensity is 40 km/mol.

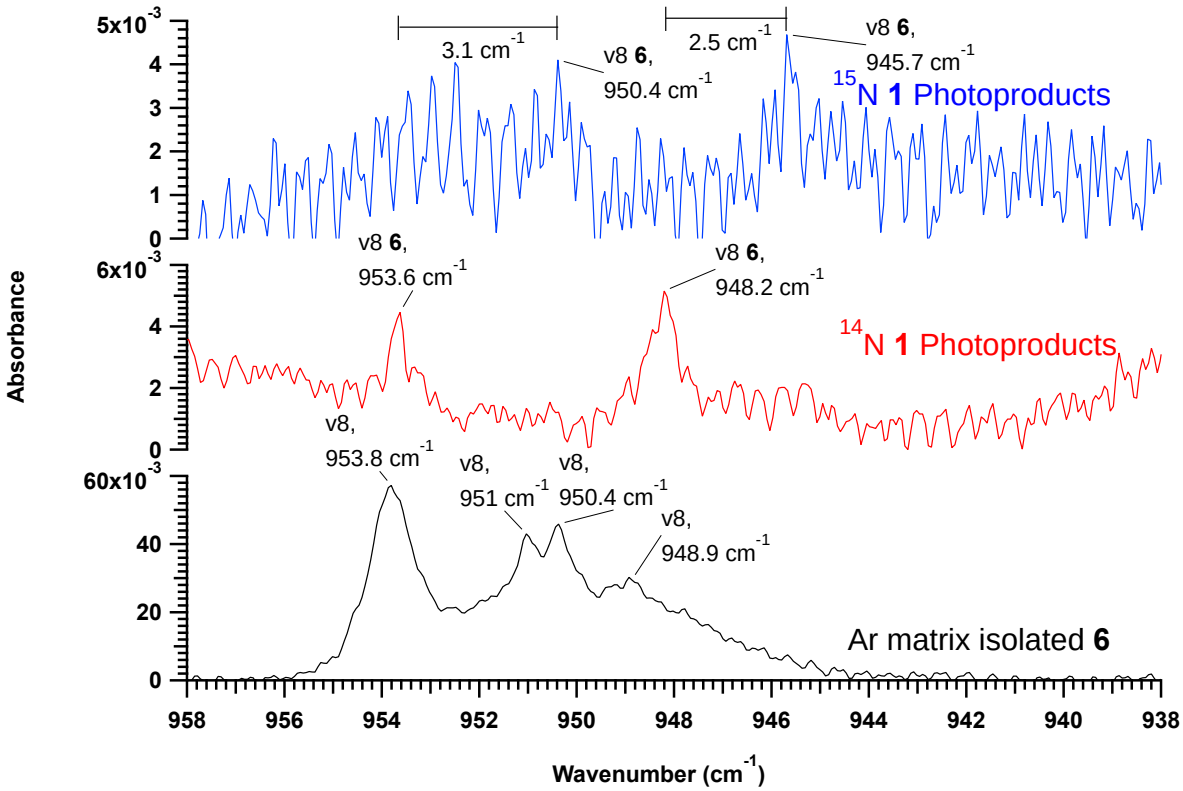

Fig. S25-Allenyl isocyanide (**6**) standard (bottom trace) in Ar and as formed following photolysis of ^{14}N-**1** (1365 min, middle trace) and ^{15}N-**1** (741 min, top trace) using Ly-α (121.6 nm) radiation. Predicted ^{14}N-^{15}N frequency shift is -3 cm^{-1}. Calculated intensity is 26 km/mol.

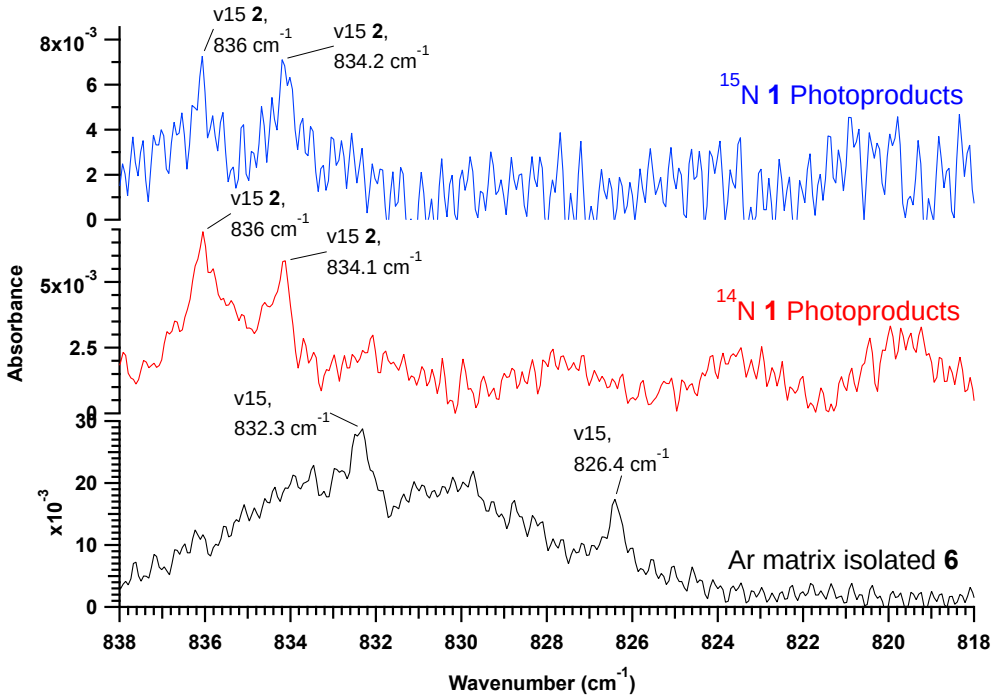

Fig. S26-Allenyl isocyanide (**6**) standard (bottom trace) in Ar and as formed following photolysis of ^{14}N-**1** (1365 min, middle trace) and ^{15}N-**1** (741 min, top trace) using Ly-α (121.6 nm) radiation. Predicted ^{14}N-^{15}N frequency shift is 0 cm^{-1}. Calculated intensity is 21 km/mol.

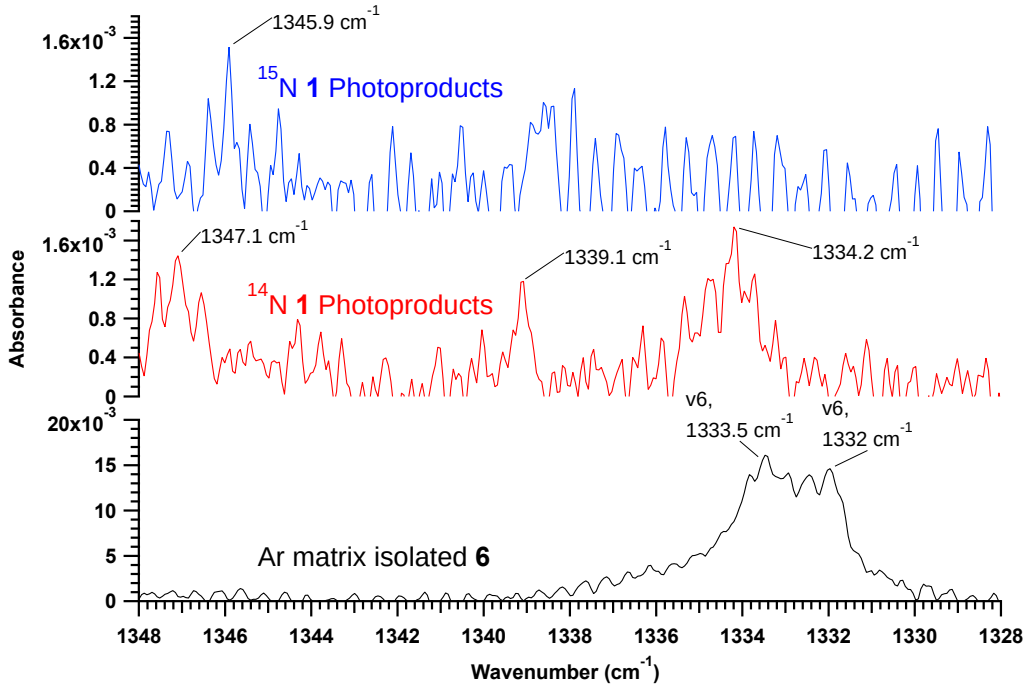

Fig. S27-Allenyl isocyanide (**6**) standard (bottom trace) in Ar and as formed following photolysis of ^{14}N-**1** (1365 min, middle trace) and ^{15}N-**1** (741 min, top trace) using Ly-α (121.6 nm) radiation. Predicted ^{14}N-^{15}N frequency shift is -1 cm^{-1}. Calculated intensity is 18 km/mol.

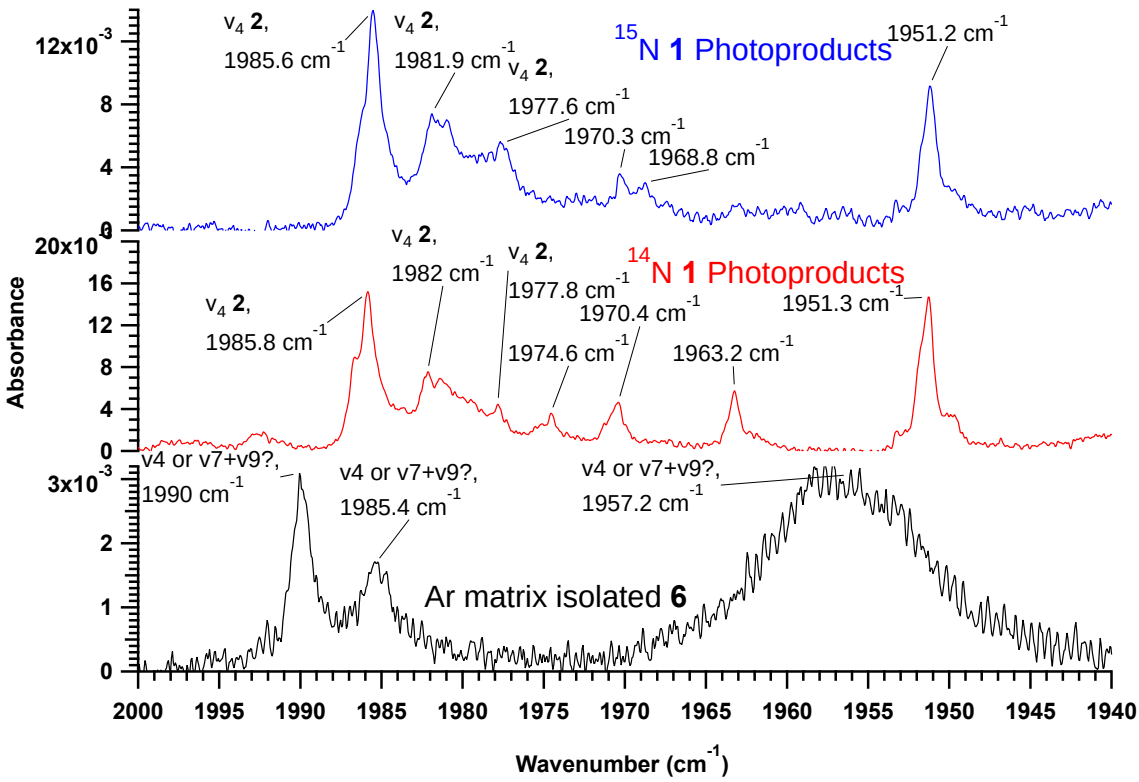

Fig. S28-Allenyl isocyanide (**6**) standard (bottom trace) in Ar and as formed following photolysis of ^{14}N-**1** (1365 min, middle trace) and ^{15}N-**1** (741 min, top trace) using Ly-α (121.6 nm) radiation. Predicted ^{14}N-^{15}N frequency shift (ν_4) is 0 cm^{-1}. Calculated intensity is 17 km/mol. Predicted ^{14}N-^{15}N frequency shift (ν_7+ν_9) is -1 cm^{-1}. Calculated intensity is 40 km/mol.

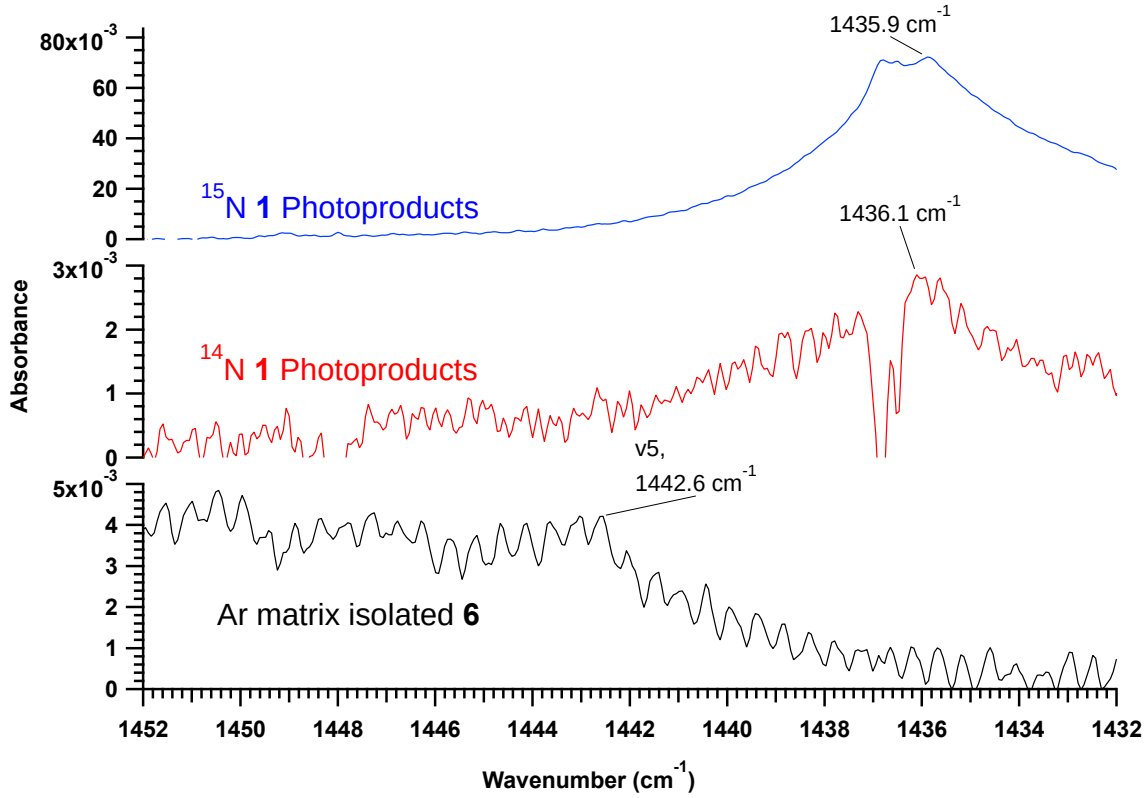

Fig. S29-Allenyl isocyanide (**6**) standard (bottom trace) in Ar and as formed following photolysis of ^{14}N-**1** (1365 min, middle trace) and ^{15}N-**1** (741 min, top trace) using Ly-α (121.6 nm) radiation. Predicted ^{14}N-^{15}N frequency shift is 0 cm^{-1}. Calculated intensity is 15 km/mol.

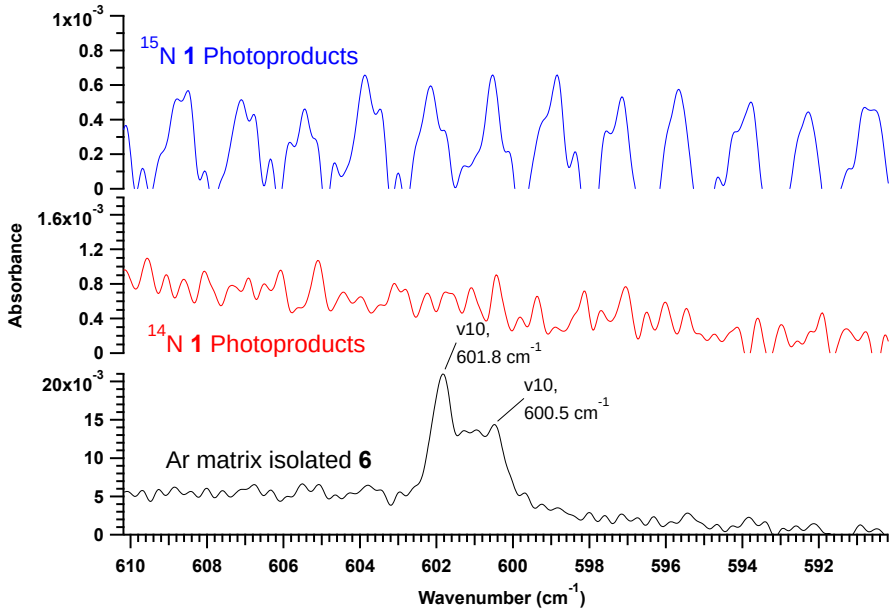

Fig. S30-Allenyl isocyanide (**6**) standard (bottom trace) in Ar and as formed following photolysis of ^{14}N-**1** (732 min, middle trace) and ^{15}N-**1** (240 min, top trace) using 193 nm radiation. Predicted ^{14}N-^{15}N frequency shift is -5 cm^{-1}. Calculated intensity is 10 km/mol.

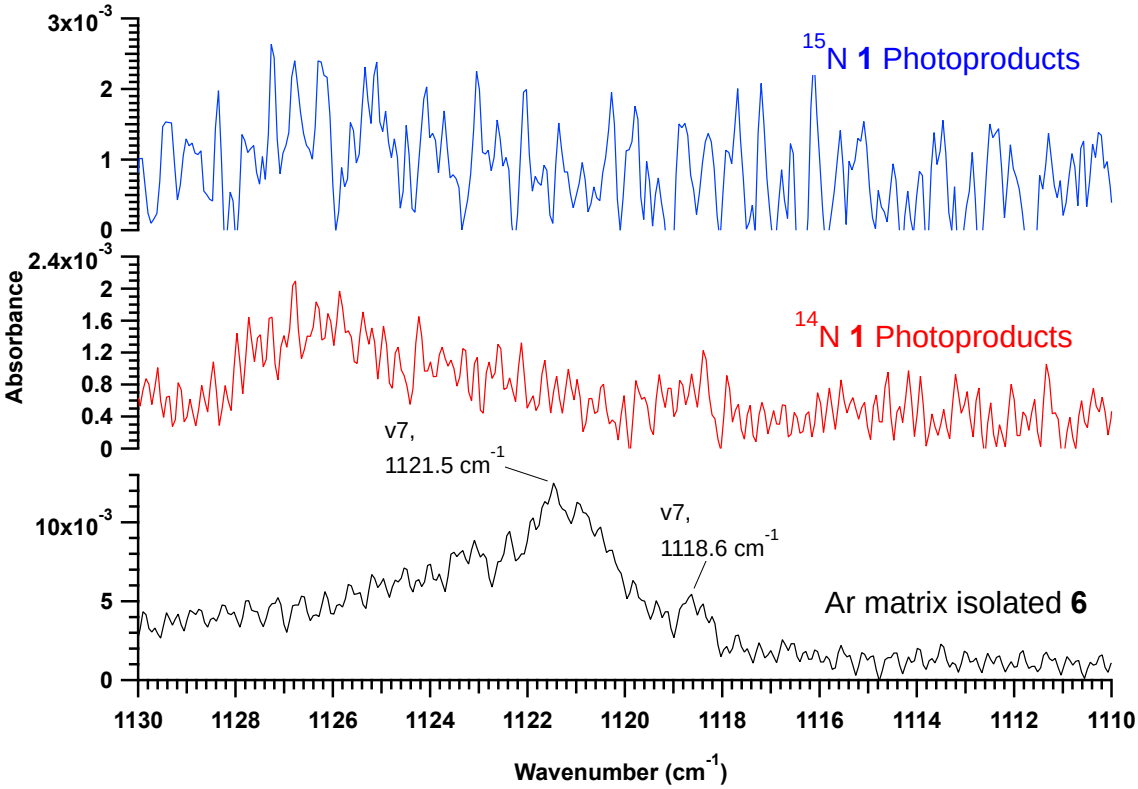

Fig. S31-Allenyl isocyanide (**6**) standard (bottom trace) in Ar and as formed following photolysis of ^{14}N-**1** (1365 min, middle trace) and ^{15}N-**1** (741 min, top trace) using Ly-α (121.6 nm) radiation. Predicted ^{14}N-^{15}N frequency shift is -1 cm^{-1}. Calculated intensity is 4 km/mol.

Propargyl isocyanide (10)

As the ν_1 mode of propargyl isocyanide (**10**) is obscured by the appearance of the strong ν_1 absorption of **3** (Fig. S33, S34, and S35, Column A), evidence for the production of **10** centers around the feature at 2160 cm^{-1} which is a candidate for the strongest band of this species (Fig. S33, S34 or S35, Column B and Fig. S37). This value is close to what is observed for ν_3 or ν_4 in the pure, matrix isolated chemical (Fig. S33, Column B, bottom) and approximately 21 cm^{-1} away from the predicted gas-phase value (Table S24). Based on recent gas-phase assignments of ν_3 and ν_4 of **10** by Benidar et al., ν_4 of **10** is centered at 2147 cm^{-1} and ν_3 at 2157 cm^{-1}. In matrix spectra, four peaks belonging to one or another of these fundamentals and reflecting a complicated site structure can be clearly discerned spanning 2147 to 2156 cm^{-1} (Fig. S33, Column B, bottom and Fig. S37). Although ν_4 and ν_3 have not been unambiguously identified in the matrix spectra, upon formation due to photolysis, only ν_4 is expected to be visible as it is predicted to have an intensity much higher than that of ν_3. Assuming a small shift due to its production as a photolysis product, the feature at 2160 cm^{-1} can be tentatively connected to one or more of the ν_3/ν_4 peaks between 2147 and 2156 cm^{-1}.

While not producible using 248 nm radiation, the feature at 2160 cm^{-1} can be generated with reasonable efficiency using both 193 nm radiation (Fig. S35, Column B) and Ly-α radiation (Figs. S33 and S34, Column B). This feature is not observed when using ^{15}N-**1** as a precursor and instead, a feature near 2122 cm^{-1} appears indicating a shift of -39 cm^{-1} (Figs. S34, Column B and S34, ESI). Calculations predict that the isotope shift for **10** should be -37 cm^{-1}, a value very close to what is measured for this pair. The connection between 2160 cm^{-1} and 2122 cm^{-1} was further confirmed by performing an experiment using an equimolar mixture of ^{14}N-**1** and ^{15}N-**1** precursors (Fig. S35, Column B, bottom). Photolysis at 193 nm of this mixture resulted in production of both peaks simultaneously and both exhibited the same time evolution (Fig. S36).

Potential C_4H_3N candidates for the 2160/2122 cm^{-1} isotopic pair can also be determined using the density functional predictions of energies, IR frequencies, and ^{14}N-to-^{15}N shifts for various isomers. Filtering this data for species which have an energy with respect to **1** of less than 200 kJ/mol in addition to having a mode with a ^{14}N-to-

^{15}N bathochromic shift of greater than -34 cm^{-1} and a position between 2100 and 2200 cm^{-1} leaves only **6**, **10**, or **13** (Tab. S25 and Fig. S32). Production of **6** has already been discussed and does not appear at 2160.0 cm^{-1}. Evidence arguing against production of **13**, the isocyano isomer of the cyclic compound **8,** hinges on the fact that little (or no) **8** was produced during photolysis. This leaves **10** as the most reasonable possibility. However, as no other band from this compound can be reliably identified (Fig. S33), its photochemical creation remains to be unambiguously proven.

Table S24. Main IR absorption bands for propargyl isocyanide (10) as theoretically predicted (harmonic approximation, frequencies scaled by 0.96) and experimentally observed. Relative intensities are given in parentheses. Empty entries were not detected. Ranges generally indicate the most intense features of a multiplet with possible weak features falling outside the range. Peak locations are rounded to the nearest wavenumber. See Appendix 3 for detailed Figs of these regions.

	Calculation			**Experiment**				
	B3LYP/aug-cc-pVTZ Vibrational frequency in cm^{-1} (Relative IR intensity)			**Experimental frequency in cm^{-1} (Relative IR intensity)**				
				Literature	**This Work**			
	Literature[21]	**This Work**		**Gas[23]**	**Ar Matrix**	**Ar Matrix From $CH_3C_3{}^{14}N$ phot.**	**Ar Matrix From $CH_3C_3{}^{15}N$ phot.**	
	^{14}N [a]	**^{15}N**	**^{14}N-^{15}N freq. shift**	**^{14}N**	**^{14}N [b]**	**^{14}N**	**^{15}N**	**^{14}N-^{15}N freq. shift**
ν_4	2139 (100)	2101	-37	2147	2156-2147 (100)[d]	2160	2122	-39
ν_1	3329 (39)	3329	0	3332	3332-3318 (66)	3332-3327[c]	3332-3327[c]	
ν_6	1321 (27)	1321	0	1350	1347-1345 (38)			
ν_{16}	657 (26)	657	0	645	645-641 (23)			
ν_9	691 (20)	691	0	667	672 (20)			
ν_7	955 (17)	953	-1	989	984 (20)			
ν_8	876 (11)	874	-2	908	906-902 (26)			
ν_3	2150 (11)	2149	-1	2157	---[d]			
ν_5	1415 (5)	1415	0	1446	1442-1440 (1)[e]			

[a]Relative to ν_4 with a value of 171 km/mol.

[b]Relative intensities in this table are lower limit as ν_3 and ν_4 cannot be distinguished.

[c]Overlap with strong bands from **3** prevent identification.

[d]Contribution from ν_4 and ν_3 cannot be separated.

[e]Assignment tentative due to nearby combination $\nu 8+\nu 10$[23]

Table S25-C_4H_3N isomers featuring the largest ^{14}N-to-^{15}N IR band shifts (see text). Results of B3LYP/aug-cc-pVTZ predictions. Isomer numbering according to Custer et al 2016[21]. See Fig. S2 for the isomeric structures.

Species	mode	^{14}N (cm^{-1})	^{15}N (cm^{-1})	Shift (cm^{-1})	Intensity (km/mol)
6	ν_3	2110	2071	-38	193.0
9	ν_3	2059.7	2025	-35	134
10	ν_4	2139	2101	-37	170.5
13	ν_4	2115.3	2077.9	-37.4	161.1
15	ν_5	1953.2	1915.3	-37.9	270.6
16	ν_3	2096.2	2057.7	-38.5	172.8
18	ν_5	1916.2	1876.4	-39.8	426.7
34	ν_4	1918.2	1884.1	-34.1	237.1
37	ν_4	1908.7	1874.5	-34.2	173.8
39	ν_2	2270.2	2234.5	-35.7	448.9
48	ν_4	2132.1	2093.8	-38.3	202.9
50	ν_4	2105.4	2066.7	-38.7	142.2

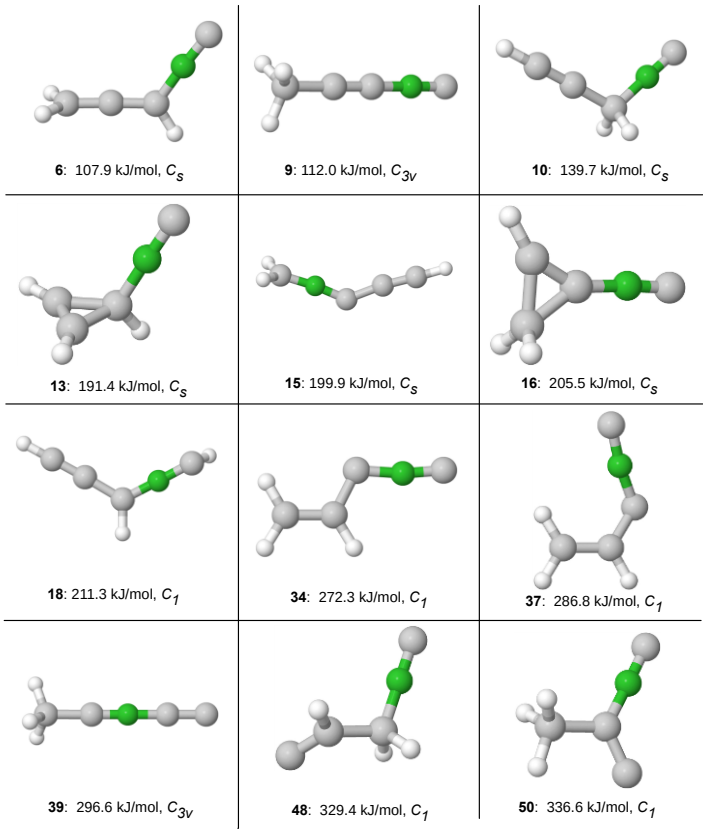

Fig. S32-structures of species corresponding to Table S24.

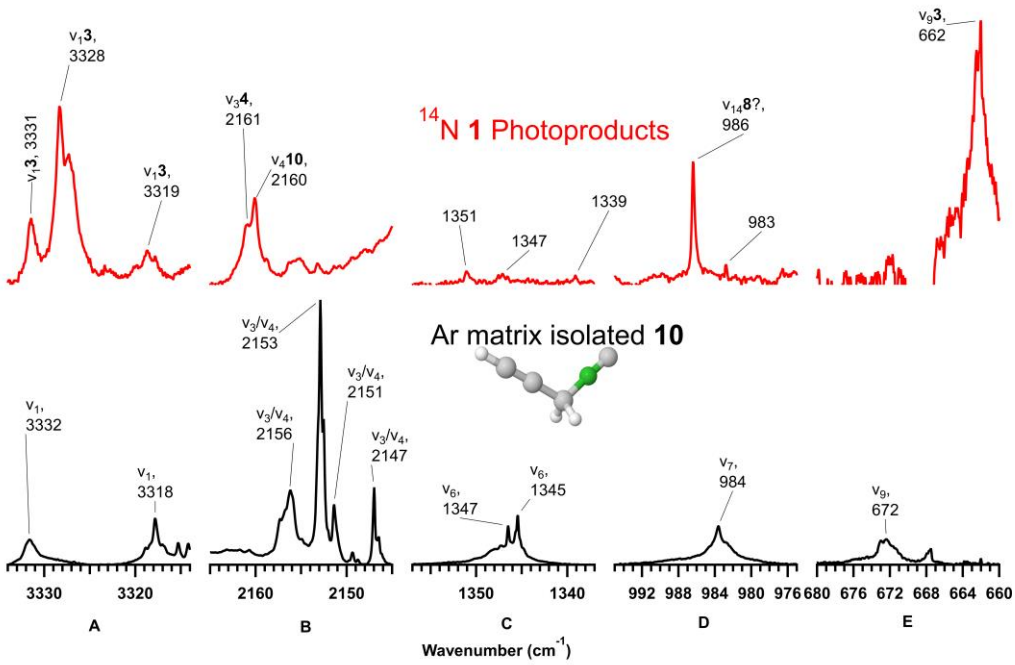

Fig. S33-Top: difference spectrum showing irradiation of ^{14}N-**1** in an Ar matrix (Ly-α, 121.6 nm, ~23h) using the unphotolyzed, freshly deposited **1** in Ar as background. Bottom: freshly deposited, Ar matrix isolated **10** for the regions surrounding bands of highest intensity for **10**. Bands assigned to **10** are indicated. Absorbance scale for all columns in a given row are identical and baselines shifted to allow direct visual intercomparison of intensities.

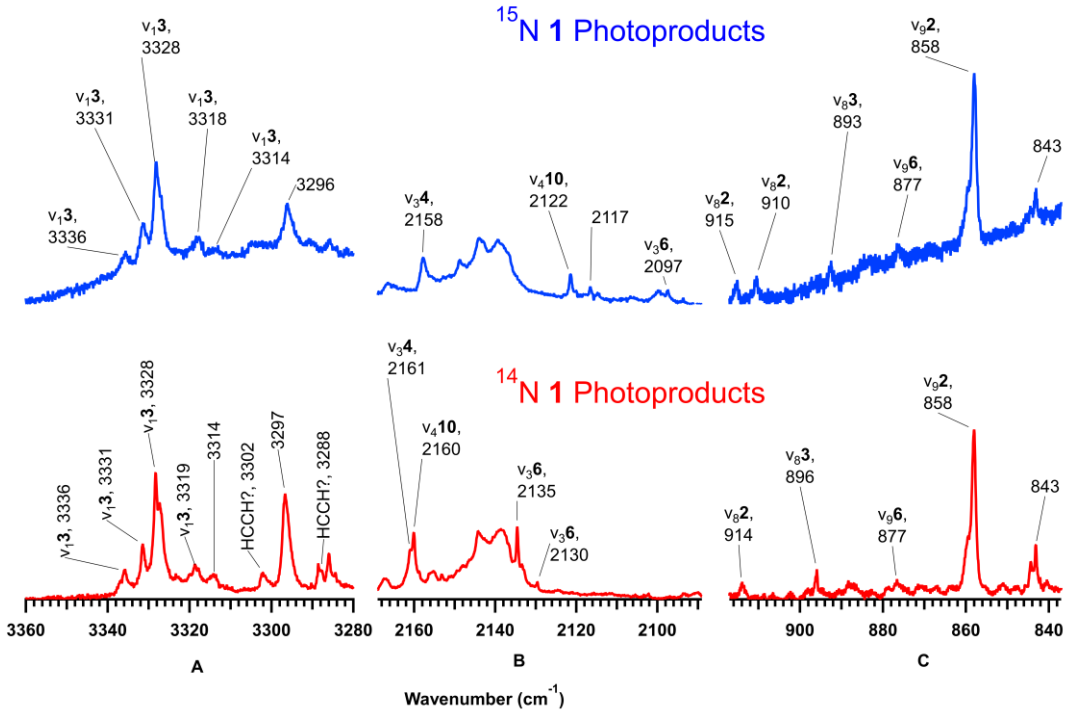

Fig. S34-Expanded view of Fig. 10, columns A and D, as well as Fig. 11, Column A. Bottom: product bands observed upon Ly-α (121.6 nm, ~23h) photolysis of ^{14}N-**1**. Top: product bands observed upon Ly-α (121.6 nm, ~12h) photolysis of ^{15}N-**1**. Absorbance scale for all columns in a given row are identical and baselines shifted to allow direct visual intercomparison of intensities.

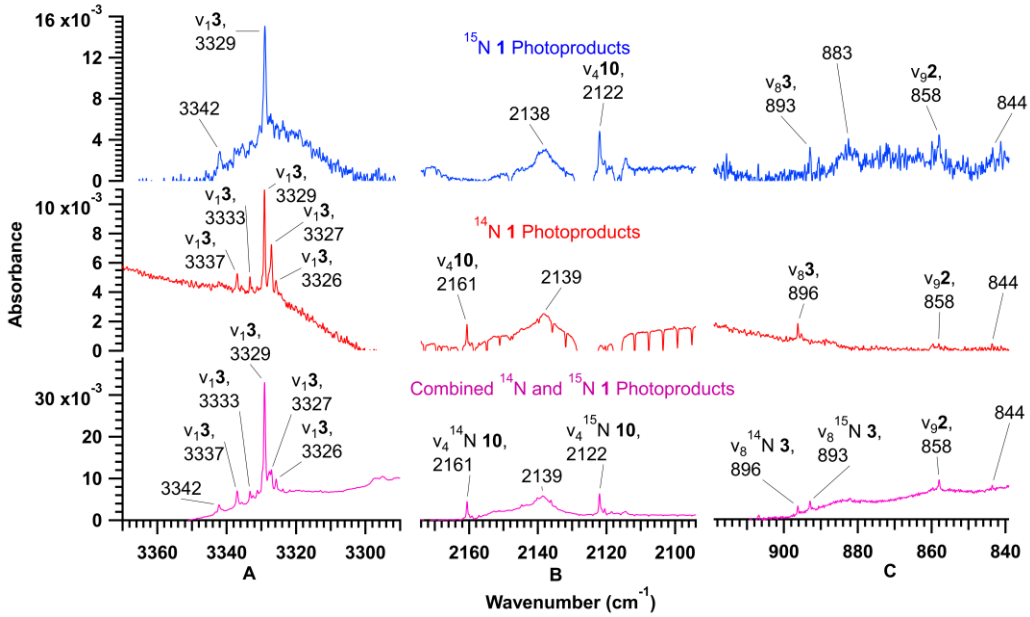

Fig. S35-Expanded view depicting compounds produced upon photolysis of ^{15}N-**1** (top), ^{14}N-**1** (middle), and a mixture of ^{14}N-**1**/^{15}N-**1** (bottom) using 193 nm laser radiation. Irradiation conditions: exposure to 10 Hz pulses of ~0.2 mJ/cm^2 for 360 min (bottom), ~0.1 mJ/cm^2 for 732 min (middle), 0.3 mJ/cm^2 for 380 min (top).

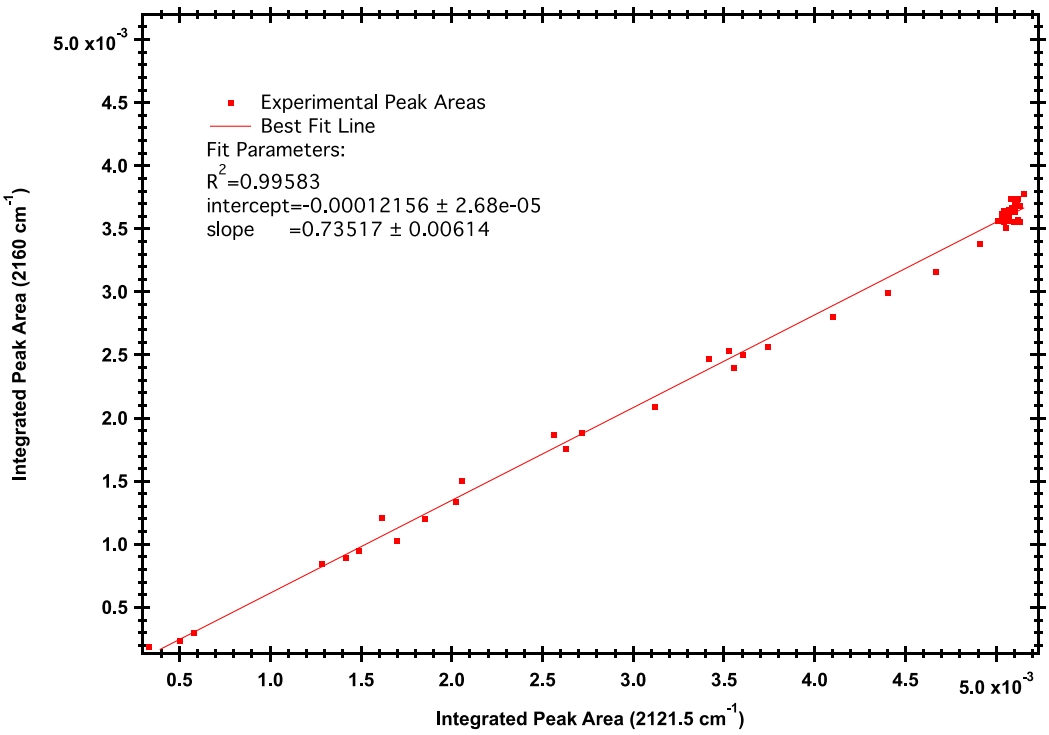

Fig. S36-Correlation between integrated intensities of bands located at 2160 and 2121.5 cm^{-1} provisionally assigned to isomer **10** produced upon irradiation of a mixture of ^{14}N-**1** and ^{15}N-**1** with 193 nm light.

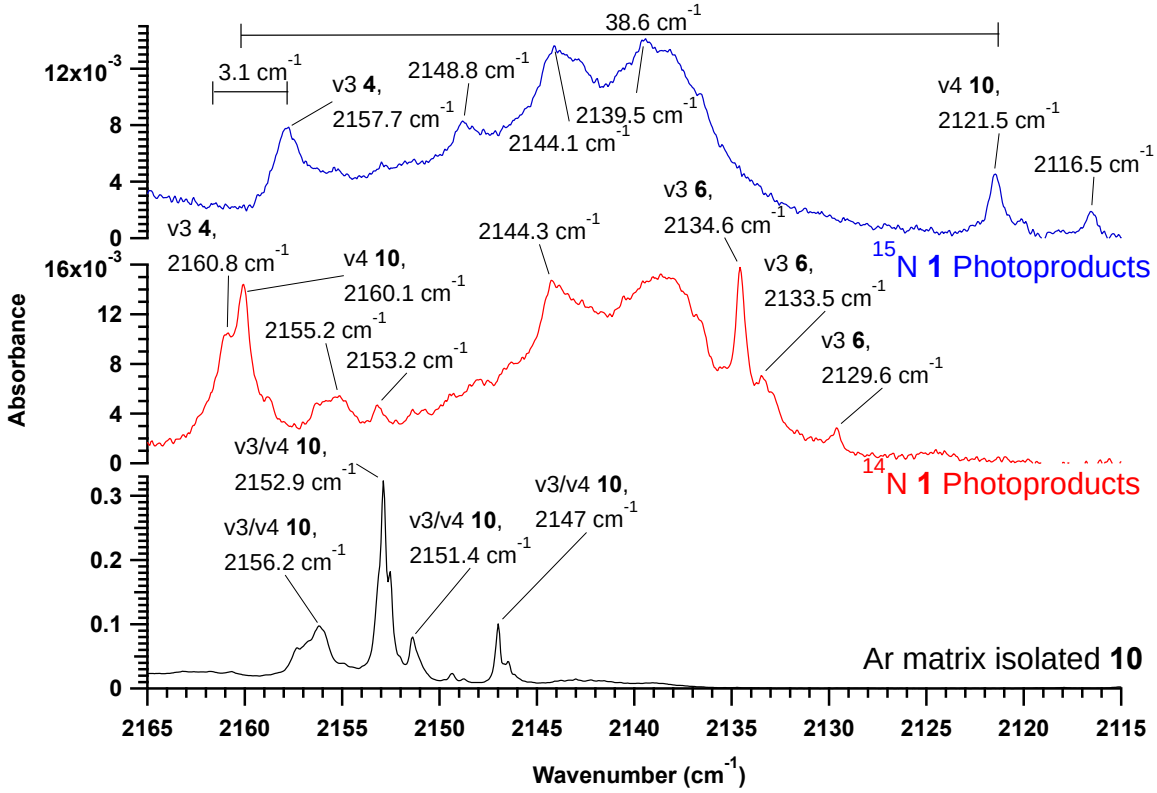

Fig. S37-Propargyl isocyanide (**10**) standard (bottom trace) in Ar and as formed following photolysis of ^{14}N-**1** (1365 min, middle trace) and ^{15}N-**1** (741 min, top trace) using Ly-α (121.6 nm) radiation. Predicted ^{14}N-^{15}N frequency shift (ν_4 of **10**) is -37 cm^{-1}. Calculated intensity is 171 km/mol. Predicted ^{14}N-^{15}N frequency shift (ν_3 of **4**) is -3 cm^{-1}. Calculated intensity is 1444 km/mol.

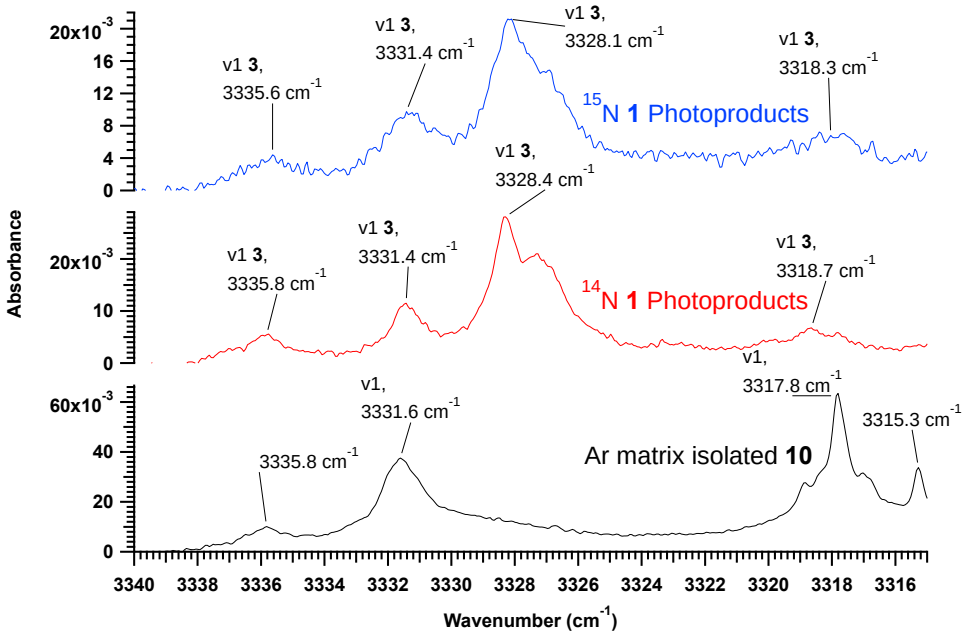

Fig. S38-Propargyl isocyanide (**10**) standard (bottom trace) in Ar and as formed following photolysis of ^{14}N-**1** (1365 min, middle trace) and ^{15}N-**1** (741 min, top trace) using Ly-α (121.6 nm) radiation. Predicted ^{14}N-^{15}N frequency shift is 0 cm^{-1}. Calculated intensity is 57 km/mol.

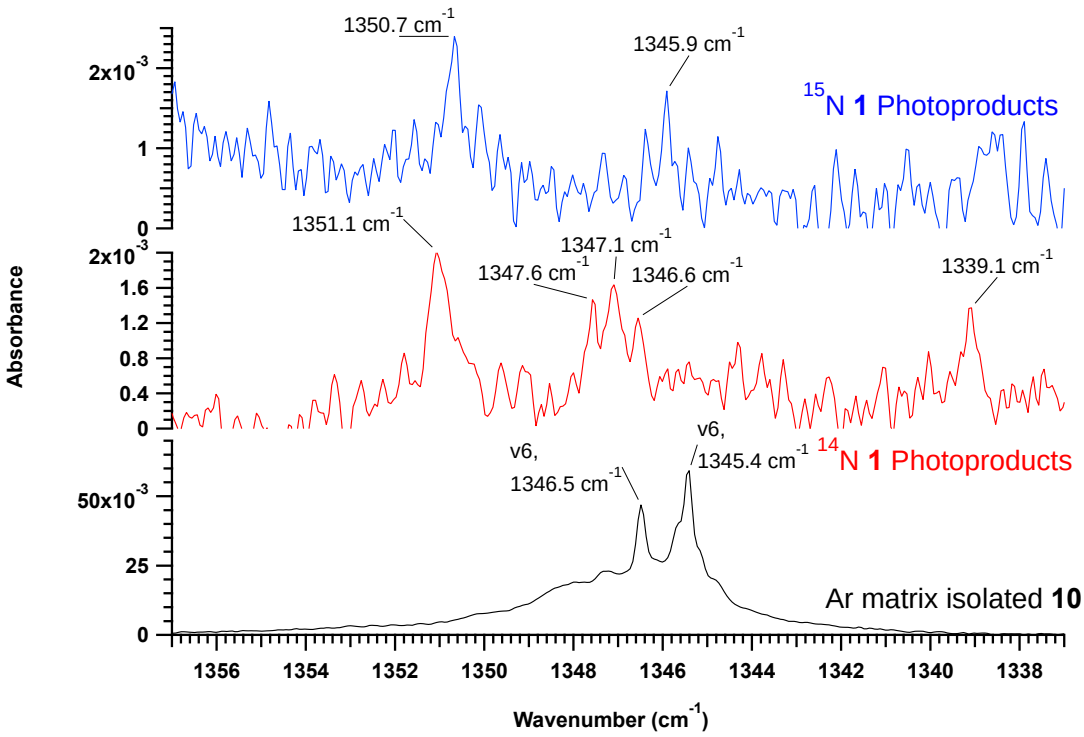

Fig. S39-Propargyl isocyanide (**10**) standard (bottom trace) in Ar and as formed following photolysis of ^{14}N-**1** (1365 min, middle trace) and ^{15}N-**1** (741 min, top trace) using Ly-α (121.6 nm) radiation. Predicted ^{14}N-^{15}N frequency shift is 0 cm^{-1}. Calculated intensity is 46 km/mol.

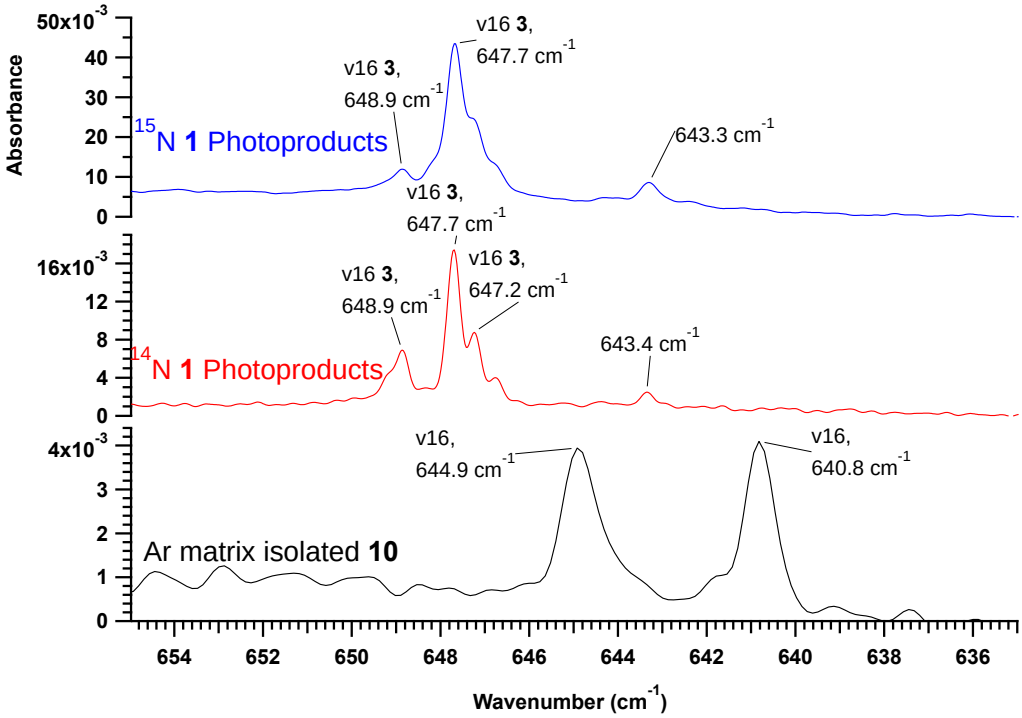

Fig. S40-Propargyl isocyanide (**10**) standard (bottom trace) in Ar and as formed following photolysis of ^{14}N-**1** (732 min, middle trace) and ^{15}N-**1** (240 min, top trace) using 193 nm radiation. Predicted ^{14}N-^{15}N frequency shift is -2 cm^{-1}. Calculated intensity is 45 km/mol.

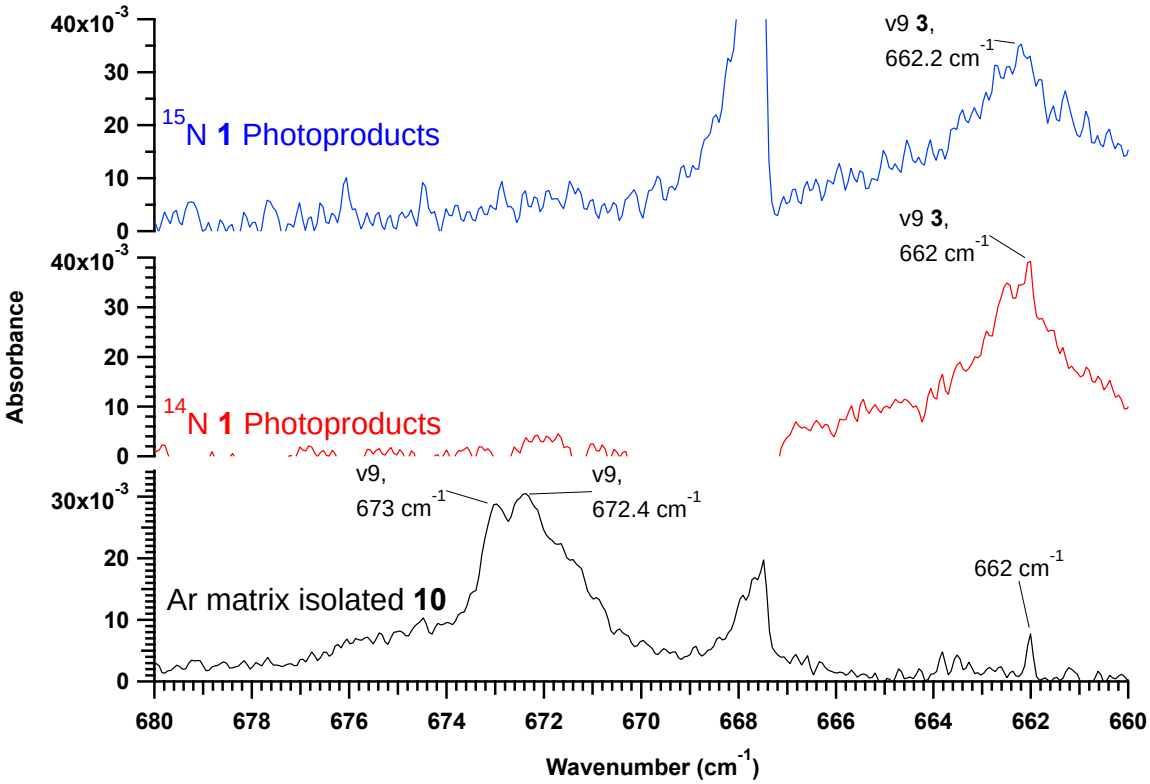

Fig. S41-Propargyl isocyanide (**10**) standard (bottom trace) in Ar and as formed following photolysis of ^{14}N-**1** (1365 min, middle trace) and ^{15}N-**1** (741 min, top trace) using Ly-α (121.6 nm) radiation. Predicted ^{14}N-^{15}N frequency shift is 0 cm^{-1}. Calculated intensity is 35 km/mol.

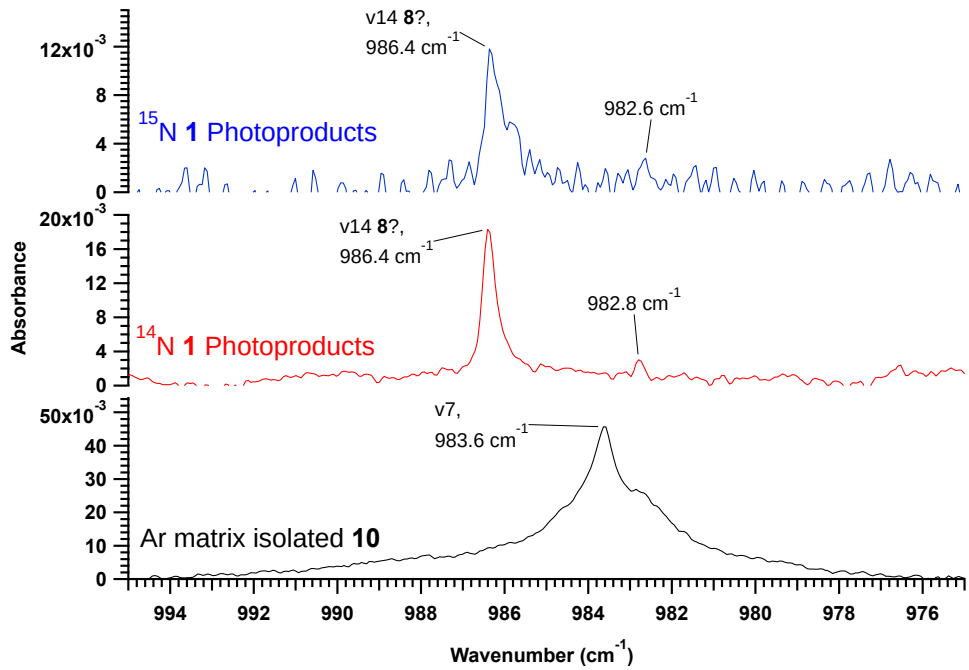

Fig. S42-Propargyl isocyanide (**10**) standard (bottom trace) in Ar and as formed following photolysis of ^{14}N-**1** (1365 min, middle trace) and ^{15}N-**1** (741 min, top trace) using Ly-α (121.6 nm) radiation. Predicted ^{14}N-^{15}N frequency shift is -1 cm^{-1}. Calculated intensity is 29 km/mol.

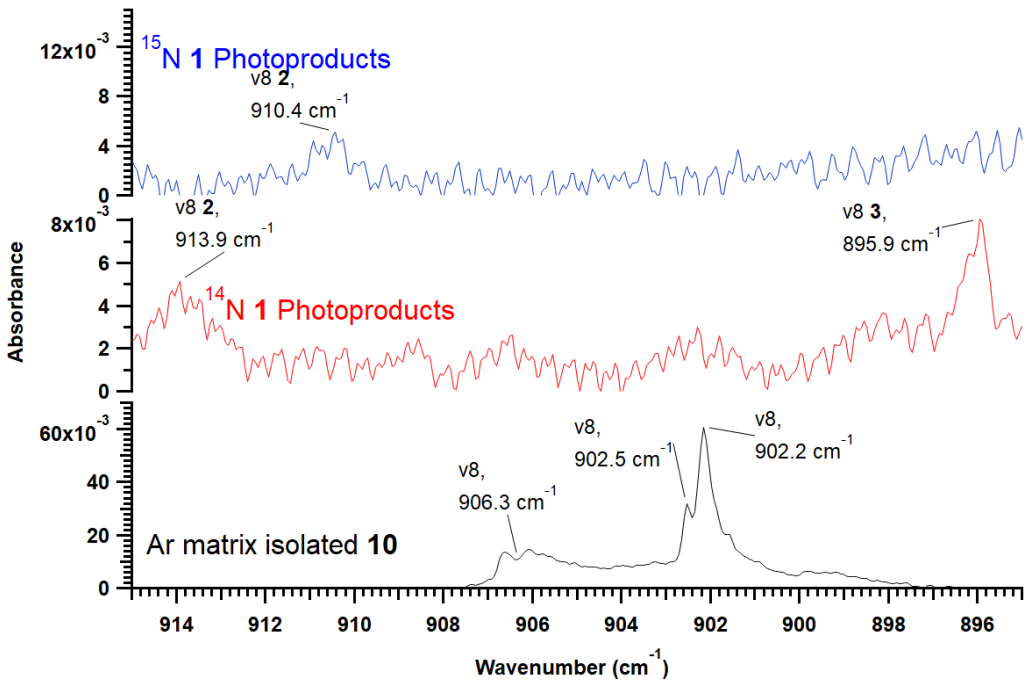

Fig. S43-Propargyl isocyanide (**10**) standard (bottom trace) in Ar and as formed following photolysis of ^{14}N-**1** (1365 min, middle trace) and ^{15}N-**1** (741 min, top trace) using Ly-α (121.6 nm) radiation. Predicted ^{14}N-^{15}N frequency shift is -2 cm^{-1}. Calculated intensity is 19 km/mol.

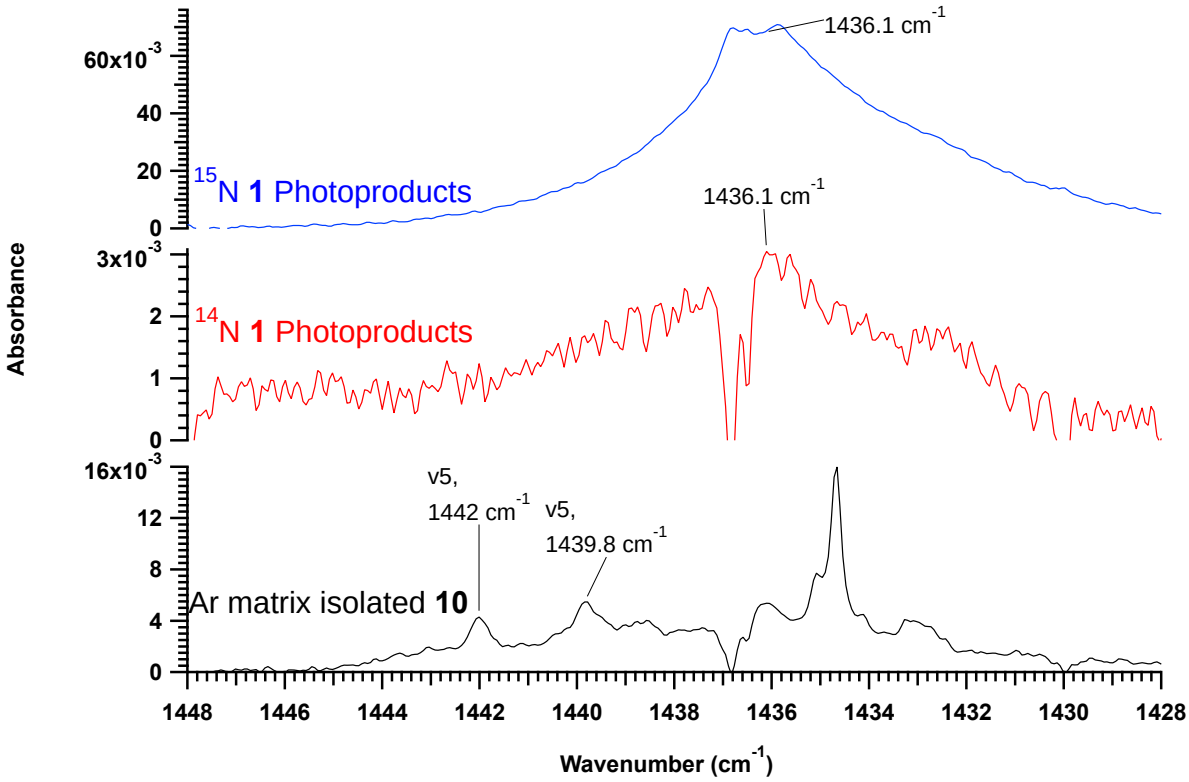

Fig. S44-Propargyl isocyanide (**10**) standard (bottom trace) in Ar and as formed following photolysis of ^{14}N-**1** (1365 min, middle trace) and ^{15}N-**1** (741 min, top trace) using Ly-α (121.6 nm) radiation. Predicted ^{14}N-^{15}N frequency shift is 0 cm^{-1}. Calculated intensity is 8 km/mol.

1,2,3-butatrien-1-imine (4)

Isomer **4**, CH_2CCCNH, is more stable than any of the three lowest-energy isonitriles on the C_4H_3N PES (Fig. 1) according to calculations. The only potential trace of **4** in this data consists of a shoulder on the peak at 2160 cm^{-1} for the most intense band of this molecule (Fig. 12, middle column, calculated intensity of 1444 km/mol) that was only visible following 121.6 nm photolysis. A partner band observed following photolysis of ^{15}N-**1** appearing at 2157.9 cm^{-1} (a shift of 3.1 cm^{-1}) is consistent with what is predicted for this species (3 cm^{-1}). There are several additional bands of **4** expected to have reasonable intensities including ν_7 (falling near 941 cm^{-1} and having an intensity of 435 km/mol), ν_5 (falling near 1448 cm^{-1} and having an intensity of 100 km/mol), ν_8 (falling near 757 cm^{-1} and having an intensity of 66 km/mol), and ν_1 (falling near 3342 cm^{-1} and 45 km/mol) (See Figs S42 to S48, ESI). While candidates exist for ν_7, there is no good evidence for any of the other bands of isomer **4** making this attribution quite tentative.

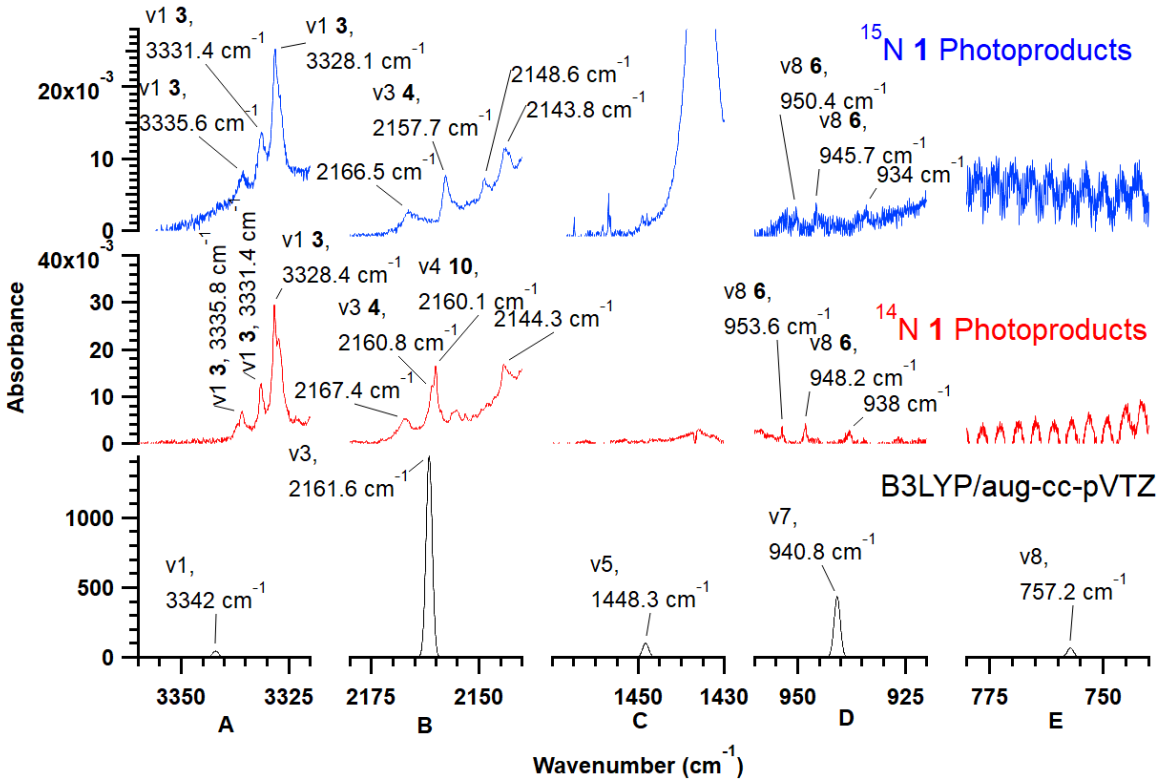

Fig. S45-1,2,3-butatrien-1-imine (**4**) theoretical spectrum (peak position and maximum are B3LYP/aug-cc-pVTZ frequency and intensity) (bottom trace) along with spectra following photolysis of ^{14}N-**1** (1365 min, middle trace) and ^{15}N-**1** (741 min, top trace) using Ly-α (121.6 nm) radiation. Only one possible assignment exists for ν_3 which is partially obscured by a band from ν_4 of **10**. No evidence of this peak can be seen for 193 nm or 248 nm photolysis experiments.

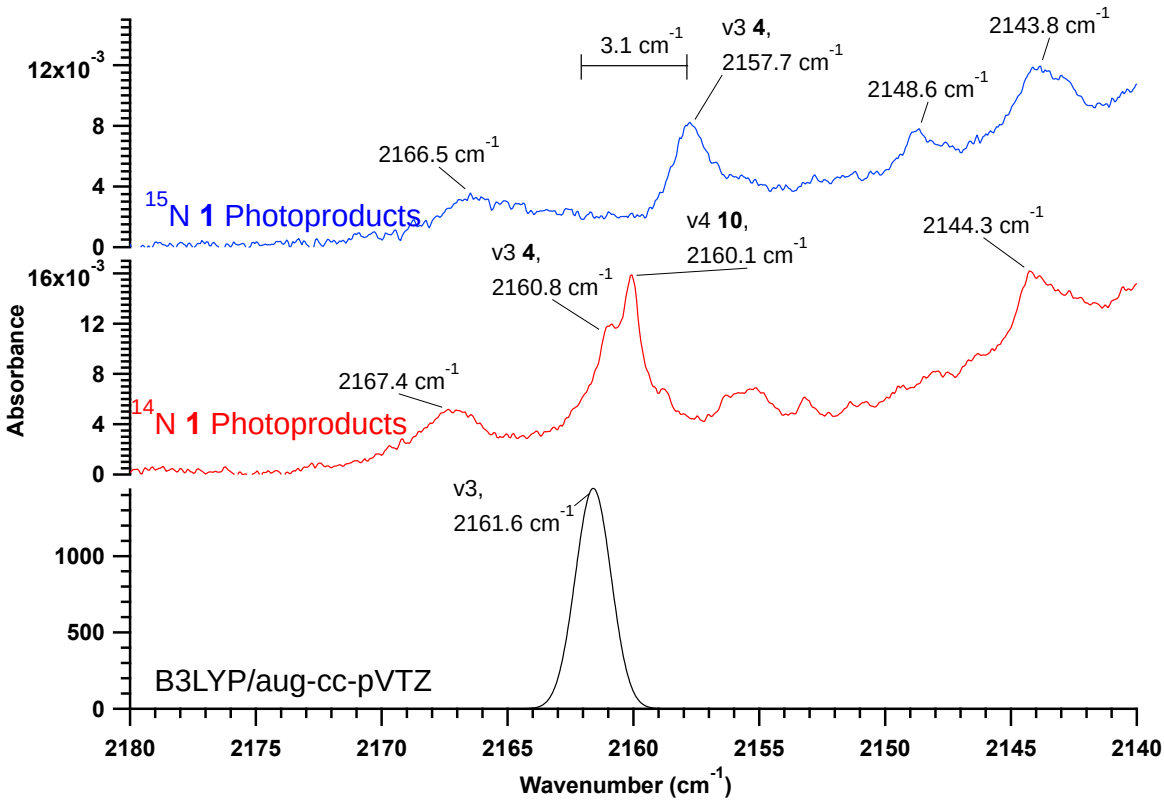

Fig. S46-1,2,3-butatrien-1-imine (**4**) theoretical spectrum (peak position and maximum are B3LYP/aug-cc-pVTZ frequency and intensity) (bottom trace) along with spectra following photolysis of ^{14}N-**1** (1365 min, middle trace) and ^{15}N-**1** (741 min, top trace) using Ly-α (121.6 nm) radiation. Only one possible assignment exists for ν_3 which is partially obscured by a band from ν_4 of **10**. No evidence of this peak can be seen for 193 nm or 248 nm photolysis experiments. Predicted ^{14}N-^{15}N frequency shift is -2.7 cm^{-1}. Calculated intensity is 1444 km/mol.

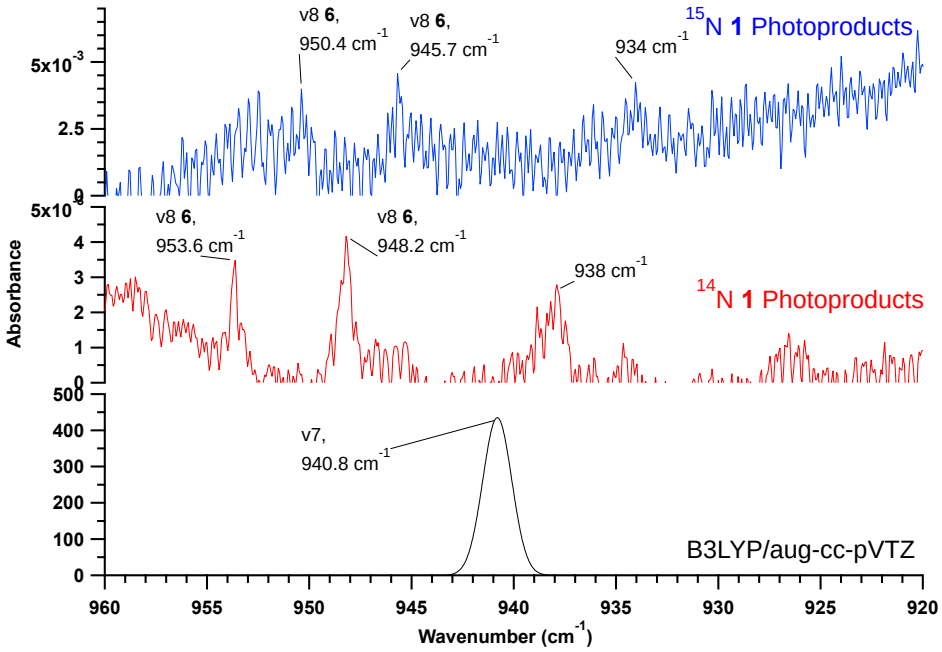

Fig. S47-1,2,3-butatrien-1-imine (**4**) theoretical spectrum (peak position and maximum are B3LYP/aug-cc-pVTZ frequency and intensity) (bottom trace) along with spectra following photolysis of ^{14}N-**1** (1365 min, middle trace) and ^{15}N-**1** (741 min, top trace) using Ly-α (121.6 nm) radiation. Predicted ^{14}N-^{15}N frequency shift is -5.7 cm^{-1}. Calculated intensity is 435 km/mol.

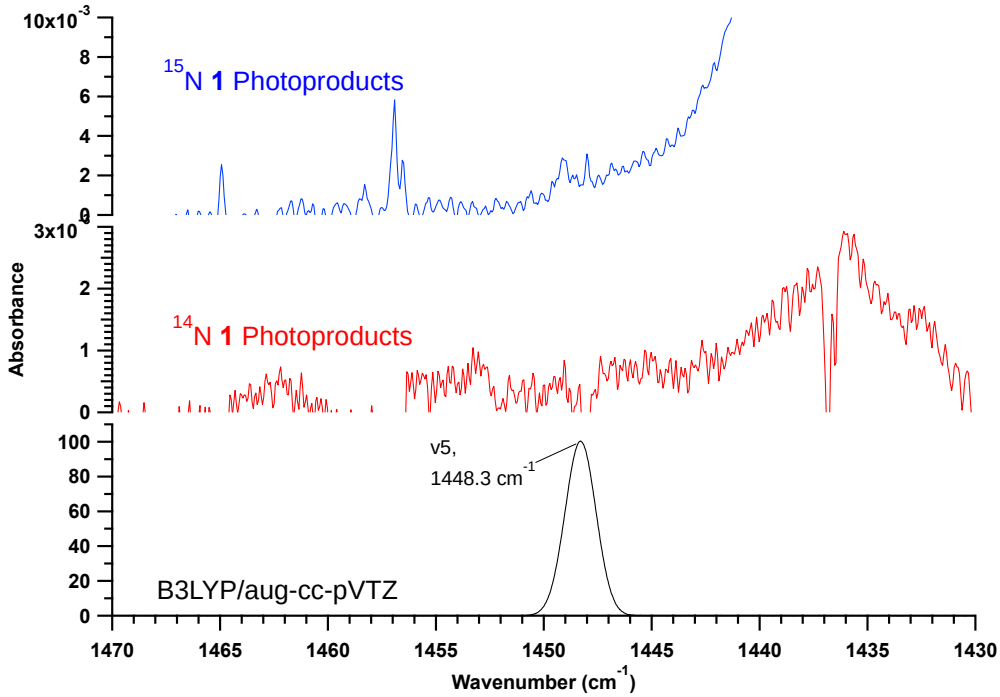

Fig. S48-1,2,3-butatrien-1-imine (**4**) theoretical spectrum (peak position and maximum are B3LYP/aug-cc-pVTZ frequency and intensity) (bottom trace) along with spectra following photolysis of ^{14}N-**1** (1365 min, middle trace) and ^{15}N-**1** (741 min, top trace) using Ly-α (121.6 nm) radiation. Predicted ^{14}N-^{15}N frequency shift is -6.1 cm^{-1}. Calculated intensity is 100 km/mol.

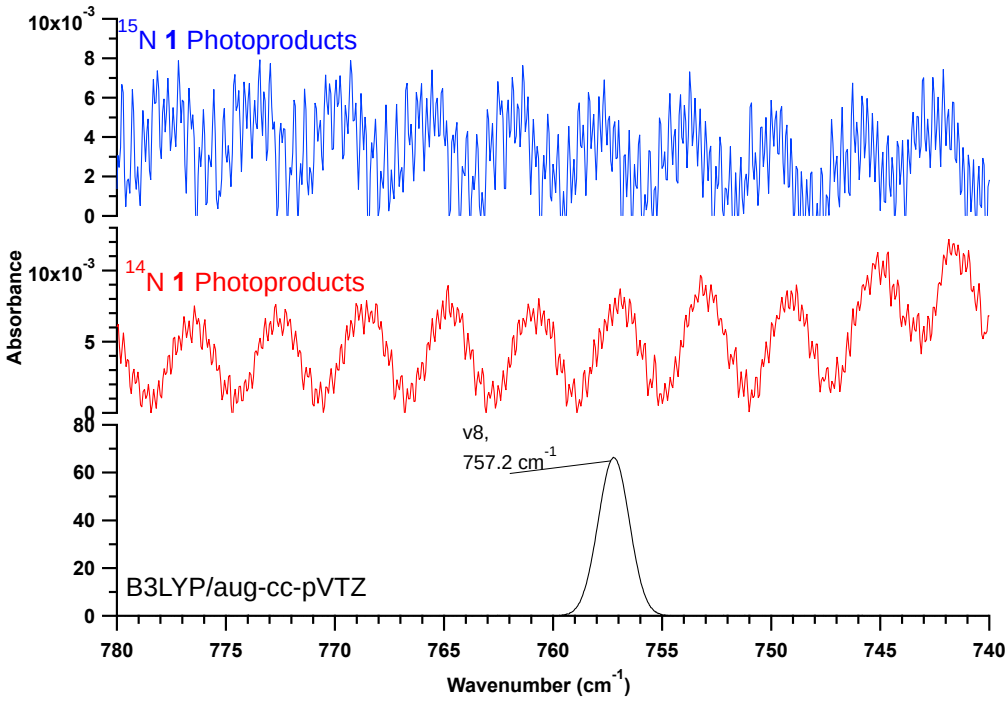

Fig. S49-1,2,3-butatrien-1-imine (**4**) theoretical spectrum (peak position and maximum are B3LYP/aug-cc-pVTZ frequency and intensity) (bottom trace) along with spectra following photolysis of ^{14}N-**1** (1365 min, middle trace) and ^{15}N-**1** (741 min, top trace) using Ly-α (121.6 nm) radiation. Predicted ^{14}N-^{15}N frequency shift is 0 cm^{-1}. Calculated intensity is 66 km/mol.

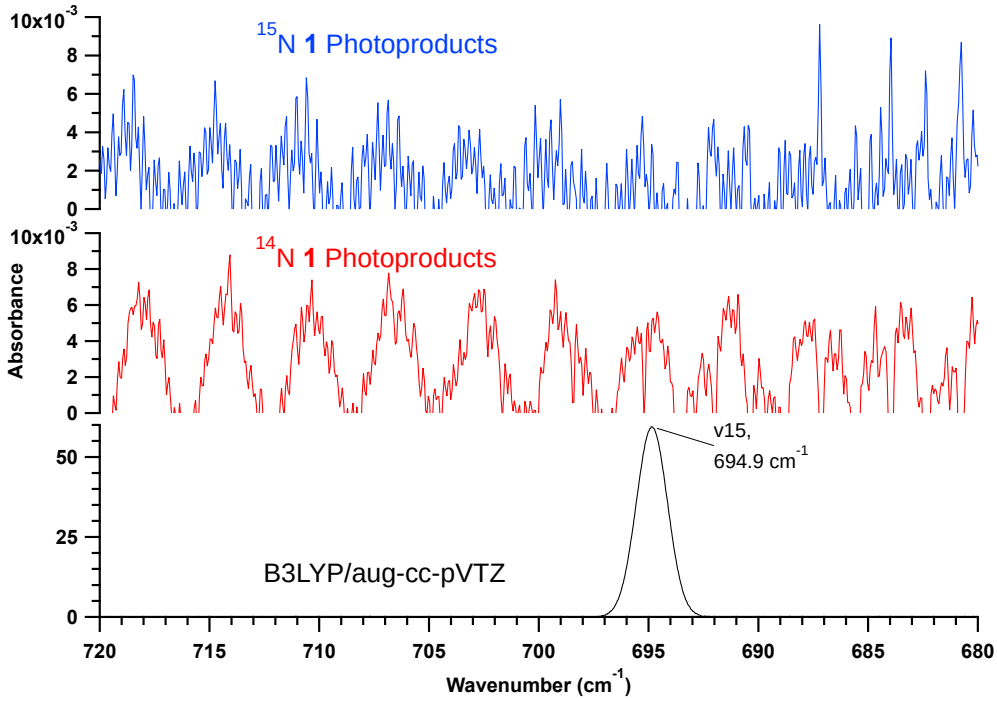

Fig. S50-1,2,3-butatrien-1-imine (**4**) theoretical spectrum (peak position and maximum are B3LYP/aug-cc-pVTZ frequency and intensity) (bottom trace) along with spectra following photolysis of ^{14}N-**1** (1365 min, middle trace) and ^{15}N-**1** (741 min, top trace) using Ly-α (121.6 nm) radiation. Predicted ^{14}N-^{15}N frequency shift is -2 cm^{-1}. Calculated intensity is 59 km/mol.

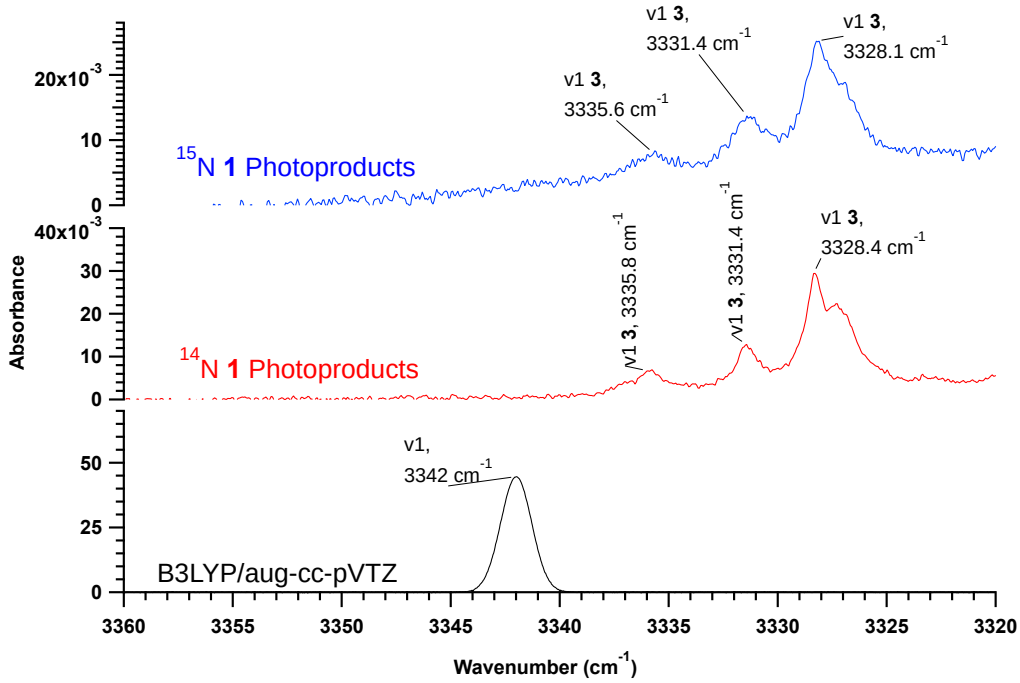

Fig. S51-1,2,3-butatrien-1-imine (**4**) theoretical spectrum (peak position and maximum are B3LYP/aug-cc-pVTZ frequency and intensity) (bottom trace) along with spectra following photolysis of ^{14}N-**1** (1365 min, middle trace) and ^{15}N-**1** (741 min, top trace) using Ly-α (121.6 nm) radiation. Predicted ^{14}N-^{15}N frequency shift is -7.6 cm^{-1}. Calculated intensity is 45 km/mol.

1-isocyano-1-propyne (9)

In addition to the isocyano species **6** and **10** which have already been discussed, additional effort was also expended to search for 1-isocyano-1-propyne (**9**). Gas-phase vibrational frequencies are available for **9** in the literature[24] which, in conjunction with the theoretical predictions, help to more narrowly constrain expected frequencies in a matrix (Figs S52 to S56). While a number of candidates for ν_3 falling within 10 cm^{-1} of its measured gas-phase band center (2083 cm^{-1}) might be postulated, it is difficult to unambiguously associate any one of these with a ^{15}N partner having a shift of -35 cm^{-1}. The congested nature of this region and small peak intensities makes integration as a function of time problematic and this strategy does not provide any additional information. Modes ν_8 and ν_1 should not exhibit any isotopic shift, but there are no promising features falling near their gas-phase band centers (1447.9 and 2941 cm^{-1} respectively) that can be considered as strong candidates. No further evidence for this species was observed during photolysis at 193 nm or 248 nm or employing a mixture of ^{14}N-**1** and ^{15}N-**1** as a starting material. Although chemical intuition might lead one to expect formation of **9**, no evidence exists pointing to its formation. This might be rationalized in part using the energies and number of isomers separating the cyano and isocyano forms. While the calculated energy difference of 112 kJ/mol[21] between **9** and **1** is similar to that separating nitriles from isonitriles discussed in the introduction, the number of isomers intervening between **1** and **9** is higher for C_4H_3N isomers than for H-CC-CC-NC, NC-CC-NC, NC-CC-CC-NC, or H-CC-NC each of which was the next most stable species following the respective most stable parent nitrile.

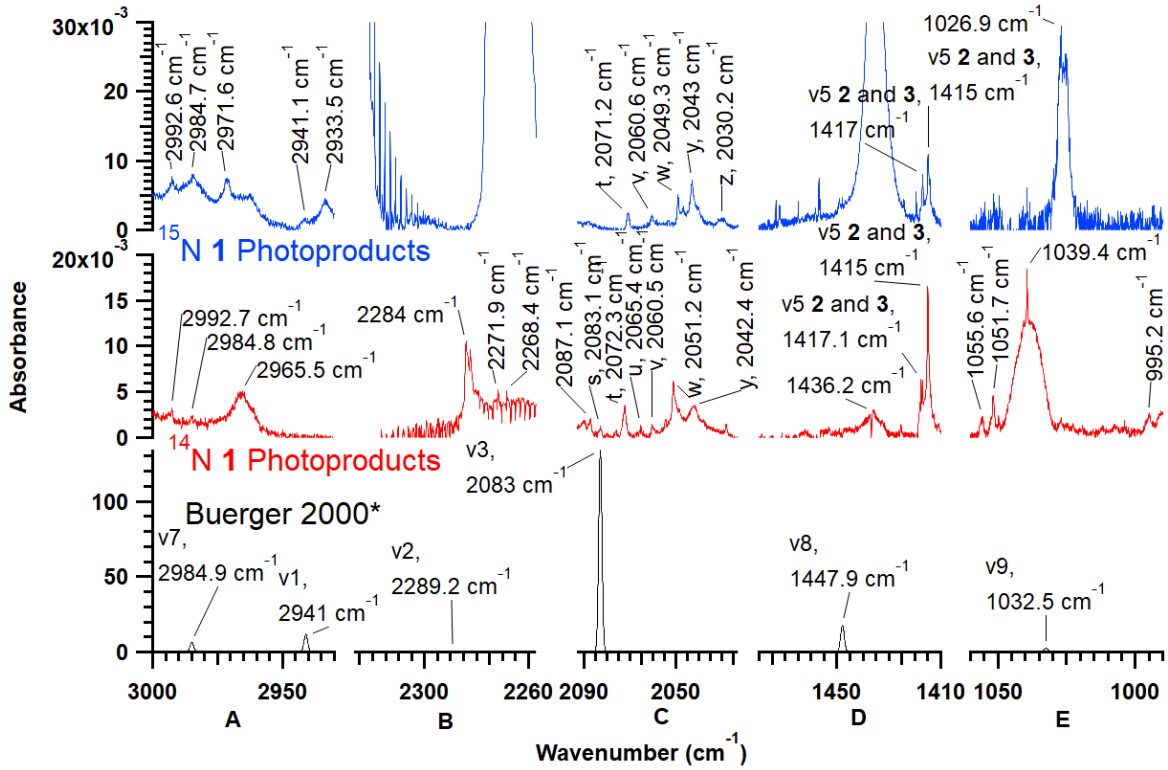

Fig. S52-1-isocyano-1-propyne (**9**) theoretical spectrum (peak position from Buerger et al. 2000[24] peak maximum B3LYP/aug-cc-pVTZ intensity) (bottom trace) along with spectra following photolysis of ^{14}N-**1** (1365 min, middle trace) and ^{15}N-**1** (741 min, top trace) using Ly-α (121.6 nm) radiation.

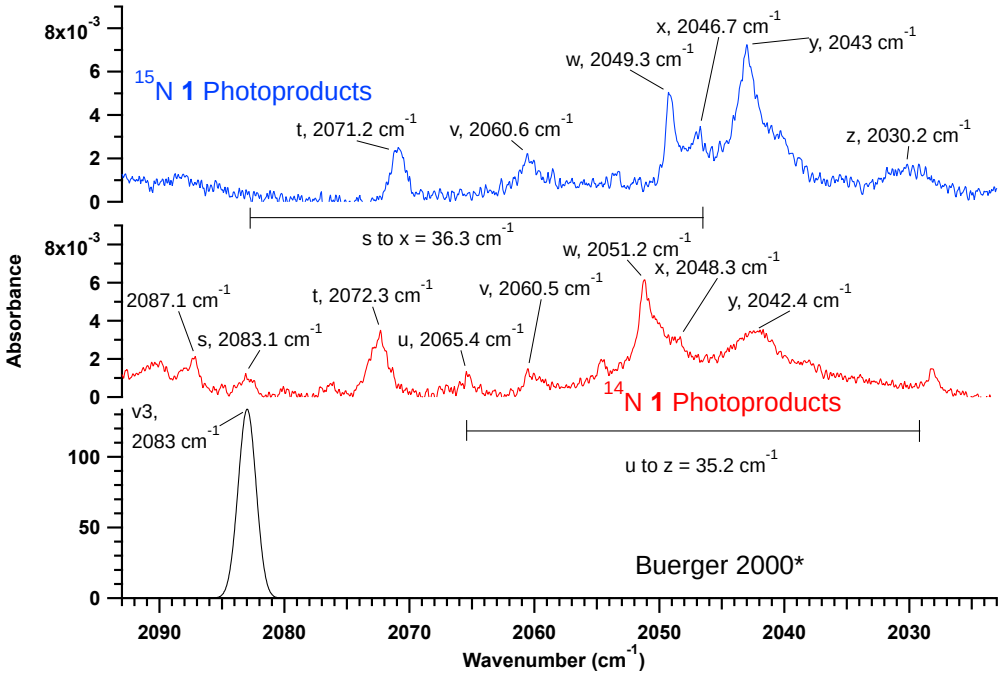

Fig. S53-1-isocyano-1-propyne (**9**) theoretical spectrum (peak position from Buerger et al. 2000[24] peak maximum B3LYP/aug-cc-pVTZ intensity) (bottom trace) along with spectra following photolysis of ^{14}N-**1** (1365 min, middle trace) and ^{15}N-**1** (741 min, top trace) using Ly-α (121.6 nm) radiation. Predicted ^{14}N-^{15}N frequency shift is -34.8 cm^{-1}. Calculated intensity is 134 km/mol. While features "s" (^{14}N, red) and "u" (^{15}N, blue) seem to shift, it is impossible to unambiguously confirm that either can be associated with **9**. Studies using 193 nm radiation and a mixture of ^{14}N and ^{15}N-**1** do not show this structure and do not aid in identification.

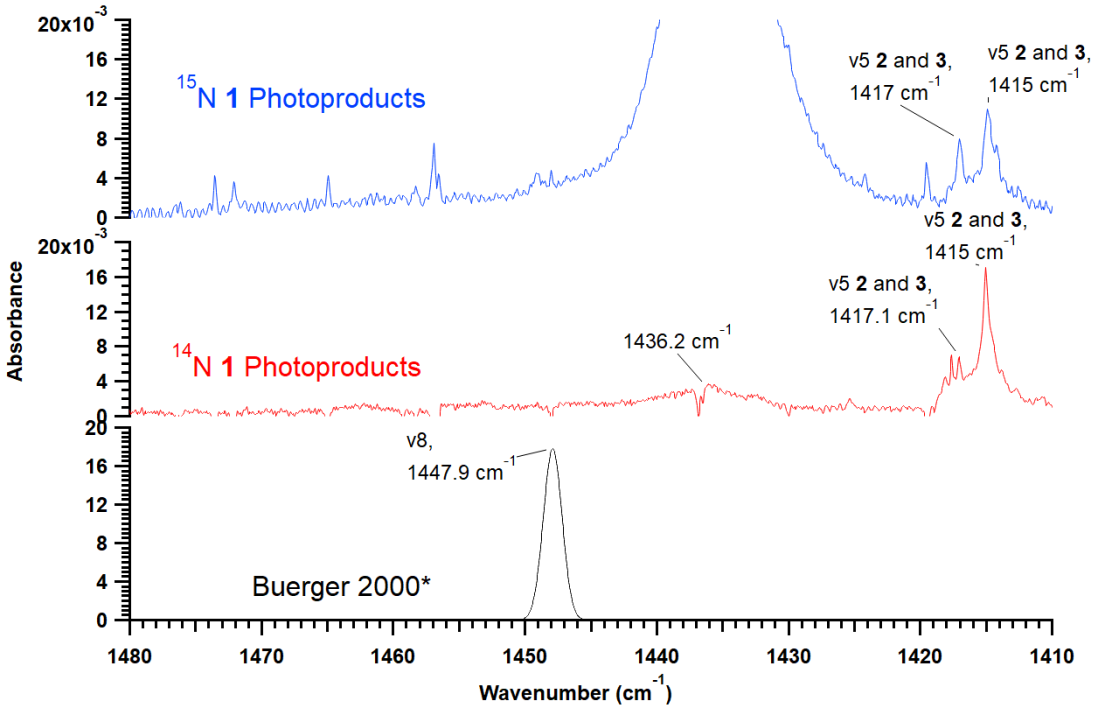

Fig. S54-1-isocyano-1-propyne (**9**) theoretical spectrum (peak position from Buerger et al. 2000[24] peak maximum B3LYP/aug-cc-pVTZ intensity) (bottom trace) along with spectra following photolysis of ^{14}N-**1** (1365 min, middle trace) and ^{15}N-**1** (741 min, top trace) using Ly-α (121.6 nm) radiation. Predicted ^{14}N-^{15}N frequency shift is 0 cm^{-1}. Calculated intensity is 18 km/mol. Features in the red curve at 1436 cm^{-1} belong to ^{14}N-**1** or ^{15}N-**1** while features at 1417 cm^{-1} and 1415 cm^{-1} belong to a combination of **2** and **3**. No convincing candidate for this band exists in experimental spectra.

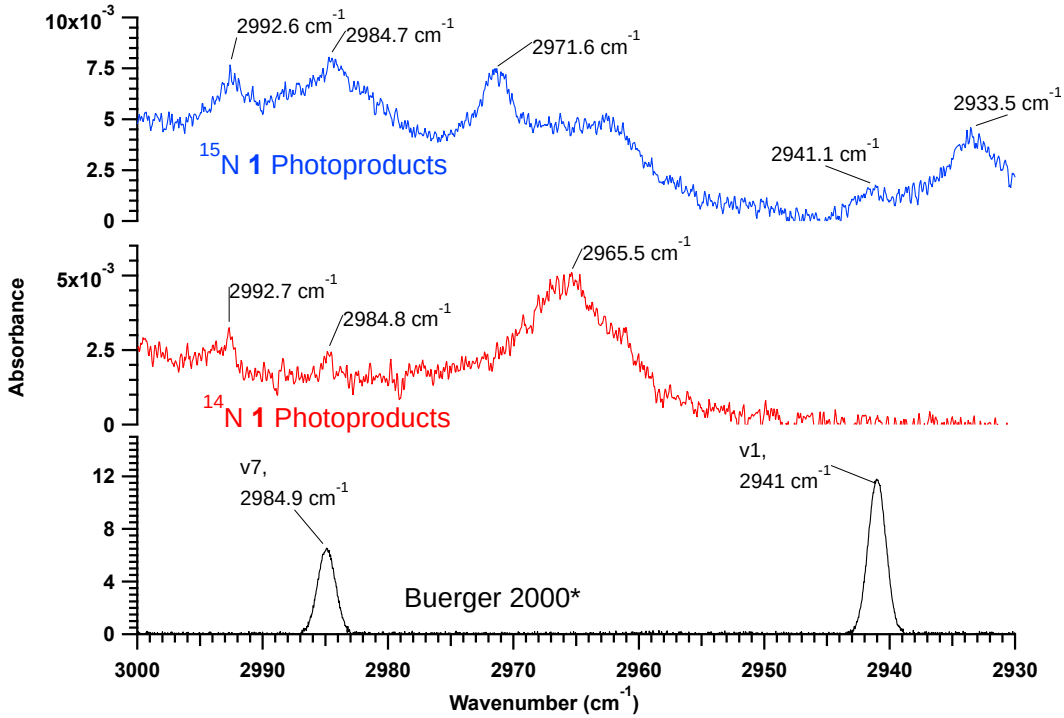

Fig. S55-1-isocyano-1-propyne (**9**) theoretical spectrum (peak position from Buerger et al. 2000[24] peak maximum B3LYP/aug-cc-pVTZ intensity) (bottom trace) along with spectra following photolysis of ^{14}N-**1** (1365 min, middle trace) and ^{15}N-**1** (741 min, top trace) using Ly-α (121.6 nm) radiation. Predicted ^{14}N-^{15}N frequency shift for ν_7 is 0 cm^{-1}. Calculated intensity is 6 km/mol. Predicted ^{14}N-^{15}N frequency shift for ν_1 is 0 cm^{-1}. Calculated intensity is 12 km/mol. Without convincing evidence of the most intense band near 2082 cm^{-1}, it is very unlikely that these unassigned features, whose intensities must be ~10% of the most intense band, can belong to **9**.

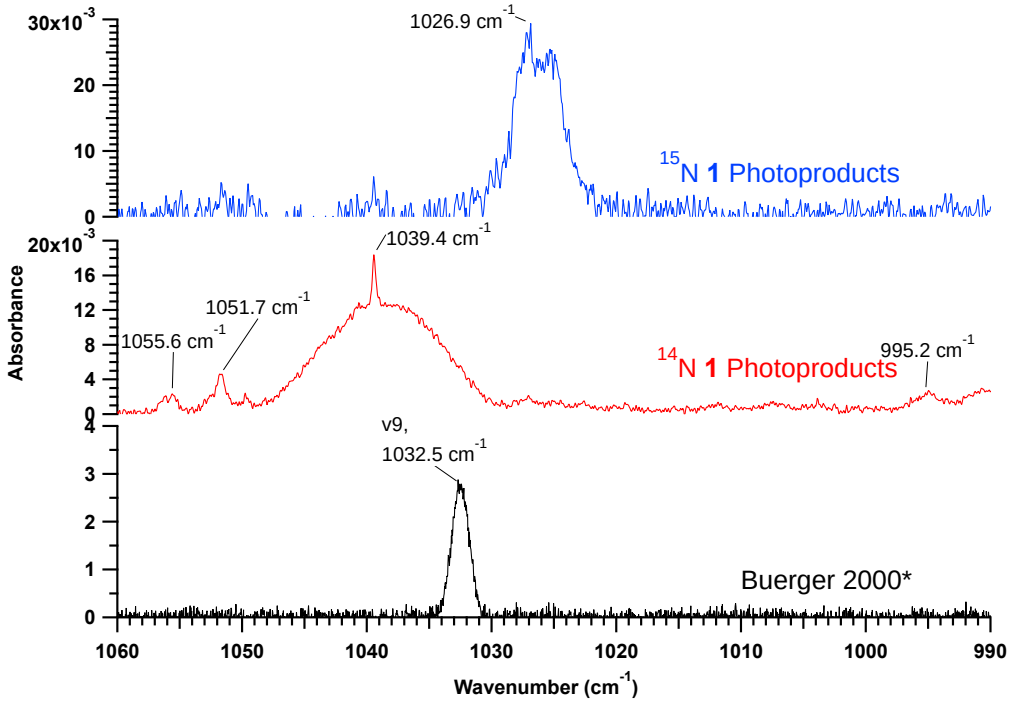

Fig. S56-1-isocyano-1-propyne (**9**) theoretical spectrum (peak position from Buerger et al. 2000[24] peak maximum B3LYP/aug-cc-pVTZ intensity) (bottom trace) along with spectra following photolysis of ^{14}N-**1** (1365 min, middle trace) and ^{15}N-**1** (741 min, top trace) using Ly-α (121.6 nm) radiation. Predicted ^{14}N-^{15}N frequency shift is 0 cm^{-1}. Calculated intensity is 2 km/mol.

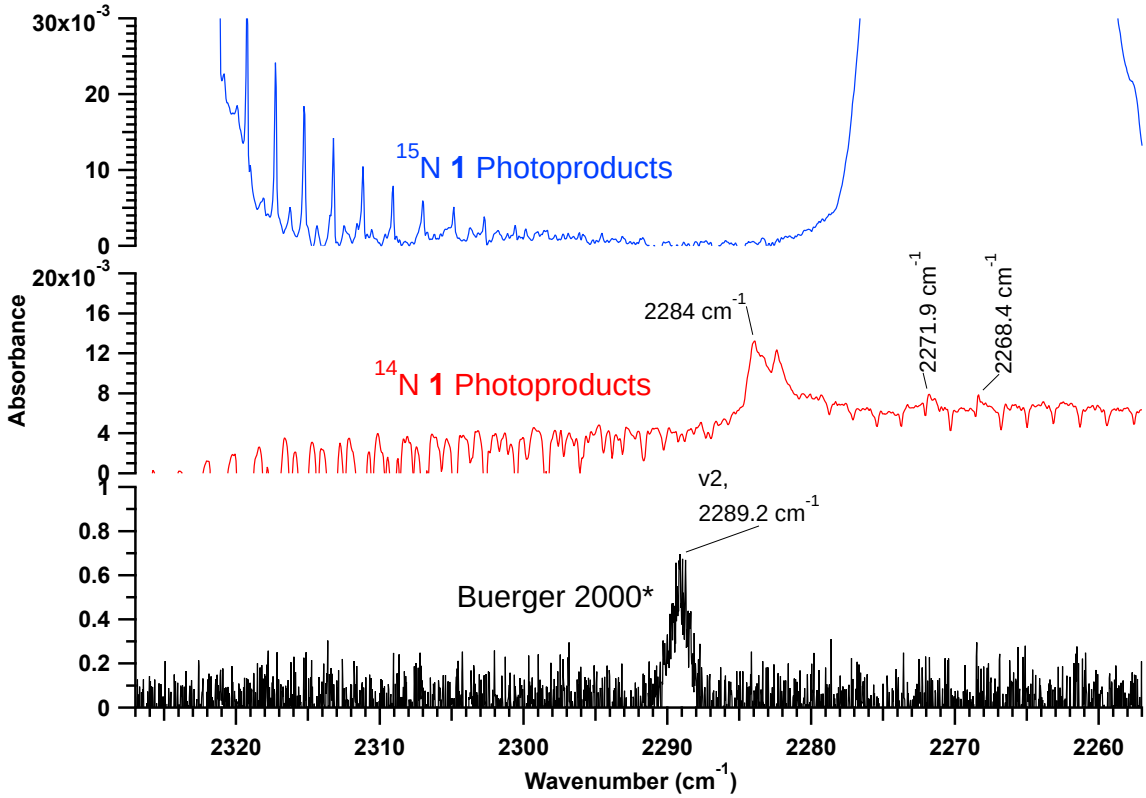

Fig. S57-1-isocyano-1-propyne (**9**) theoretical spectrum (peak position from Buerger et al. 2000[24] peak maximum B3LYP/aug-cc-pVTZ intensity) (bottom trace) along with spectra following photolysis of ^{14}N-**1** (1365 min, middle trace) and ^{15}N-**1** (741 min, top trace) using Ly-α (121.6 nm) radiation. Predicted ^{14}N-^{15}N frequency shift is -5 cm^{-1}. Calculated intensity is 1 km/mol.

3-cyanocyclopropene (8)

Cyclic species 3-cyanocyclopropene (**8**) should be considered as a potential, if not probable, product. Up to thirteen different modes were reportedly observed in earlier studies and are listed in Table S26. Comparing our own results with these values (Figs S58 to S63), one would expect to reproduce at least some of the most intense bands which include ν_9, ν_{14}, ν_4, ν_3, ν_{10}, and ν_2 with calculated intensities of 67, 46, 26, 18, 18, and 15 km/mol, respectively. At all irradiation wavelengths, a feature in the same location as was previously reported for ν_{14} of **8** (986 cm^{-1}) can be found (Fig. S33, Column D). Much like peaks attributed to **6** and **10**, the time evolution of this band strongly resembles that of **2**, although its attribution to this chemical can be ruled out. No trace of this feature was seen in a pure sample of **2**. This peak is strong for both 248 nm experiments and 121 nm experiments but much weaker during 193 nm photolysis. The more intense mode for **8** (ν_9 reportedly at 624 or 623 cm^{-1}) can be clearly seen following 248 nm photolysis and falls at 623 cm^{-1} with an isotope shift of -2 cm^{-1}, close to the predicted value of -1 cm^{-1} (Fig. S58, Column E and S63). The ν_9 band was out of range for 121 nm radiation experiments and not observable for 193 nm experiments, although for 193 nm radiation the intensity of the ν_{14} band at 986 cm^{-1} was also much smaller than at other wavelengths possibly putting ν_9 below our limit of detection. No further bands can be identified from laser photolysis experiments. However, very small features at 1664 and 1671 cm^{-1} can be found in 121.6 nm irradiation experiments which were also reported to belong to ν_4, although only one or another of these bands were described in the different publications and never the two together. If a reversal in the intensities of bands ν_9 and ν_{14} is assumed to occur upon its formation by photolysis, a reasonable assumption as changes in intensity are frequently observed in such products, these measurements may support the observation of **8**. However, the low intensity of these signals and limits in the data-sets used for analysis prevent any firm conclusions from being reached.

Table S26-Ar matrix isolated observations of species **8**, 3-cyanocyclopropene.

	Custer 2016[21]			Torker et al. 2014[25]				Hill and Platz 2003[26]		
	B3LYP/aug-cc-pVTZ			B3LYP/6-31G*		Experiment		B3LYP/6-31G*		Experiment
Mode	Scaled Harmonic Freq. (cm^{-1})	Intensity (km mol^{-1})	Shift	Scaled Harmonic Freq. (cm^{-1})	Intensity (km mol^{-1})	Freq. (cm^{-1})	Intensity	Scaled Harmonic Freq. (cm^{-1})	Intensity (km mol^{-1})	Freq.(cm^{-1})
ν_1	3176.3	2.5	0	3162	5			3208	0.9	2193
ν_{12}	3129.3	7.1	0					3162	2.7	3160
ν_2	2972.5	14.8	0	2990	37	2995	m	2990	22.5	
ν_3	2240.6	18.1	-29	2260	22	2241	m	2261	12.2	2239
ν_4	1671.5	25.9	0	1691	33	1664	m	1691	18.8	1670
ν_5	1314.4	4	0	1331	8	1352	w	1332	4.6	1316
ν_6	1091.8	4.1	-1	1113	6			1113	3.6	
ν_{13}	1007.3	0.5	0	1011	8			1012	4.5	1027
ν_{14}	969.98	46	0	974	77	986	s	975	46.8	983
ν_7	924.37	7	-3	932	11	949	w	933	6.7	948
ν_8	869.28	11	-3	876	21	888	m	876	11.8	859
ν_{15}	827.44	0	0					812	0	
ν_{16}	790.15	1.9	0	800	2			800	1.2	837
ν_9	620.37	67.1	1	619	100	623	s	618	57.1	624
ν_{17}	551.17	3.9	1	554	8			554	4.3	559
ν_{10}	536.53	17.6	2	535	29	543	m	535	16.7	543
ν_{18}	220.3	1.5	2					223	1.2	
ν_{11}	210.3	4.1	3					211	3.4	

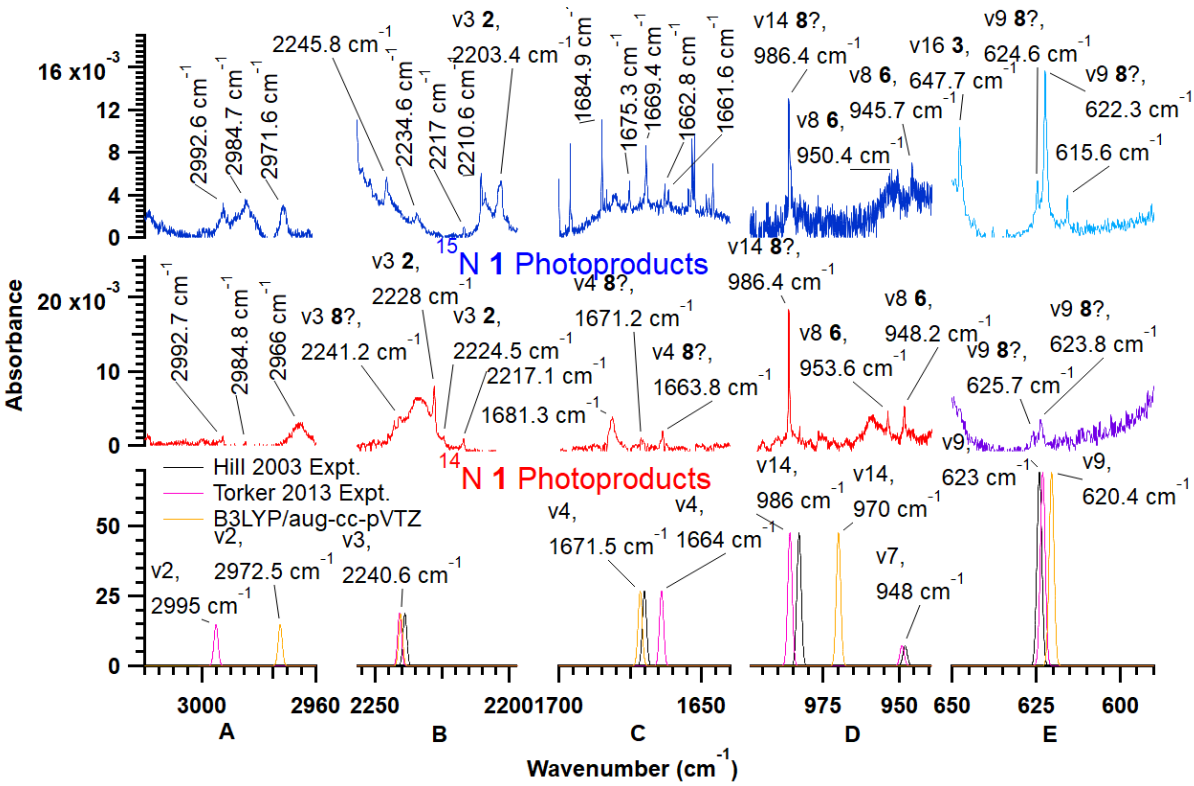

Fig. S58-3-cyanocyclopropene (**8**) theoretical spectrum (peak position and maximum from B3LYP/aug-cc-pVTZ frequency and intensity) (bottom trace) in addition to frequencies reported by Hill and Platz 2003[26] and Torker et al. 2013[25] (peak maximum from B3LYP/aug-cc-pVTZ intensities). Spectra following photolysis of ^{14}N-**1** (1365 min, middle trace) and ^{15}N-**1** (741 min, top trace) using Ly-α (121.6 nm) radiation. For the ν_9 region, which was out of range for the Ly-α measurements, spectra following 248 nm photolysis of ^{14}N-**1** (319 min, middle trace) and ^{15}N-**1** (320 min, top trace) are given. Intensities for the ν_9 region cannot be compared to other regions.

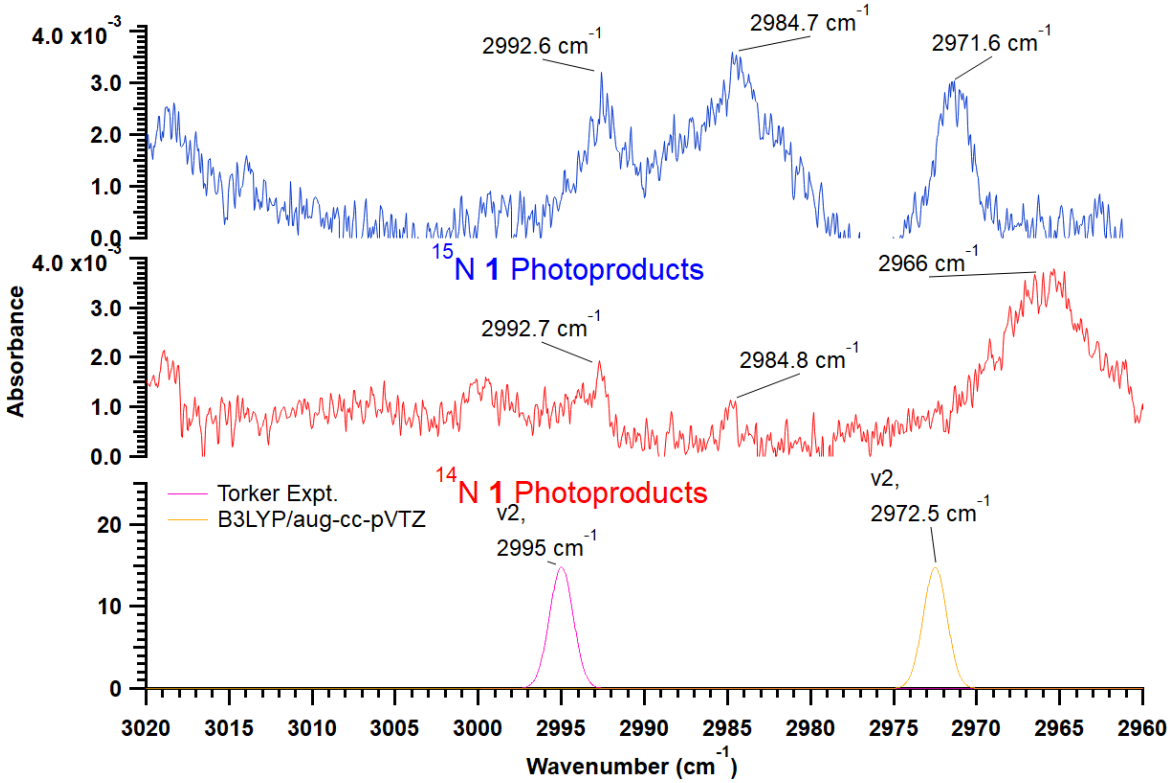

Fig. S59-3-cyanocyclopropene (**8**) theoretical spectrum (peak position and maximum from B3LYP/aug-cc-pVTZ frequency and intensity) (bottom trace) in addition to frequencies reported by Torker et al. 2013[25] (peak maximum from B3LYP/aug-cc-pVTZ intensities). Spectra following photolysis of ^{14}N-**1** (1365 min, middle trace) and ^{15}N-**1** (741 min, top trace) using Ly-α (121.6 nm) radiation. Predicted ^{14}N-^{15}N frequency shift is 0 cm^{-1}. Calculated intensity is 15 km/mol.

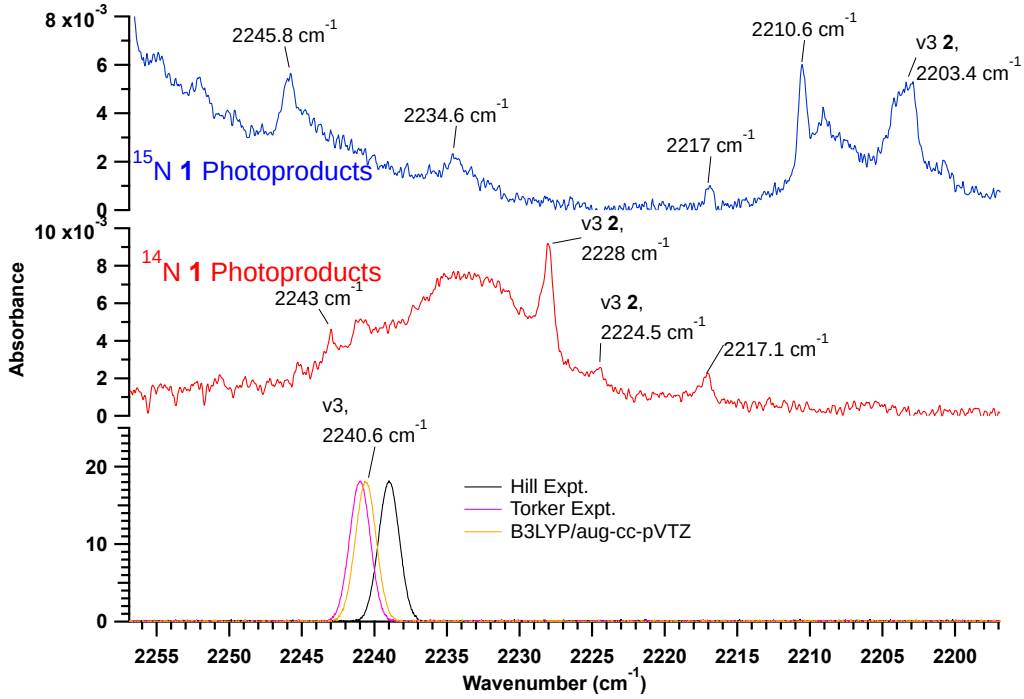

Fig. S60-3-cyanocyclopropene (**8**) theoretical spectrum (peak position and maximum from B3LYP/aug-cc-pVTZ frequency and intensity) (bottom trace) in addition to frequencies reported by Hill and Platz 2003[26] and Torker et al. 2013[25] (peak maximum from B3LYP/aug-cc-pVTZ intensities). Spectra following photolysis of ^{14}N-**1** (1365 min, middle trace) and ^{15}N-**1** (741 min, top trace) using Ly-α (121.6 nm) radiation. Predicted ^{14}N-^{15}N frequency shift is -29 cm^{-1}. Calculated intensity is 18 km/mol.

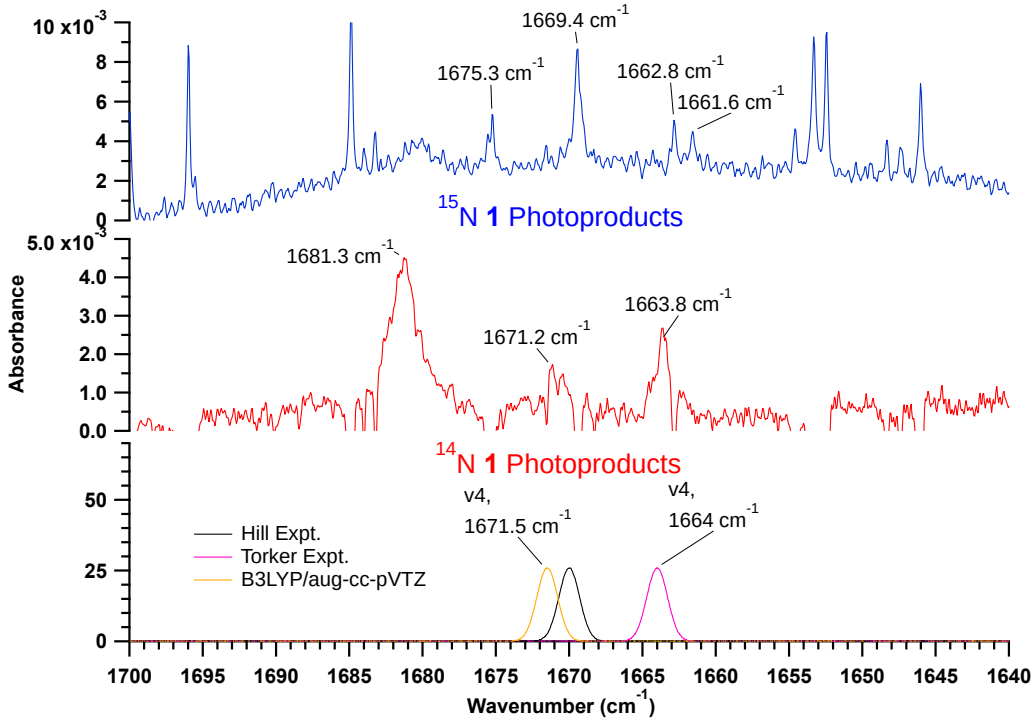

Fig. S61-3-cyanocyclopropene (**8**) theoretical spectrum (peak position and maximum from B3LYP/aug-cc-pVTZ frequency and intensity) (bottom trace) in addition to frequencies reported by Hill and Platz 2003[26] and Torker et al. 2013[25] (peak maximum from B3LYP/aug-cc-pVTZ intensities). Spectra following photolysis of ^{14}N-**1** (1365 min, middle trace) and ^{15}N-**1** (741 min, top trace) using Ly-α (121.6 nm) radiation. Predicted ^{14}N-^{15}N frequency shift is 0 cm^{-1}. Calculated intensity is 26 km/mol.

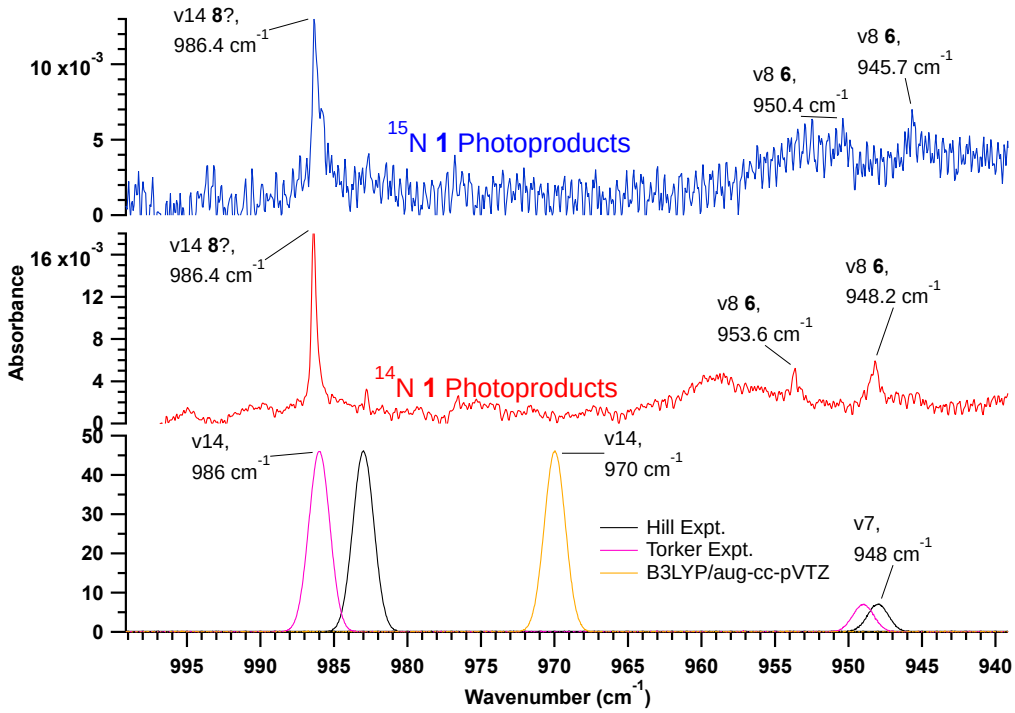

Fig. S62-3-cyanocyclopropene (**8**) theoretical spectrum (peak position and maximum from B3LYP/aug-cc-pVTZ frequency and intensity) (bottom trace) in addition to frequencies reported by Hill and Platz 2003[26] and Torker et al. 2013[25] (peak maximum from B3LYP/aug-cc-pVTZ intensities). Spectra following photolysis of ^{14}N-**1** (1365 min, middle trace) and ^{15}N-**1** (741 min, top trace) using Ly-α (121.6 nm) radiation. Predicted ^{14}N-^{15}N frequency shift for ν_{14} is 0 cm^{-1}. Calculated intensity is 46 km/mol. Predicted ^{14}N-^{15}N frequency shift for ν_7 is -2.5 cm^{-1}. Calculated intensity is 7 km/mol.

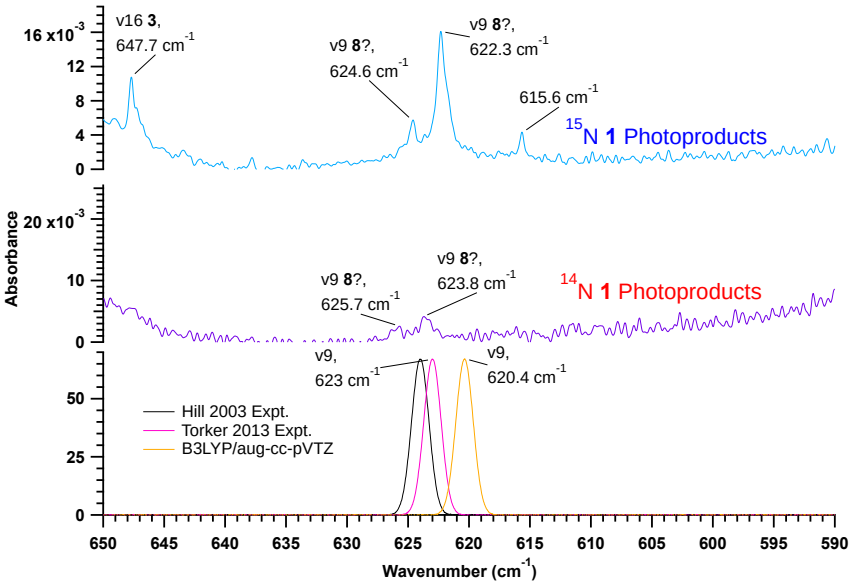

Fig. S63-3-cyanocyclopropene (**8**) theoretical spectrum (peak position and maximum from B3LYP/aug-cc-pVTZ frequency and intensity) (bottom trace) in addition to frequencies reported by Hill and Platz 2003[26] and Torker et al. 2013[25] (peak maximum from B3LYP/aug-cc-pVTZ intensities). Spectra following photolysis of ^{14}N-**1** (319 min, middle trace) and ^{15}N-**1** (320 min, top trace) using 248 nm radiation. Predicted ^{14}N-^{15}N frequency shift is -1.4 cm^{-1}. Calculated intensity is 67 km/mol.

1-cyano-2-propeneylidene (triplet) (19)

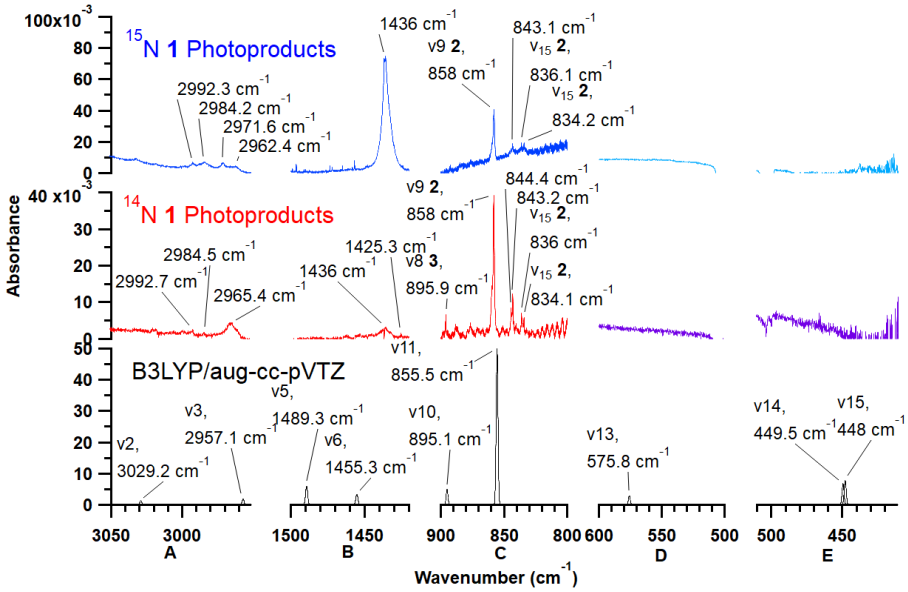

Fig. S64-Triplet 1-cyano-2-propeneylidene (**19**) theoretical spectrum (peak position and maximum are B3LYP/aug-cc-pVTZ frequency and intensity) (bottom trace). Spectra following photolysis of ^{14}N-**1** (1365 min, middle trace) and ^{15}N-**1** (741 min, top trace) using Ly-α (121.6 nm) radiation. For ν_{13}, ν_{14}, and ν_{15}, which were out of range for the Ly-α measurements, spectra following photolysis of ^{14}N-**1** (732 min, middle trace) and ^{15}N-**1** (240 min, top trace) using 193 nm radiation are given.

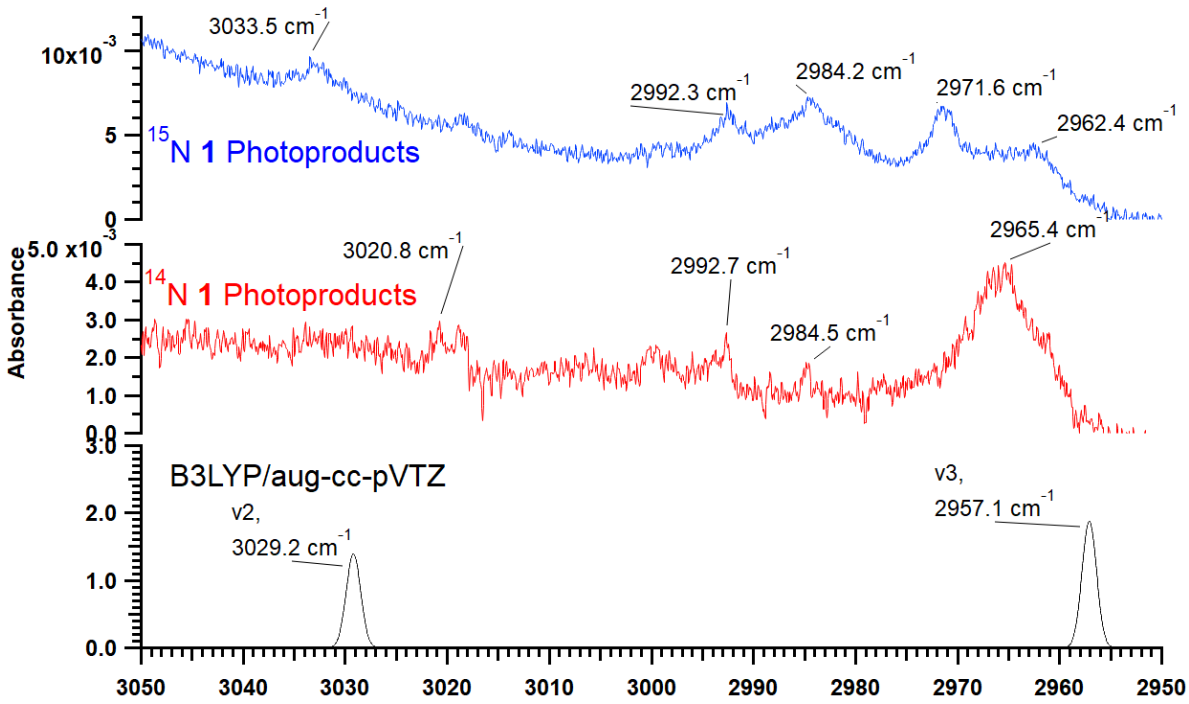

Fig. S65-Triplet 1-cyano-2-propeneylidene (**19**) theoretical spectrum (peak position and maximum are B3LYP/aug-cc-pVTZ frequency and intensity) (bottom trace). Spectra following photolysis of ^{14}N-**1** (1365 min, middle trace) and ^{15}N-**1** (741 min, top trace) using Ly-α (121.6 nm) radiation. Predicted ^{14}N-^{15}N frequency shift for v_2 is 0 cm^{-1}. Calculated intensity is 1 km/mol. Predicted ^{14}N-^{15}N frequency shift for v_3 is 0 cm^{-1}. Calculated intensity is 2 km/mol.

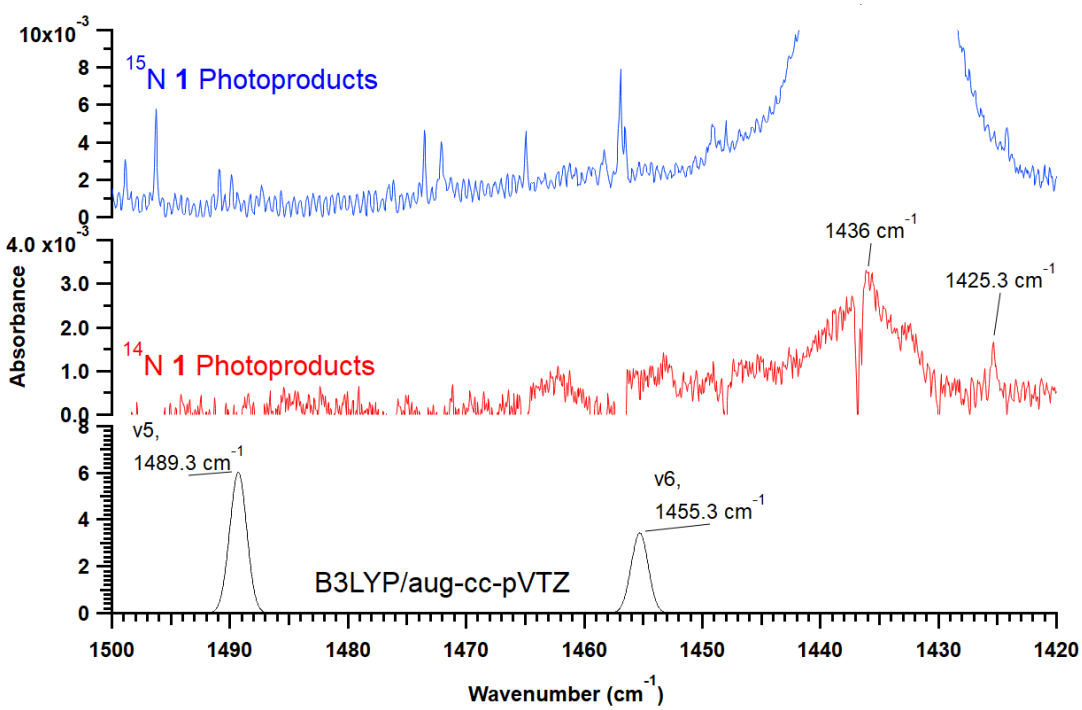

Fig. S66-Triplet 1-cyano-2-propeneylidene (**19**) theoretical spectrum (peak position and maximum are B3LYP/aug-cc-pVTZ frequency and intensity) (bottom trace). Spectra following photolysis of ^{14}N-**1** (1365 min, middle trace) and ^{15}N-**1** (741 min, top trace) using Ly-α (121.6 nm) radiation. Predicted ^{14}N-^{15}N frequency shift for v_5 is -5.3 cm^{-1}. Calculated intensity is 6 km/mol. Predicted ^{14}N-^{15}N frequency shift for v_6 is 0 cm^{-1}. Calculated intensity is 3 km/mol.

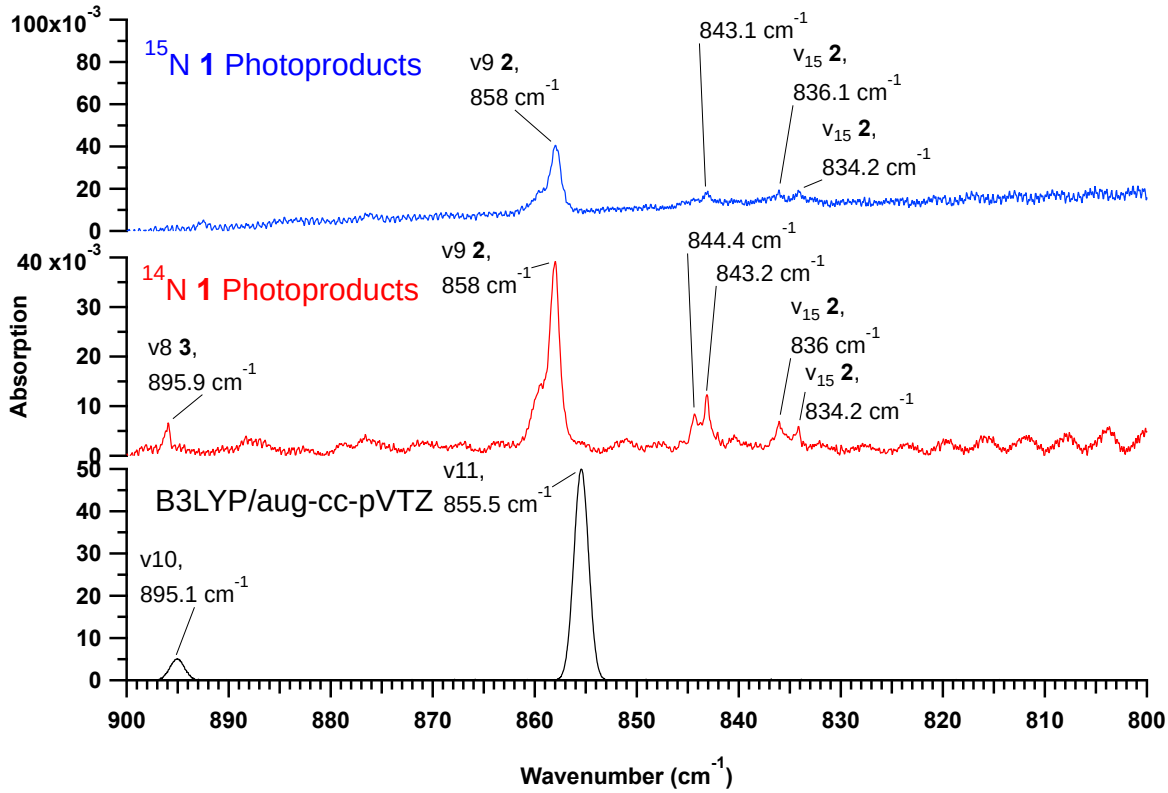

Fig. S67-Triplet 1-cyano-2-propeneylidene (**19**) theoretical spectrum (peak position and maximum are B3LYP/aug-cc-pVTZ frequency and intensity) (bottom trace). Spectra following photolysis of ^{14}N-**1** (1365 min, middle trace) and ^{15}N-**1** (741 min, top trace) using Ly-α (121.6 nm) radiation. Predicted ^{14}N-^{15}N frequency shift for ν_{10} is 0 cm^{-1}. Calculated intensity is 5 km/mol. Predicted ^{14}N-^{15}N frequency shift for ν_{11} is 0 cm^{-1}. Calculated intensity is 50 km/mol.

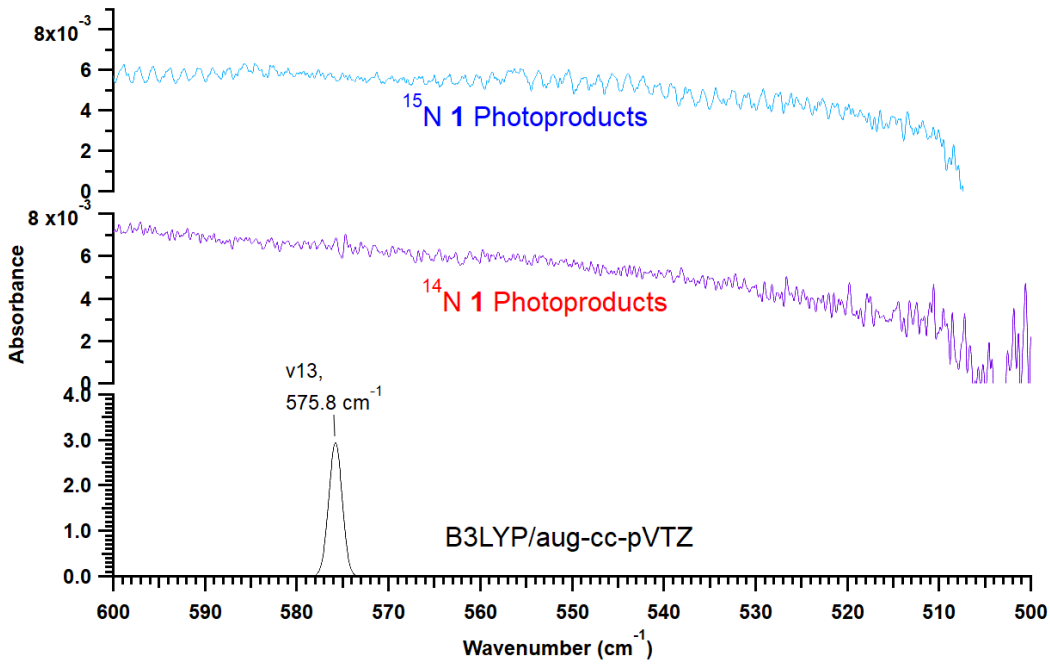

Fig. S68-Triplet 1-cyano-2-propeneylidene (**19**) theoretical spectrum (peak position and maximum are B3LYP/aug-cc-pVTZ frequency and intensity) (bottom trace). Spectra following photolysis of ^{14}N-**1** (732 min, middle trace) and ^{15}N-**1** (240 min, top trace) using 193 nm radiation. Predicted ^{14}N-^{15}N frequency shift for ν_{13} is 0 cm^{-1}. Calculated intensity is 3 km/mol.

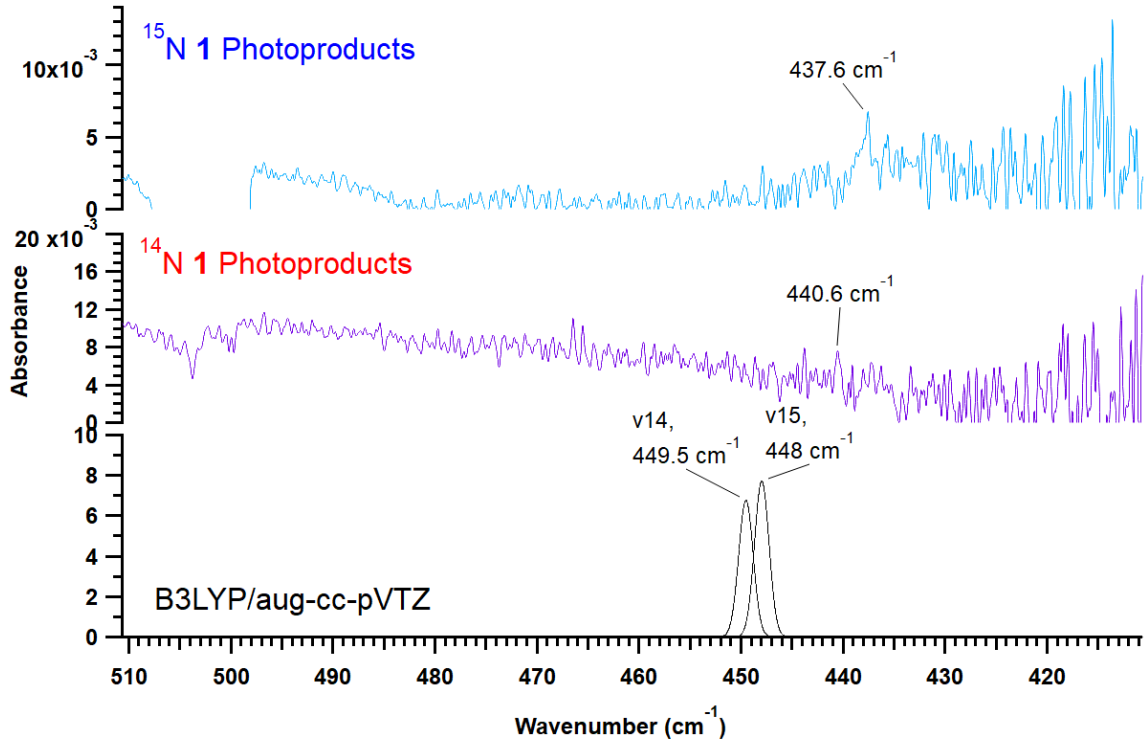

Fig. S69-Triplet 1-cyano-2-propeneylidene (**19**) theoretical spectrum (peak position and maximum are B3LYP/aug-cc-pVTZ frequency and intensity) (bottom trace). Spectra following photolysis of ^{14}N-**1** (732 min, middle trace) and ^{15}N-**1** (240 min, top trace) using 193 nm radiation. Predicted ^{14}N-^{15}N frequency shift for v_{14} is -2 cm^{-1}. Calculated intensity is 7 km/mol. Predicted ^{14}N-^{15}N frequency shift for v_{15} is -2 cm^{-1}. Calculated intensity is 8 km/mol.

Acetylene

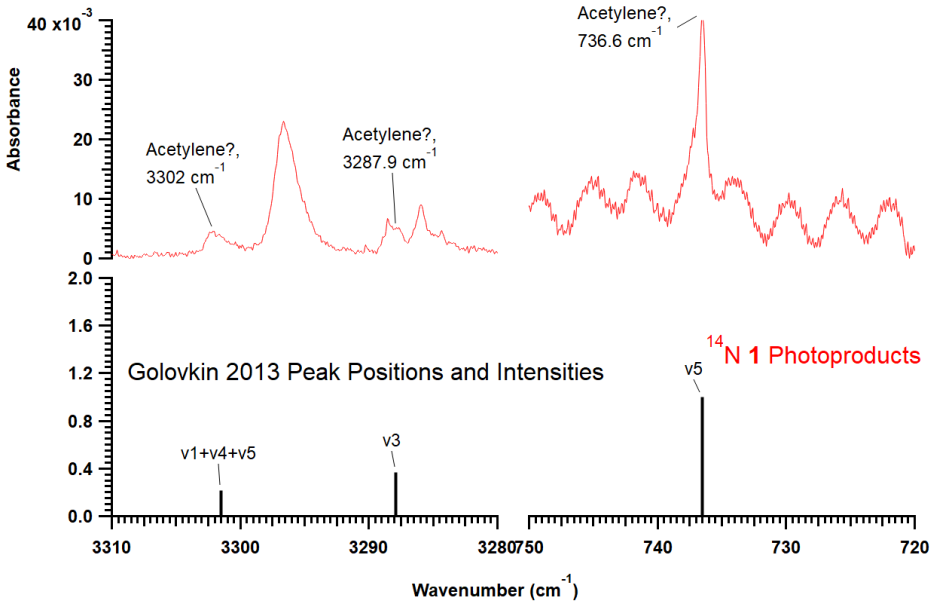

Fig. S70-Acetylene spectrum (peak position and maximum following experimental measurement of Golovkin 2013[27]) (bottom trace). Spectra following photolysis of ^{14}N-**1** (1365 min, top trace) using Ly-α (121.6 nm) radiation.

Full Spectra

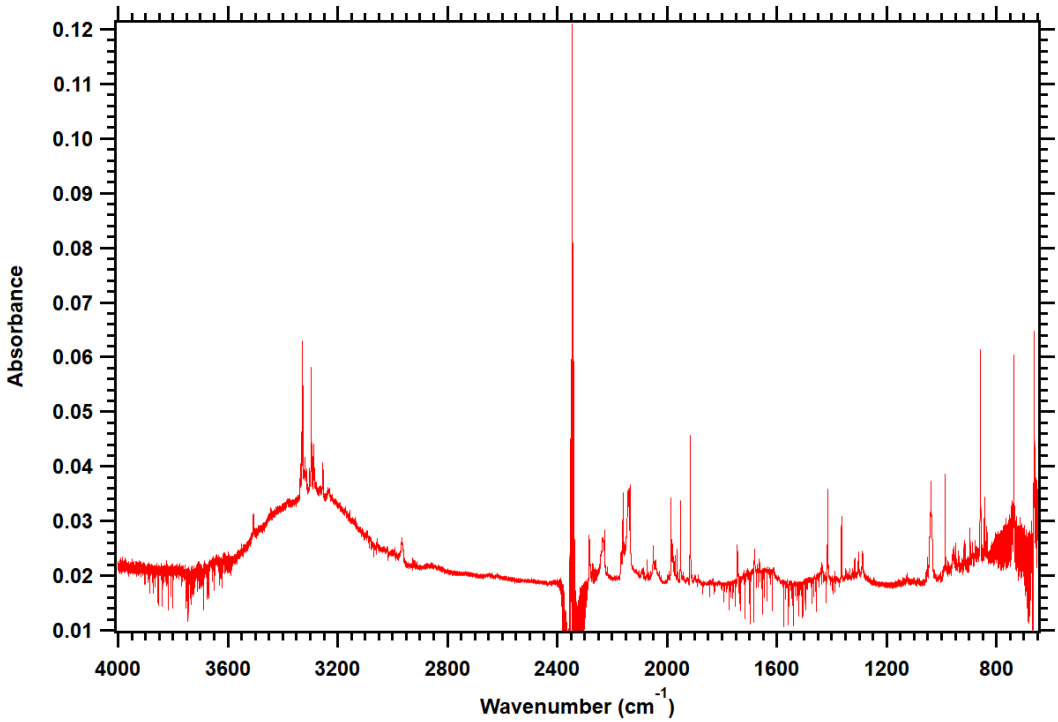

Fig. S71-IR spectrum after 1365 min of 121 nm photolysis of ^{14}N-**1** using the H_2 discharge lamp.

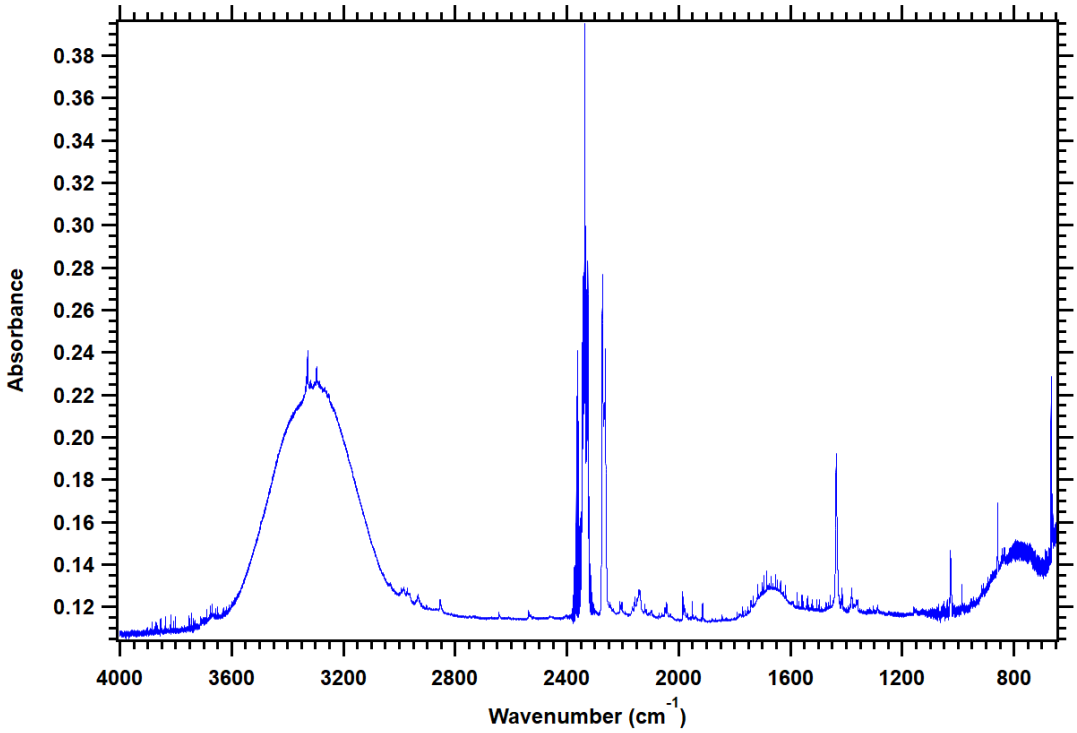

Fig. S72-IR spectrum after 741 min of 121 nm photolysis of ^{15}N-**1** using the H_2 discharge lamp.

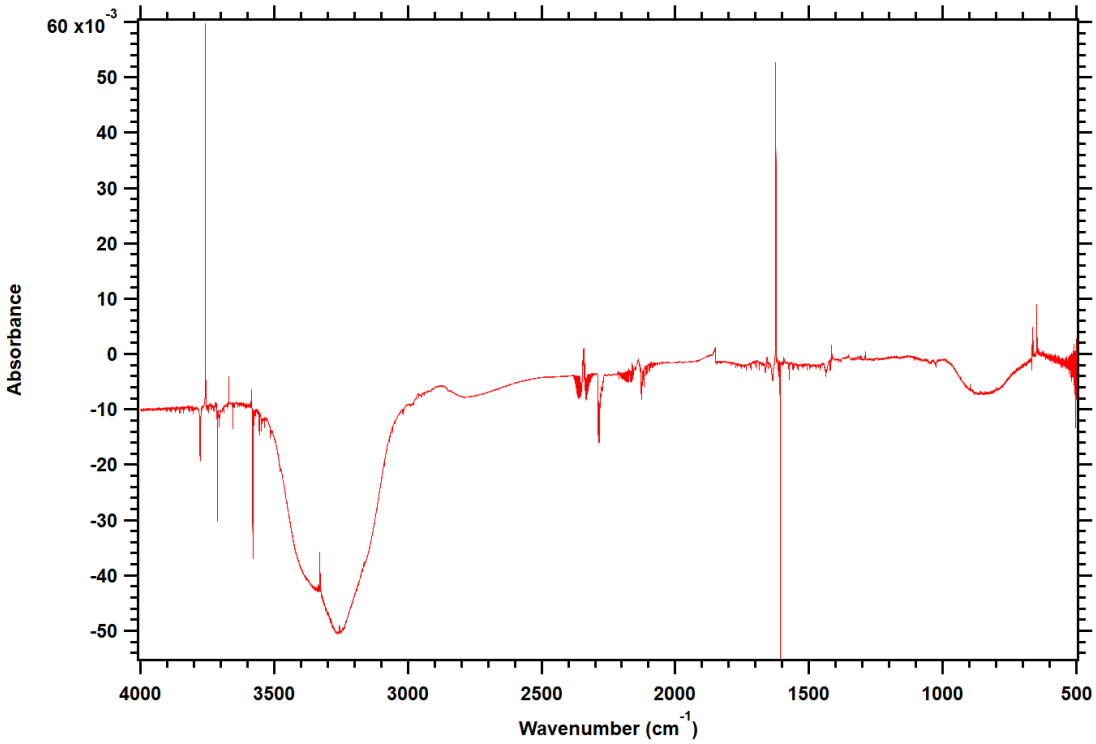

Fig. S73-IR difference spectrum following 731 min photolysis of ^{14}N-**1** at 193 nm (10 Hz, ~0.1 mJ cm^{-2} pulse^{-1} or ~10^{14} photons cm^{-2} pulse^{-1}).

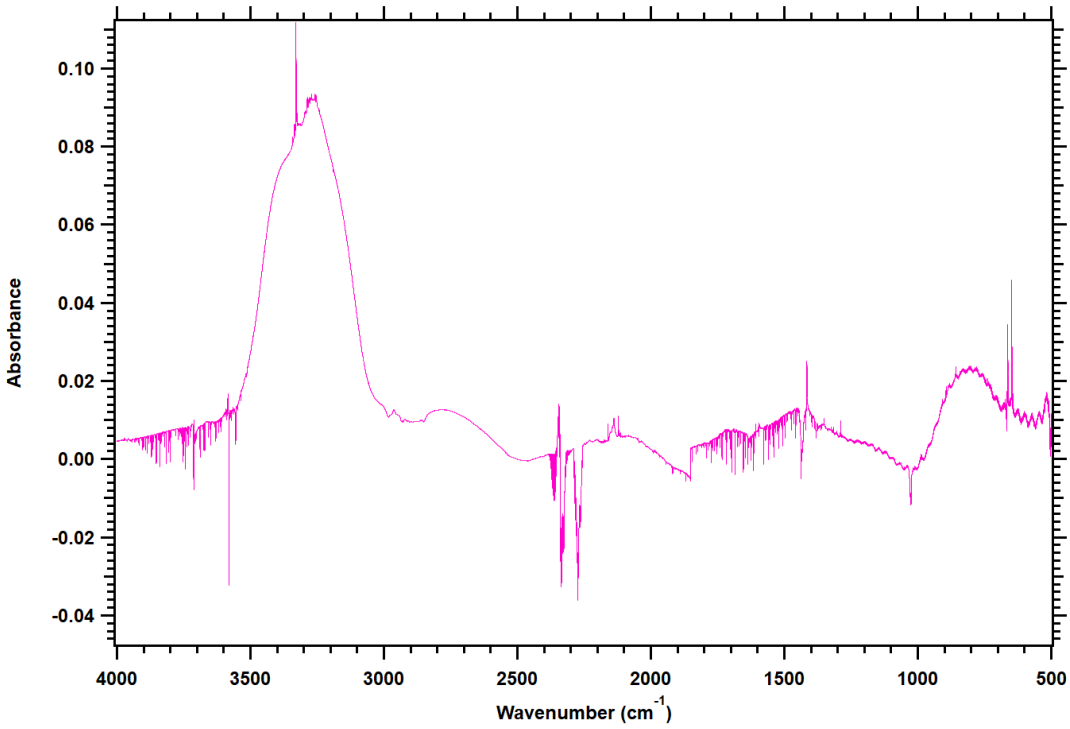

Fig. S74-IR difference spectrum following 360 min photolysis of a mixture of ^{14}N-**1**/^{15}N-**1** at 193 nm (10 Hz, ~0.2 mJ cm^{-2} pulse^{-1} or ~2x10^{14} photons cm^{-2} pulse^{-1}).

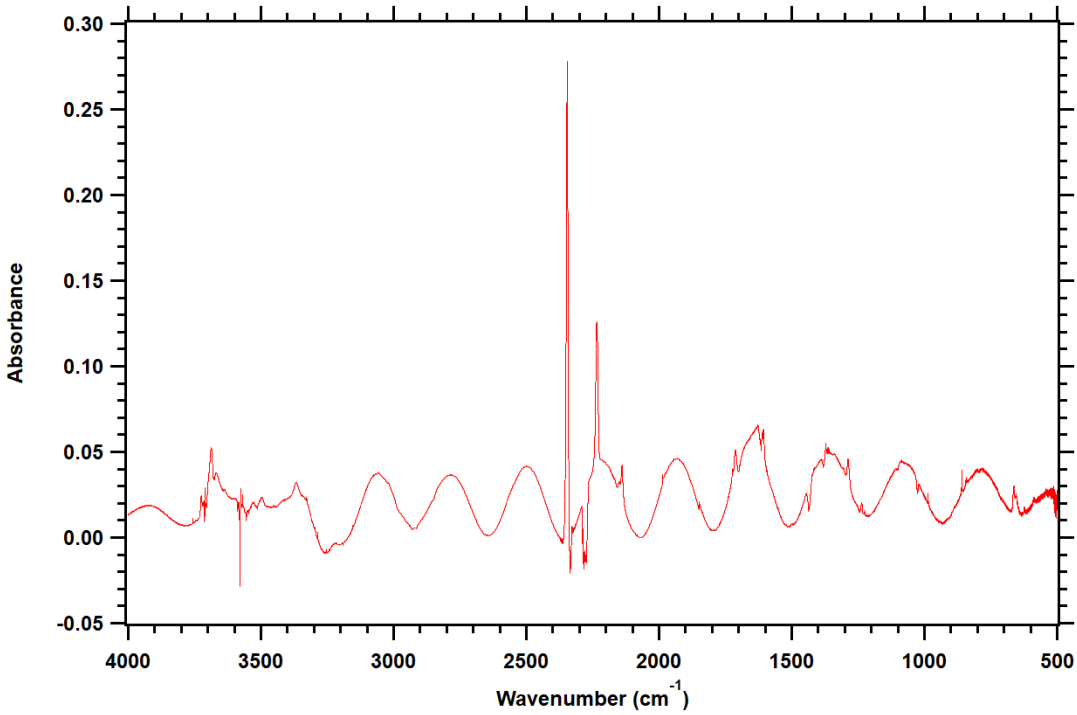

Fig. S75-IR difference spectrum following 319 min photolysis of ^{14}N-**1** at 248 nm (10 Hz, ~7 mJ cm^{-2} pulse^{-1} or 1016 photons cm^{-2} pulse^{-1}).

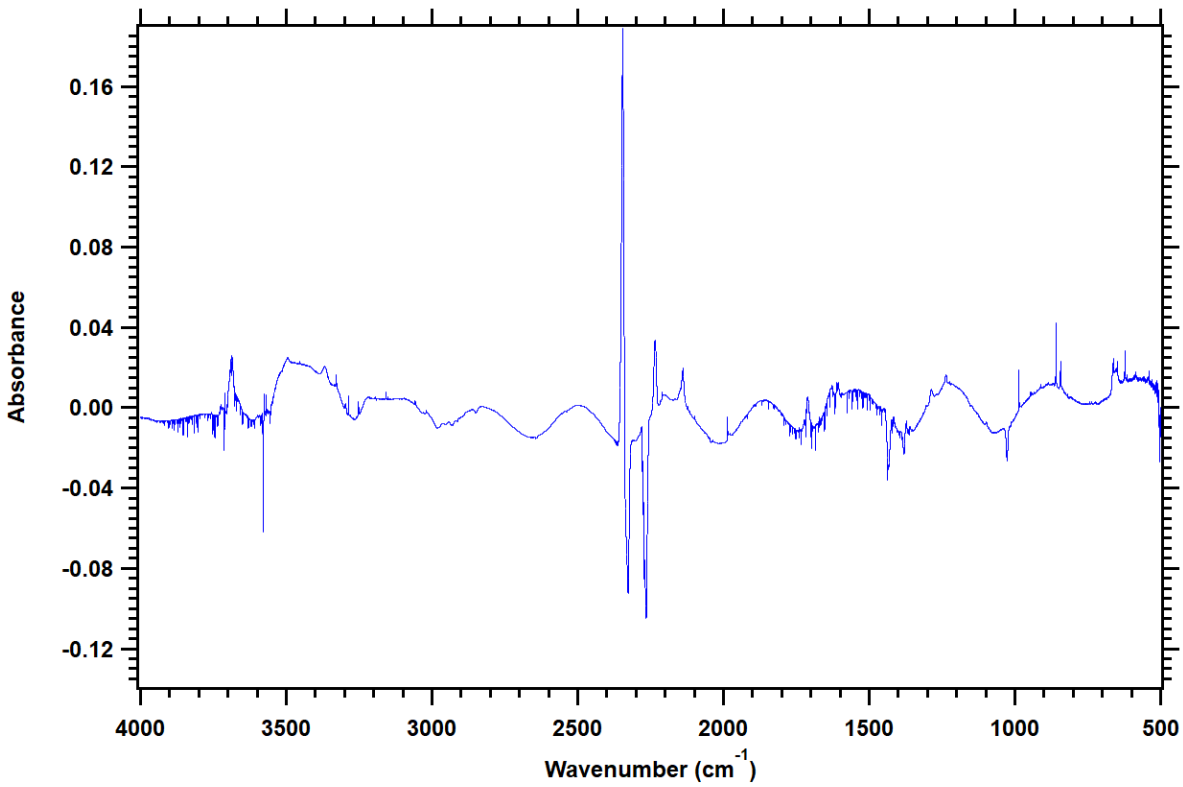

Fig. S76-IR difference spectrum following 320 min photolysis of ^{15}N-**1** at 248 nm (10 Hz, ~6 mJ cm^{-2} pulse^{-1} or ~10^{16} photons cm^{-2} pulse^{-1}).

Appendix 4-Rate Coefficients and Excited State Potential Energy Surface

Table S27-Rate coefficients obtained by fitting data from Fig. 13, panels A, B, and C to equations 1 to 3.

Rate Coefficient (s^{-1})	
$k_{1,2}$	0.0019
$k_{1,3}$	0.00035
$k_{2,3}$	0.00027
$k_{3,2}$	0.00051
k_1	0.0030
k_2	0.0045
k_3	0.0018
k_{Phot}	0.0024

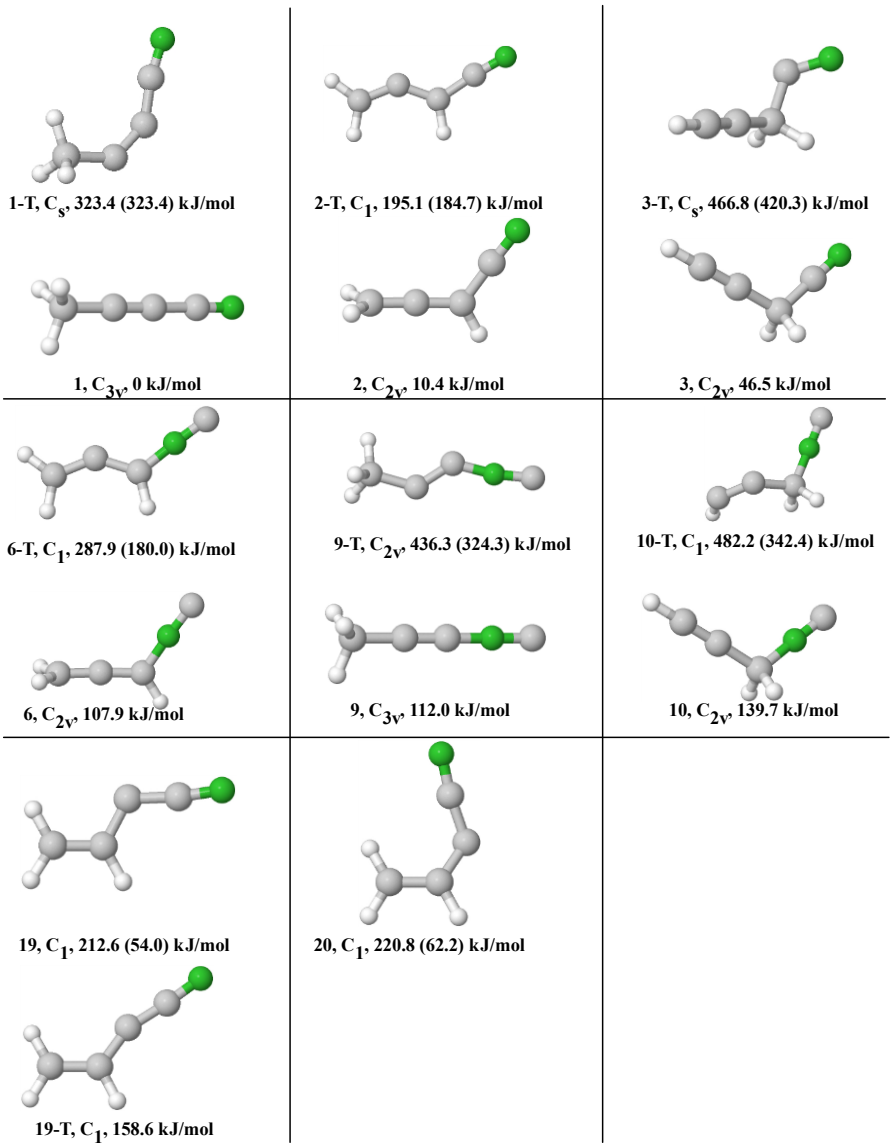

Fig. S77-Optimized singlet structures and their associated, optimized triplets. Both **19** and **20** share the lower energy triplet **19 T**. Structures and energies of geometries reached upon vertical excitation will differ from the optimized values pictured here.

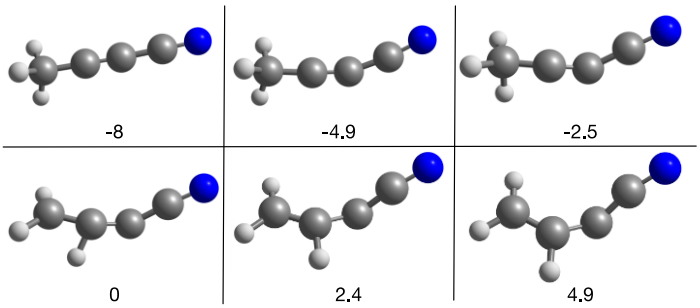

Fig. S78-Structures representing the reaction coordinate for transformation of **1** into **19** on the S_0 surface (Column B, Fig. 7). Numbering follows the reaction coordinate of Fig. 7 starting with -8 and ending at 8.

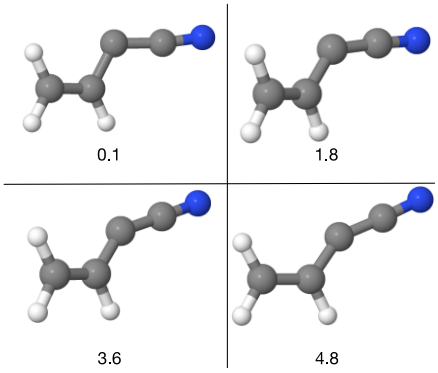

Fig. S79-Structures representing the reaction coordinate for transformation of **19S** into **19T** on the T_0 surface (Column C, Fig. 7). Numbering follows the reaction coordinate of Fig. 7 starting with 0 and ending at 4.5.

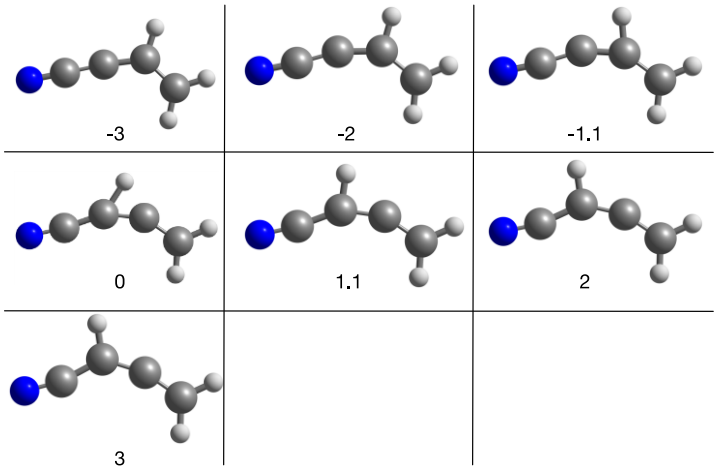

Fig. S80-Structures representing reaction coordinate of the transformation of **19** to **2** on the "T_1" potential energy surface (Column D, Fig. 7). Numbering follows the reaction coordinate of Fig. 7 starting with -3 and ending with 7.

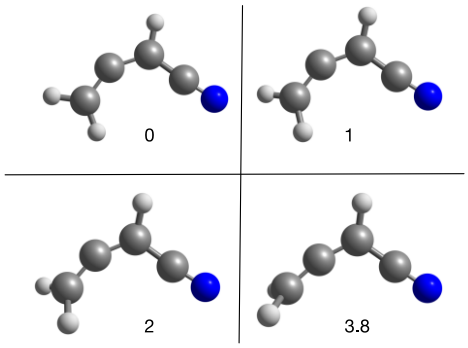

Fig. S81-Structures representing the reaction coordinate for relaxation of **2** from its T_1 state to the ground state (Column E, Fig. 7). Numbering follows the reaction coordinate of Fig. 7 starting with 0 and ending at 6.

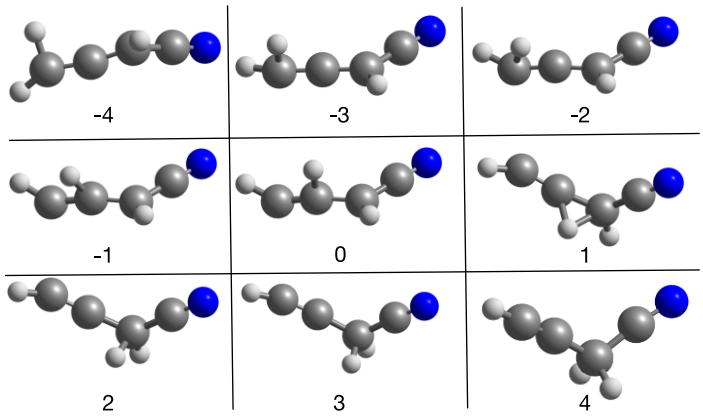

Fig. S82-Structures representing the reaction coordinate of **2** converting to **3** (Column F, Fig. 7). Numbering follows the reaction coordinate of Fig. 7 starting from -5 and ending at 5.

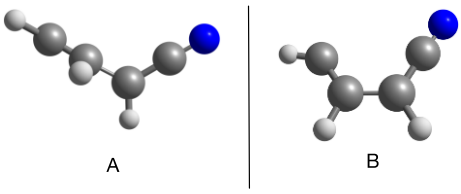

Fig. S83-Comparison of transition state on the ground-state potential energy surface linking **2** and **3** (A) and closest structure on the triplet-state energy surface (B) in Fig. 7.

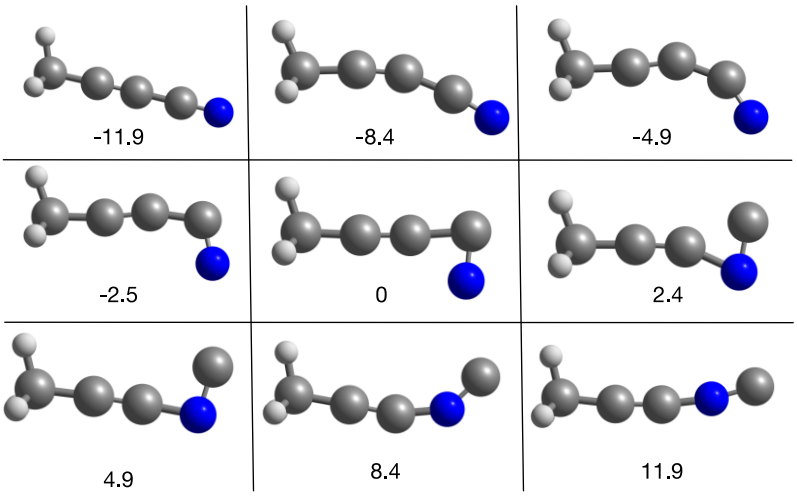

Fig. S84-Structures following the reaction coordinate for the transformation of **1** to **9** on the S_0 surface (Column A, Fig. 7). Numbering follows the reaction coordinate of Fig. 7 starting with -11.9 and ending at 11.9.

References

1. N. Lamarre, C. Falvo, C. Alcaraz, B. Cunha de Miranda, S. Douin, A. Flütsch, C. Romanzin, J. C. Guillemin, S. Boyé-Péronne and B. Gans, *J. Mol. Spectrosc.*, 2015, **315**, 206-216.
2. D. Strübing, H. Neumann, S. Klaus, S. Hübner and M. Beller, *Tetrahedron*, 2005, **61**, 11333-11344.
3. A. Chrostowska, A. Matrane, D. Maki, S. Khayar, H. Ushiki, A. Graciaa, L. Belachemi and J.-C. Guillemin, *ChemPhysChem*, 2012, **13**, 226-236.
4. H. Møllendal, S. Samdal, A. Matrane and J. C. Guillemin, *J. Phys. Chem. A*, 2011, **115**, 7978-7983.
5. J. W. Zwikker and R. W. Stephany, *Synth. Commun.*, 1973, **3**, 19-23.
6. E. K. A. Wolber, M. Schmittel and C. Rüchardt, *Chem. Ber.*, 1992, **125**, 525-531.
7. V. A. Apkarian and N. Schwentner, *Chem. Rev.*, 1999, **99**, 1481-1514.
8. V. E. Bondybey, M. Rasanen and A. Lammers, *Annu. Rep. Prog. Chem., Sect. C: Phys. Chem.*, 1999, **95**, 331-372.
9. B. Meyer, *Low Temperature Spectroscopy*, American Elsevier Pubishing Company, Inc., New York, 1971.
10. S. Radhakrishnan, J. Mieres-Perez, M. S. Gudipati and W. Sander, *J. Phys. Chem. A*, 2017, **121**, 6405-6412.
11. T. A. B. Miller, Vladimir. E., in *Molecular Ions: Spetroscopy, Structure, and Chemistry*, ed. T. A. B. Miller, Vladimir E., North-Holland Publishing Company, Amsterdam, New York, Oxford, 1983, pp. 126-173.
12. J. Fulara, S. Leutwyler, J. P. Maier and U. Spittel, *J. Phys. Chem.*, 1985, **89**, 3190-3193.
13. N. Lamarre, B. Gans, L. A. Vieira Mendes, M. Gronowski, J. C. Guillemin, N. De Oliveira, S. Douin, M. Chevalier, C. Crépin, R. Kołos and S. Boyé-Péronne, *J. Quant. Spectrosc. Radiat. Transfer*, 2016, **182**, 286-295.
14. R. Kołos, M. Gronowski and P. Botschwina, *J. Chem. Phys.*, 2008, **128**, 154305.
15. M. Turowski, M. Gronowski, S. Boyé-Péronne, S. Douin, L. Monéron, C. Crépin and R. Kołos, *J. Chem. Phys.*, 2008, **128**, 164304.
16. A. Coupeaud, M. Turowski, M. Gronowski, N. Piétri, I. Couturier-Tamburelli, R. Kołos and J.-P. Aycard, *J. Chem. Phys.*, 2008, **128**, 154303.
17. J. Sadlej and B. O. Roos, *Chem. Phys. Lett.*, 1991, **180**, 81-87.

18. J. A. Halpern, G. E. Miller, H. Okabe and W. Nottingham, *J. Photochem. Photobiol., A*, 1988, **42**, 63-72.
19. F. Borget, S. Müller, D. Grote, P. Theulé, V. Vinogradoff, T. Chiavassa and W. Sander, *Astron. Astrophys.*, 2017, **598**, A22.
20. U. Szczepaniak, R. Kołos, M. Gronowski, M. Chevalier, J.-C. Guillemin, M. Turowski, T. Custer and C. Crépin, *J. Phys. Chem. A*, 2017, **121**, 7374-7384.
21. T. Custer, U. Szczepaniak, M. Gronowski, E. Fabisiewicz, I. Couturier-Tamburelli and R. Kolos, *J. Phys. Chem. A*, 2016, **120**, 5928-5938.
22. A. Coupeaud, R. Kołos, I. Couturier-Tamburelli, J. P. Aycard and N. Piétri, *J. Phys. Chem. A*, 2006, **110**, 2371-2377.
23. A. Benidar, D. Begue, F. Richter, C. Pouchan, M. Lahcini and J.-C. Guillemin, *ChemPhysChem*, 2015, **16**, 848-854.
24. H. Bürger, D. Lentz, B. Meisner, N. Nickelt, D. Preugschat and M. Senzlober, *Chem.-Eur. J.*, 2000, **6**, 3377-3385.
25. S. Torker, D. Kvaskoff and C. Wentrup, *J. Org. Chem.*, 2014, **79**, 1758-1770.
26. B. T. Hill and M. S. Platz, *Phys. Chem. Chem. Phys.*, 2003, **5**, 1051-1058.
27. A. V. Golovkin, D. I. Davlyatshin, A. L. Serebrennikova and L. V. Serebrennikov, *J. Mol. Struct.*, 2013, **1049**, 392-399.